Alma Mater Studiorum
Università degli Studi di Bologna

Facoltà di Ingegneria

Dottorato di Ricerca in:	Meccanica e scienze avanzate dell'ingegneria.
Progetto n°4:	Meccanica dei materiali e dei processi tecnologici.
Ciclo	XXV
Settore concorsuale di afferenza:	09/A3
Settore scientifico disciplinare:	ING/IND 14

Electrospun nanofibrous interleaves in composite laminate materials

Candidato:
ROBERTO PALAZZETTI

Tutore:
Andrea Zucchelli, PhD

Co-tutori:
Irina Trendafilova, PhD
Giangiacomo Minak, PhD

Esame finale Anno 2012

a Laura.

Abstract

The present work aims for investigate the influence of electrospun Nylon 6,6 nanofibrous mat on the behavior of composite laminates. The main idea is that nanofibrous interleaved into particular ply-to-ply interfaces of a laminate can lead to significant improvements of mechanical properties and delamination/damage resistance. Experimental campaigns were performed to investigate how nanofibers affect both the static and dynamic behavior of the laminate in which they are interleaved.
Mode I and Mode II fracture mechanics tests were initially performed on virgin and 8 different configuration of nanomodified specimens. The purposes of this first step of the work are (1) to understand which geometrical parameters of the nanointerleave influence the behavior of the laminate and, (2) to find the optimal architecture of the nanofibrous mat in order to obtain the best reinforcement. In particular, 3 morphological parameters are investigated: nanofibers diameter, nanofibers orientation and thickness of the reinforce. Two different values for each parameter have been used, and it leads to 8 different configurations of nanoreinforce. Acoustic Emission technique is also used to monitor the tests.
Once the optimum configuration has been found, attention is focused on the mechanism of reinforce played by the nanofibers during static and dynamic tests. Low velocity impacts and free decay tests are performed to attest the effect of nanointerlayers and the reinforce mechanism during the dynamic loads. Bump tests are performed before and after the impact on virgin and two different nanomodified laminates configurations. The authors focused their attention on: vibrational behavior, low velocity impact response and post impact vibration behavior of the nano-interleaved laminates with respect to the response of non-nanomodified ones.
Experiments attest that nanofibers significantly strength the delamination resistance of the laminates and increase some of their mechanical properties, such as energy absorbing capability, G_{IC}, maximum stress before material crisis, absorbed energy during impact and residual strength. It is demonstrated that the nanofibers are capable to continue to carry on the loads even when the matrix

around them is broken.

Sommario

Scopo del presente lavoro è quello di studiare l'interazione tra strati di nanofibre polimeriche e laminati compositi a matrice epossidica. La tesi che si intende dimostrare sostiene che attraverso l'utilizzo di materiale nanofibroso posizionato in determinate interfacce di laminati compositi, si possa ottenere un significativo aumento di proprietà mecaniche e di resistenza alla propagazione della delaminazione.
Attività principale di questo lavoro è un'intensa campagna sperimentale volta a studiare il modo in cui le nanofibre influenzano sia il comportamento statico che quello dinamico del laminato nel quale sono inserite, prestando particolare attenzione al meccanismo attraverso il quale esse agiscono. Il tessuto di rinforzo è stato prodotto in laboratorio mediante processo di electrospinning di Nylon 6,6.
La prima fase del lavoro ha riguardato lo studio di quelle caratteristiche geometriche e morfologiche del nanorinforzo che hanno influenza sul comportamento finale del laminato, al fine di trovare la configurazione migliore. Le caratteristiche ritenute rilevanti sono 3: il diametro e l'orientamento delle nanofibre e lo spessore del rinforzo. Si sono quindi realizzate 8 diverse configurazioni di nanofibre, assegnando ad ogni caratteristica due valori. Attraverso test di Modo I e di Modo II di meccanica della frattura su provini vergini e nanomodificati, si è determinata la configurazione in gradi di migliorare più delle altre le caratteristiche del laminato di base. Durante ogni prova sono inoltre state misurate le emissioni acustiche.
Le prove dinamiche sono state effettuate su laminati nanomodificati con nanofibre aventi la configurazione trovata precedentemente. Si sono eseguiti impatti a bassa velocità e prove di vibrazione, queste ultime eseguite prima e dopo impatto. Le prove erano focalizzate, in particolare: sul comportamento vibrazionale, sulla risposta all'impatto e sul comportamento vibrazionale post-impatto.
I risultati mostrano che l'utilizzo di nanofibre può significativamente migliorare la resistenza alla delaminazione del laminato e allo stesso tempo aumentarne alcune proprietà e caratteristiche meccaniche. Le prove statiche hanno dimostrato che nella loro configurazione ottimale, le nanofibre sono in grado di aumentare la capacita di assorbimento di energia meccanica del laminato nel quale sono inserito, G_{IC}, la tensione massima sopportabile, la capacita di assorbimento di energia durante l'impatto e la loro resistenza residua.
Si dimostra che il principale meccanismo di rinforzo dovuto alle nanofibre è il cosiddetto fiber bridging: la capacità, cioè, da parte delle fibre, di continuare a sopportare carichi anche quando la matrice che le avvolge è danneggiata.

Contents

List of Figures

List of Tables

Introduction

This work finds its place into the composite materials world. Composite materials are a solution to one of the biggest challenge of our times: manufacture components at the same time lighter and stronger than their counterparts made by traditional materials. In many fields such as aerospace, automotive, transportation, constructions, and so on, working with lighter structures and manufactures leads to save energy. The BP Statistical Review of World Energy shown that in 2008, in the world, 11.3 billions of Tons of Oil Equivalent (TOE) have been burned and in particular:

- North America 24.8% (USA 20.4%);
- Central and South America: 5.1%;
- Europe and Eurasia: 26.2% (UE 15.3%);
- Middle East: 5.4%;
- Africa: 3.2%;
- Asia and Pacific area: 35.3% (China 17.7%; Japan 4.5%; India 3.8%).

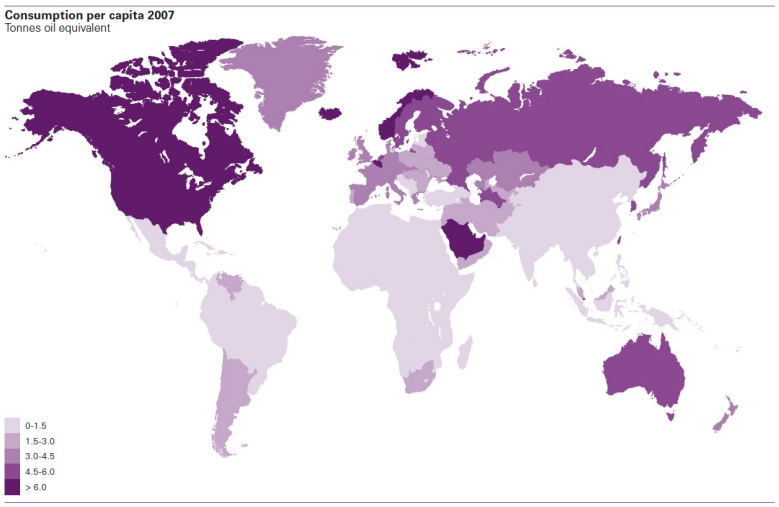

Figure 1: Consumption per capita 2007 [1].

Since these numbers are increasing year after year, it is clear to everyone that our society can not continue on this path in terms of energy consumption: if we want longer survive on this planet we need to find the manner to reduce our energy needs. In our everyday life two main causes of expenditure of energy are individuated: heating and transportation. Leaving aside the heating, which is not in our interest, composite material are related with the second matter. The impact of the large use and of the cost of the oil is heavily strong on our finance, and moreover, on our planet, its survival and the health of its environment. Saving propellent is one of the most important issues that we should keep in mind to preserve our planet and the health of us all and of our children. Research, which should always be focused to improve our quality of life, has made and is making many efforts in this direction. With this considerations, the invention of composite materials gets a great importance. By the definition of the Oxford Dictionary of English, a *composite material* is a "material made up of recognizable constituents". In engineering, a composite material is that material, non present in nature, characterized by a non-homogeneous structure, made by two or more different substances, physically separated, which presents different physical and mechanical characteristic respect to the single constituents. Commonly the base materials are called "matrix" and "reinforce". In this meaning, the first composite material produced by the man was the brick, made by straw and mud. Of course we are interested in something different and much more evolutes, but the definition is perfectly applicable to a wide range of materials, already applied in the past, and widely present in nature, already.
The importance of composites in transport industry is related to the weight saving introduced by this materials and the fact that at the same time they also possess very interesting mechanical properties, which are comparable, and often superior, of those of steel and aluminium, usually used in industry (§1.1). Due to their good performances, composite materials can find many applications from cars to aircrafts, from sport equipment to medical devices, for both civil and military applications, in mechanical and civil engineering, and in general for all those applications for which it is important to save weight and at the same time improve the performances. At the state of the art manufacturing with composite is still a bit expensive, thus these materials are almost reserved to high-quality and/or high-performance equipment (§1.1.1).
Many kinds and configurations of composites can be found in all the mentioned applications; the attention of this work in focused on laminate (§1.1.2), which is probably the most important and used structure of composite. Mainly due to their heterogeneous and stacked nature, laminate failure modes are strongly different from those of traditional materials like metals or plastics, and among all the failure modes the most common one is the delamination (§1.1.3).
Core of this work is to give contribution to one of the last developed techniques born to mitigate the delamination effects and the damage progression: the use of nanofibers. Many techniques are developed to face the delamination (§1.2.1) and the one this work is interested in involves to the use of polymeric nanofibers (§2.2.1).
Attention of the author is focused on nanofibers manufactured by electrospinning process (§2.1.1) and on their capability to improve the delamination resistance and the mechanical properties of the laminates where they are interleaved in. From the literature review it is already clear that nanofibers have the potential to significantly strength epoxy-based composite laminates but there are

still some questions which necessitates to find their answers (§2.2.2). A huge experimental campaign is performed (§3.4) in order to compensate the lack of the literature and to obtain enough data to understand how Nylon 6,6 nanofibers can affect the behavior of an epoxy-based composite material under many points of view. Both static and dynamic tests are performed. A preliminary analysis made by the use microscope (see §4.4) revealed the nature and the characteristics of the nanomodified interfaces and the fact that the nanoreinforce is clearly visible and affects the resin content of the interfaces.

Figure 2: SEM image of resin-carbon fiber-nanofibers system.

The electrospinning is probably the most versatile technique to manufacture nanofibers and it is driven by many process parameters, each of them affecting the final morphology and the shape of the nanofibers in its own way. The features of the nanofibers will also affect the behavior of the interface where they are interleaved in and than the whole laminate. The first part of this work is focused to find that morphological aspect of the nanoreinforce that allows the best reinforcement for the laminate, in order to help those designer who will apply nanofibers to their structures to maximize the reinforce effect (§4.1). Nanofiber diameter, nanofibers orientation, and nanolayer thickness are individuated to be the most characterizing features for a nanoreinforce, and an optimization process was carried out by two static tests (§3.2.1): DCB and ENF. 8 different configuration of nanofiber mats were manufactured and interleaved into specimens to be tested. Mode I and Mode II fracture mechanics tests are performed on laminates in which a nanointerlayer was placed in between the delaminated interface. Acoustic emission technique is also applied for the first time to this kind of problem (§3.3.2) in order to understand the mechanical behavior of the crack propagation in interlayers both non-nanomodified and nanomodified, and the role played by the nanofibers.
Once the optimum conditions for the nanoreinforce are determined, two dynamic tests (§3.2.2) were performed to complete the investigation: Low velocity impact (§4.6) and free decay vibration (see §4.5) tests were carried out to investigate the dynamic behavior of the nanomodified composite under different

impulsive loads. Vibration tests were performed before and after an impact event and used as a tools to detect and evaluate the damage induced by the impactor.
A complete presentation, analysis and discussion of the results is reported (§4). Experiments enhanced the capability of the polymeric nanofibers to significantly improve delamination resistance of the laminates without loss of mechanical performances or increase of thickness. Static tests determined that nanofibers are significantly capable to reinforce a composite laminate, especially when it is solicited under Mode II loads and at the same time the optimization process revealed the importance of an accurate geometrical choice of the characteristics of the fibers to achieve the desired reinforce. Mode I tests have, in fact, demonstrated that in many cases nanofibers may weak the interface if they are not properly designed.
Dynamic tests revealed that with the proper nanointerlayer, it is possibly to significantly improve mechanical performances and delamination resistance of the laminate. In particular it is evinced the capability of the nanofibers to bridge the crack while it propagates improving the residual mechanical characteristics of the damaged/delaminated specimen (§4.7).

1. Composite materials

Cominciate col fare ciò che è necessario
poi ciò che è possibile.
E all'improvviso vi sorprenderete a fare l'impossibile.
S. Francesco d'Assisi - patrono d'Italia

1.1. Introduction to composites

A composite material is made by the combination of two or more materials, different in form or in composition at macroscale. Constituents maintain their identities and work together, even if in different way and with different role when subjected to loads. The concept of composites was not invented by human beings since it is already present in nature, for example the wood is a composite of cellulose fibers in a matrix of natural glue called lignin. The main concept of a composite is that it contains matrix materials. Typically, a composite material is formed by reinforcing fibers in a matrix resin. The reinforcements can be fibers, particulates or whiskers, and the matrix materials can be metals, plastics, or ceramics. The reinforcements can be made from polymers, ceramics, and metals. The fibers can be continuous, long, or short. Composites made with a polymer matrix have become more common and are widely used in various industries. The wildest, and at the same time one of the first, composite introduced in industry is the reinforced concrete used for buildings: the concrete matrix carries on the compressive load give by the mass of the structure and keeps the steel bars together; at the same time, those bars carry the flexural component of the loads during winds, earthquakes and so on. In mechanical engineering, the most important class of composite is the so-called "Fiber Reinforced Plastic" (FRP) materials. FRPs are made of long fibers (usually carbon, glass or Kevlar) embedded into a resin matrix (thermosetting or thermoplastic). Fibers are high-modulus and high strength and carry on the loads in their direction, while the resin keeps them together and carries out-of-plane loads.
Composites are mainly designed and manufactured for applications in which high performance and light weight are needed since they offer several advantages over traditional engineering materials [2]:

1. higher specific stiffness (stiffness-to-density ratio): composites offer the stiffness of steel at one fifth the weight and equal the stiffness of aluminium at one half the weight;

2. higher specific strength (strength-to-density ratio): typically in the range of 3 to 5 times that of steel and aluminum alloys. Due to this higher specific stiffness and strength, composite parts are lighter than their counterparts;

3. higher fatigue strength: steel and aluminium alloys exhibit good fatigue strength up to about 50% of their static strength. Unidirectional carbon/epoxy composites have good fatigue strength up to almost 90% of their static strength;

4. higher corrosion resistance. Iron and aluminium corrode in the presence of water and air and require special coatings and alloying. Because the outer surface of composites is formed by plastics, corrosion and chemical resistance are very good;

5. complex parts, appearance, and special contours, which are sometimes not possible with metals, can be fabricated using composite materials without welding or riveting the separate pieces. This increases reliability and reduces production times and offers greater manufacturing feasibility;

6. higher impact properties: glass and Kevlar composites provide higher impact strength than steel and aluminium;

7. by utilizing proper design and manufacturing techniques, cost-effective composite parts can be manufactured. Composites offer design freedom by tailoring material properties to meet performance specifications, thus avoiding the over-design of products. This is achieved by changing the fiber orientation, fiber type, and/or resin systems;

Al these characteristics lead composite to be ideal materials for applications in which performances are of particular importance, such as aerospace, aeronautic, competition, shipbuilding and many more [8–11].

1.1.1. Manufacturing of composites

Working with composites means to work with many types of materials, including fibers, resins, mats, fabrics, prepregs, moulds, compounds, and many more, and each of them needs its own particular treatment, storage condition, process and so on. Each manufacturing technique requires different types of support materials, different processing conditions, and different tools for part fabrication. For this reason, manufacturing process of composites has to take into account a great number of variables and often is particularly complicated. Since the use of composite material is relatively new in mechanical engineering, many manufacturing processes are still quite raw and under develop. Production process of composites faces with high costs and low production rate, compared to processes which involve traditional materials, and it is another reason for which, at the moments, composites are dedicated to top-class applications. In Figure 1.1, the most used manufacturing techniques of composites are presented, and divided into groups selected by the type of resin (thermosetting or thermoplastic) and the length of the fibers (short of long).
For each component, the choose of the best process depends on many parameters, such as production rate, cost, strength required, size, shape, type of raw

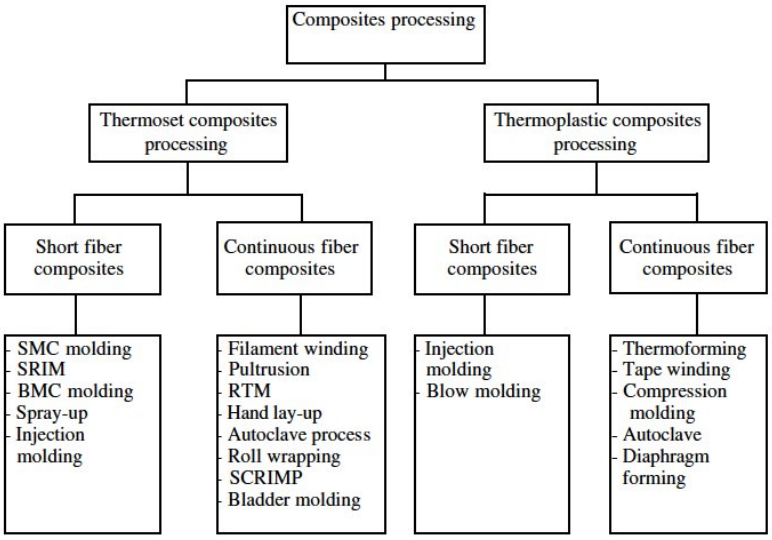

Figure 1.1: Composite process techniques [2].

material, and often they are linked each other.
Among the wide world of composites, present work is focused on laminates, which are made of plies of long fibers commonly embedded into a thermosetting resin.

1.1.2. Composite laminates

This work focuses its attention of laminates, thus it is important to give a comprehensive explanation on what a composite laminate is: a sequence of unidirectionally or bidirectionally reinforced plies stitched together by uncured polymer matrix material. Usually the resin used for industrial applications is a thermosetting one, due to its much better mechanical properties compared to the thermoplastic ones. Composites usually exhibit the best qualities of their constituents and qualities that neither of the constituents possesses. Each ply is typically a thin (approximately 0.2 mm) sheet made by fibers placed in one or two direction stitched together by the resin and the orientation of each ply into the manufactured depends on the final needs of the component, thus the lay-up sequence is tailored to achieve the properties desired for the laminate. Each ply is placed one over the other into a mould which gives the shape to the final component. If row sheets are dry, many techniques and many processes have been developed to make the resin flow and wet the fibers, such as Resin Transfer Moulding (RTM), Vacuum Assisted Resin Transfer Moulding (VARTM), Infusion and so on. When the plies are pre-impregnated with the resin, curing process takes place into an autoclave which provides the temperature and pressure needed to cure the resin and the whole manufactured. A vacuum bag is then prepared to compact the laminate over the mould (Figure 1.2(a)) and all is placed into the autoclave where a temperature-pressure cycle takes place to cure the resin, as the example shown in Figure 1.2(b).
The process needs few hours to be completed and after cooling the component

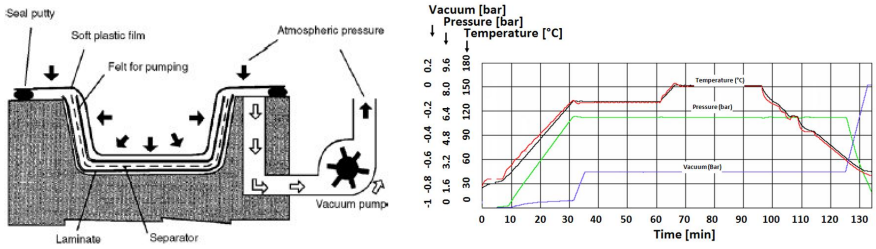

(a) Vacuum bag [3]. (b) Cure cycle.

Figure 1.2: Lamination process into autoclave.

is took out and ready for the use. Even if this process is the slowest one, it has applications particularly for aircraft structures since it ensures the best quality in terms of avoid defects such as air bubbles or partially-cured resin.

1.1.3. Failure and damage modes for laminates

Due to their complex nature and structure, composite materials exhibit different modes of failure and damage respect to metals or other conventional materials. The main aspects influencing damage are related to the non-homogeneity and the non-isotropy of the structure of composites. The presence of different materials (e.g. fiber and matrix) and the combination of layers which usually have different orientations, lead to a great number of modes of failure and damage. In Figure 1.3 laminates modes of failure are presented.

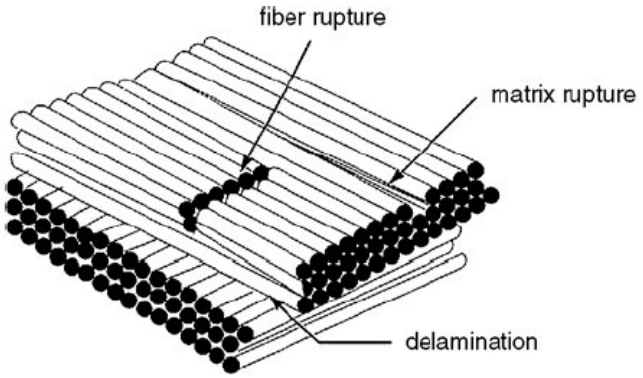

Figure 1.3: Modes of failure [3].

The failure mode is strongly affected by the material of the matrix as well as its compatibility with the fibers. Since the matrix is the weakest component, it is usually the first element to fail. When external load or deformation become stronger, even the fibers can broke. One of the most common failure mode is the so-called "delamination", and it takes place when two adjacent plies debond (§1.2).
In Figure 1.4 modes of damage are presented.

(a) Tension.

(b) Compression.

(c) Shear.

Figure 1.4: Modes of damage [3].

Due to the fiber-nature of the reinforce, composites show different behavior between tension and compression load-states and present different resistance: in particular long fiber reinforced plastics present an higher resistance to tension loads respect the compression one. Compression and shear loads are able to induce the phenomena of delamination, which is one of the most critical factors related to laminates, and of particular interest in this work. To introduce the delamination topic it is important to spend some words about the interlaminar properties of laminates.

1.2. Delamination problem: state of the art

Fiber reinforced resin composites are typically formed by laying up a plurality of plies made of reinforcing fibers and resin, cured by applying heat and pressure or by using a catalyst-promoter system. Since the properties in fiber directions are different from the other two orthogonal ones, a unidirectional (0-degree) ply can be modelled as an orthotropic material, as well as a bi-directional ply. From an absolute reference system, the material properties of an angle ply (for example, a 45-degree ply) can be obtained using the properties of the unidirectional, the fiber angle, and the appropriate space-transformations. The global properties of a whole laminate are given by the sum of those of each ply and often the resulting material properties show anisotropic behavior [12]. Due to the laminate nature, ply-to-ply interfaces of composite laminates represent the weak points of the structure. Delamination is a crack formed between adjacent plies and can be viewed as an interface crack between two anisotropic materials. Susceptibility to delamination along interlaminar planes is an intrinsic and severe problem of laminates that can ultimately undergo structural failure. Delamination can be caused by many factors (Figure 1.5) such as interlaminar stresses concentration at free edges, joints, matrix cracks, out-of-plane loading,

physical discontinuities or mismatch in mechanical properties between adjacent layers: all these are often principle of fails like delamination, but also buckling and so on.

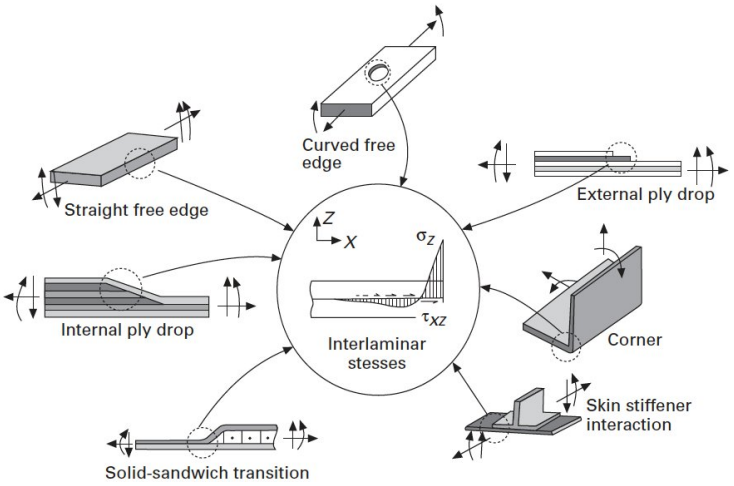

Figure 1.5: Causes of delamination [4].

Delamination is probably the most common failure mode for laminates and over the years many techniques have been developed to investigate and mitigate this phenomena, which results to be particularly dangerous since it appear and grows under the surface: a laminate can lost up to 60% of its compressive residual strength and stiffness and still remains visibly unchanged. Over the past 25 years, significant progresses had been made in research by the use of fracture mechanics principles to characterize and predict delamination failures in composite laminates. Although these studies have demonstrated the promise of this approach, they have also highlighted some of the difficulties and differences relative to the well-established use of fracture mechanics for damage tolerance assessment of metallic structures. One notable difference is the propensity for cracks in composites to propagate in a mixed-mode fashion. This aspect can be attributed to the fact that delaminations are constrained to grow between composite layers. Delamination cracks do not immediately turn toward the opening mode direction as typically occurs in metals.

1.2.1. Literature review

The interest of the research community on this problem is highly connected to the world of the industry since many companies are facing this problem, which is particularly critical for aerospace and aeronautical applications. Brunner and their research group published two interesting works on delamination resistance testing regarding reinforced plastic materials [13, 14]. From those papers it clear appears that the fracture mechanics theory is particularly suitable to face the problem and that the interlaminar fracture test methods are the widest used [13], due to three main aspects:

1. laminate materials are made by stacked plies, which lead to a weak interlaminar region. Among the many techniques developed to improve

interlaminar efficiency (as it will be further illustrated), one of the easiest consists to tough the matrix resin. Intense effort has been devoted to this activity in recent years, with new modified epoxies, phenolics, polyimides and thermoplastics appearing regularly accompanied by promises of tougher composites: fracture test methods enable the users to assess the virtues of new matrix polymers on a common basis;

2. a major concern in the aerospace industry has been damage tolerance. The allowable damage which a composite structure can incur is a key parameter in determining the safety of aircraft and so measuring fracture energies is a simple way of screening the damage tolerance of composite materials;

3. the perceived need for values of G_C, the critical strain energy release rate, for structural calculations.

The state of the art of fracture mechanics used to calculate interlaminar fracture toughness and delamination onset and growth with the standards given by the American Society for Testing of Materials (ASTM) published for composites: Mode I (double cantilever beam, DCB) [15] and mixed-Mode I and II (mixed-mode bending, MMB) [16] interlaminar fracture toughness are the most suitable tests for these purposes. Although there are still no standard methods for pure Modes II and III, two promising test methods have been developed: the End Notched Flexure (ENF) test for Mode II and the Edge Cracked Torsion (ECT) test for Mode III. In the present work, interlaminar fracture tests cover a large part of the experiments, as it will be illustrated in §3.
During the years many techniques were carried out in order to mitigate the delamination problem and to arrest the crack propagation. As it was said before, one of the easiest way to improve interlaminar resistance is the matrix-toughening which mainly consists in placing an interlayer between two adjacent plies in order to arrest the crack propagation. Marieta et al. [17] used ester matrix and focused their research on the interfacial behavior. In particular they considered the influence of carbon fiber surface treatments (sizing and oxidation) and also the modification of thermosetting matrix by the addition of a thermoplastic. They performed an experimental campaign by the pull-out test, short beam-shear test, and end-notched flexure test to determine the apparent interfacial shear strength, the interlaminar shear strength and the Mode II delamination fracture toughness (G_{IIC}) respectively. Characterization of carbon fibers and matrix showed that the unsized and oxidised carbon fibers do not have a clear effect on the cure of the resin, in an opposite way to the epoxy sizing, which decreases slightly the heat of reaction. Concerning the influence of fiber surface treatments and toughening of thermosetting matrix on the interfacial behavior of the composites, the commercial sizing of epoxy is effective in promoting adhesion and improving of fracture toughness. They also showed that the incorporation of 10 wt% PEI thermoplastic in thermosetting matrix improves composite fracture toughness. Hojo et al. [18] investigated Mode I delamination fatigue crack growth in carbon fiber/epoxy matrix with two kinds of interlayers: one was the heterogeneous interlayer with fine polyamide particles, and the other was a new types of thermoplastic resin, an ionomer. They performed DCB tests and have found that by the use of polyamide, fatigue crack resistance of the modified laminates growth from 1.5 to 3 times higher than that of the

reference CFRP, and similar results have been found by using the ionomer. The difference in the toughening mechanism for these interlayer/interleaf laminates is related to the fact that the crack propagation takes place into heterogeneous toughened interlayer region instead of going to interlayer/base lamina interface. An interesting work presented by Yang [19] studied into a new type of stitched fiber/polymer laminate that combines high interlaminar toughness with self-healing repair of delamination damage by stitching Poly(ethylene-co-methacrylic acid) (EMAA) filaments into carbon fiber/epoxy laminate. Authors created a three-dimensional self-healing fiber system that also provides high fracture toughness. Double cantilever beam testing revealed that the stitched EMAA fibers increased the mode I interlaminar fracture toughness of the laminate of about 120% , and reduced the amount of delamination damage that must subsequently be repaired by the self-healing stitches. The 3D stitched network was effective in delivering self-healing EMAA material extracted from the stitches into the damaged region, and it resulted in high recovery in the delamination fracture toughness (around 150% compared to the original material). The new self-healing stitching method provides high toughness which resists to delamination growth while also have the functionality to repeatedly repair multiple layers of damage in epoxy matrix laminates.

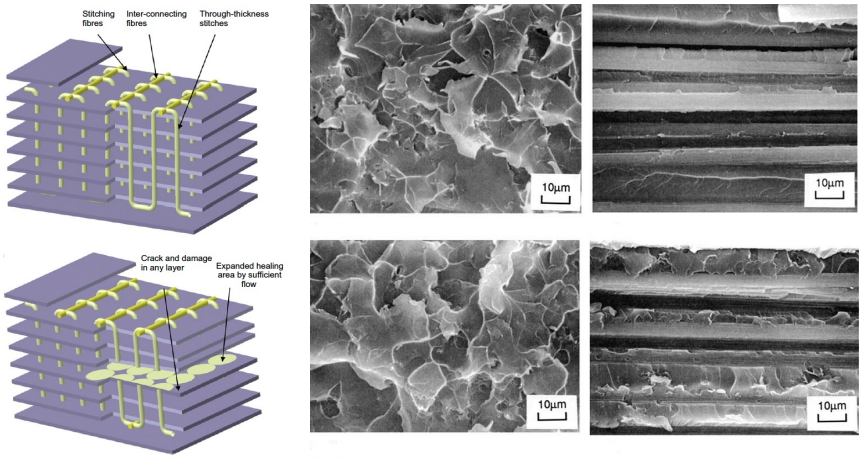

(a) 3D stitched network [19]. (b) Interlayer with fine polyamide particles [18].

Figure 1.6: .

A different approach to the problem regards the stacking sequence of the plies. From the theory of laminates [20], many mechanical properties, such as stress field in through-the-thickness direction, stiffness, strength and deformation depend on stacking sequence. Many efforts have been made in the direction of finding an optimized stacking sequence capable to minimize stress concentrations and thus delamination initiations. Fuoss et al. [21] in their work investigated the effect of the staking sequence of a laminate subjected to impacts, focusing their attention on three parameters: interface angle, ply orientation relative to a fixed angle and ply grouping. Research has found that each parameter influences the damage resistance differently and concluded with some important guidelines to design with laminates, such as avoiding ply grouping

and stacking adjacent plies in similar orientation, particularly at interface angles below 45°. Basing on it, same authors also developed a prediction method [22] for impact damage. Kere et al. [23] developed a technique to optimize stacking sequence of laminates subjected to multiple loads. By an iteration process they have found an optimized stacking sequence with respect to laminate failure. Ghiasi et al. [24, 25] in their papers present a wide review of the literature on this topics, in order to find a tool which allows designers to minimize the number of layers and to design with the best fiber orientation and thickness for each layer. Several optimization methods have been introduced, which are often non-linear, non-convex, multimodal, and multidimensional, and might be expressed by both discrete and continuous variables. They studied the optimization by two techniques: constant stiffness design and variable stiffness design. The first one deal with laminates with uniform stacking sequence through their entire structure and authors describe the main optimization methods and their characteristic features. The second paper explains the different parametrization and optimization algorithms and discusses the advantages and shortcomings of each algorithm. Pereira et al. [26, 27] performed an experimental study on Mode II interlaminar fracture mechanics of epoxy-based woven fabric laminates to choose the best stacking sequences for End-Notched Flexure specimens with starter delaminations on $\theta/-\theta$ and $0°/-\theta$ interfaces. They demonstrated that G_{IIC} is highly dependent on the angles of the plies at the interface and proposed a coefficient to predict that value.

Another interesting technique, even if quite complicated sometimes, regards the use of through-the-thickness 3D reinforcements. The first author who introduced this kind of solution was Howard, in 1986 [28] by bonding of a U-shaped caps to the edge of a laminate. He performed static and tension-tension fatigue loads on symmetric 11-layer graphite-epoxy laminates with a one-layer cap of Kevlar-epoxy cloth. Those new specimens were found to be from 130% to 140% stronger than uncapped laminates under static tensile and tension-tension fatigue loading. In addition, the coefficient of variation of the static tensile failure load decreases from 24% to 8% when edge caps are added. Following this idea, other researchers started investigations in the same field. Partridge et al. [29] presented an introduction into the technology of through-the-thickness reinforcement of thermosetting composites by the insertion of Z-Fiber® pins. The insertion of the Z-pins adds only one extra step during the manufacturing process of the composite: just prior to bagging in the case of autoclave cure of prepreg based parts or prior to resin injection in the case of RTM process. They carefully described the manufacture of the raw materials and the method of pin insertion and performed Mode I and Mode II fracture mechanics tests over 3 mm thick unidirectional continuous carbon fiber/epoxy prepreg, with and without a block of Z-pins in the crack path.

A similar technique regards the stitched composites. The work of Chen et al. [31] is one of the most important on this topic: they present both an experimental campaign and a finite element models to determine the Mode I and Mode II fracture toughness of stitched composites. They also present two new test methods to measure the Mode I and Mode II fracture toughness of stitched composites. Their best results was that improving the fracture toughness of laminates by increasing the cross-sectional area of the stitches, is more effective than increasing the density of stitching.

Another solution regards the three-dimensional braided composites, particu-

(a) Z-Pinn [14]. (b) Micrography of fracture of braided composites[30].

Figure 1.7: Two kind of 3D reinforcement proposed in literature.

larly suitable in the fields of astronaut and aeronautic. Tange et al. [30] studied the effect of the braiding process and the test parameters on the mechanical properties of a carbon fiber/epoxy resin braided composites. They used optical and SEM microscopes to analyse the macro- and micro-fracture morphology of the composite, loaded under different rates. The results indicate that the mechanical properties can be significantly affected by the parameters of braiding: by decreasing the braided angle, the elastic moduli and the ultimate tensile strength showed an obvious increase. The fracture process, indeed, depends on stress transfer behavior. The fracture characteristic is brittle, originated from plastic constraint at the fiber. Fiber fracture is caused by a defect on their surface in low loading rate. Authors also performed explosive impact tests, carried out in a special attachment: superior energy absorption capability and damage tolerance are found compared to traditional 2D laminates. Mouritz et al. [32] studied the behavior under mode I loading conditions of vinyl ester-based composites reinforced with glass fiber manufactured by braiding, knitting, stitching and through-the-thickness weaving, and compared to a variety of traditional composites such as unidirectional or woven roving. They have found that the use of advanced textile technologies leads to superior Mode I interlaminar fracture toughness properties respect to the common used composites. Advanced textile composites were found to have G_{IC} values at least twice as high as traditional fiberglass composites, although only the braided materials showed higher G_{IIC} values. The magnitude of the improvement in G_{IC} appears to be dependent upon the textile processing parameters, such as the braiding angle, the knit yarn density or the tensile strength, thickness and density of the through-thickness stitch/binder. The improved interlaminar toughness in braided and knitted composites was found to be the result of extensive crack branching combined with the delamination being forced to follow a tortuous path through the fiberglass network. The toughening in the stitched and through-the- thickness woven composites was mainly because of crack bridging, although crack branching and stitch/binder pull-out effects also contributed.
This work faces the problem of delamination by the use of nanofibers manufactured by electrospinning process. In the next chapter a brief illustration of the process is proposed and the state-of-the-art regarding composites addicted with nanofibers is presented.

2. Electrospinning

Lo spirito e la bizzarria vanno adoperati con cautela,
come tutte le sostanze corrosive.
G.C. Lichtenberg - fisico

2.1. Electrospinning

The electrospinning is a technology developed for electrostatic fiber formation by the use of electrostatic forces. It produces polymeric fibers with diameters ranging from few nanometers to several micrometers. Fibers are made using polymer solutions of both natural and synthetic polymers and the electrospinning has seen a tremendous increase in research and commercial attention over the past decade even if it is an old-know technique, observed for the first time by Raileigh in 1897 and then developed by further researches [33–37]. With smaller pores and higher surface area than regular fibers, electrospun fibers have been successfully applied in various fields, such as, nanocatalysis, tissue engineering scaffolds, protective clothing, filtration, biomedical, pharmaceutical, optical electronics, healthcare, biotechnology, defence and security, environmental engineering [38–42]. Overall, this is a relatively robust and simple technique to produce nanofibers from a wide variety of polymers. Spun nanofibers also offer several advantages such as an extremely high surface-to-volume ratio, tunable porosity, malleability to conform to a wide variety of sizes and shapes and the ability to control the nanofiber composition to achieve the desired results.
Despite the several advantages offered by the electrospinning, the throughput of nanofibers has been a serious bottleneck problem that limits their application. Many solutions have been found to increase the manufacturing rate, mainly adopting multiple nozzles systems arranged in a line/circle/matrix, or bottom-up gas-jet electrospinning (in this case the system is called bubble electrospinning), but it still one the main challenges to lead this technology into a large-scale processes.

2.1.1. Electrospinning process

Electrospinning is a unique approach that uses electrostatic forces to produce fine fibers from polymer solutions or melts: the fibers thus produced have thinner diameter (from nanometers to micrometers) and larger surface area than those obtained from conventional spinning processes. Furthermore, a DC voltage in

the range of several tens of $kV\,s$ is necessary to start the process. Electrospinning is normally conducted at room temperature and atmosphere conditions. When the humidity increases over a certain level, it is common to use air conditioner to maintain temperature and humidity into certain range. The typical set up of electrospinning apparatus is shown in Figure 2.1.

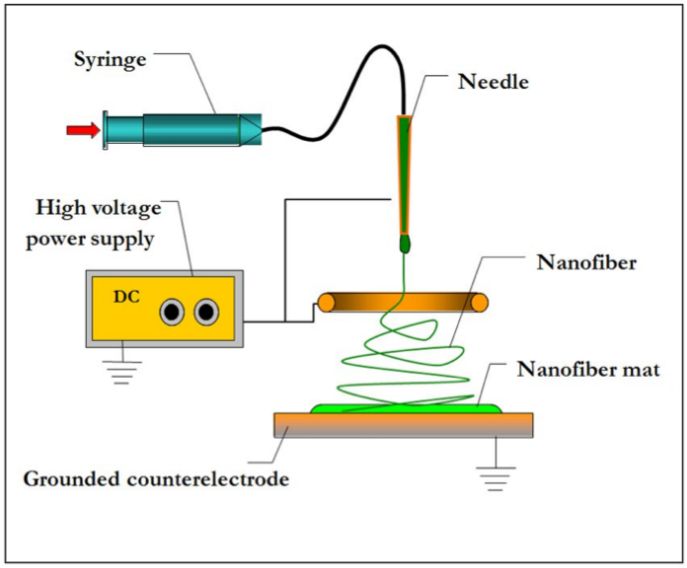

Figure 2.1: Electrospinning apparatus.

Basically, an electrospinning system consists of three major components: a high voltage power supply, a needle filled with a polymeric solution and a grounded collecting plate (usually a metal screen, flat, or rotating mandrel). The process utilizes a high voltage source to inject charge of a certain polarity into the polymer solution (or the melt, in case of "Melting electrospinning"), which is then accelerated towards a collector of opposite polarity. Most of the polymers are dissolved in some solvents before electrospinning to form the polymer solution. This fluid is then introduced into the capillary tube for the electrospinning process. The polymeric solution held by its surface tension at the end of a capillary tube is subjected to an electric field which induces an electric charge on the liquid surface. When the electric field reaches a critical value, the repulsive electrical forces overcome the surface tension ones. Eventually, a charged jet of the solution is ejected from the tip of the Taylor cone and an unstable and rapid whipping of the jet occurs in the space between the capillary tip and collector. This motion leads to the evaporation of the solvent, leaving the polymer behind. There are many parameters that influence the electrospinning process and so the final morphology of the fibers. In particular in Figure 2.2, traditional fibers (Figure 2.2(a)), porous fibers (Figure 2.2(b)), core-shell fibers (Figure 2.2(c)) and pearly fibers (Figure 2.2(d)) are shown.
The process parameters can be classified into three main groups [43]:

- polymer solution parameters: molecular weight and solution viscosity, surface tension, solution conductivity and dielectric effect of solvents;

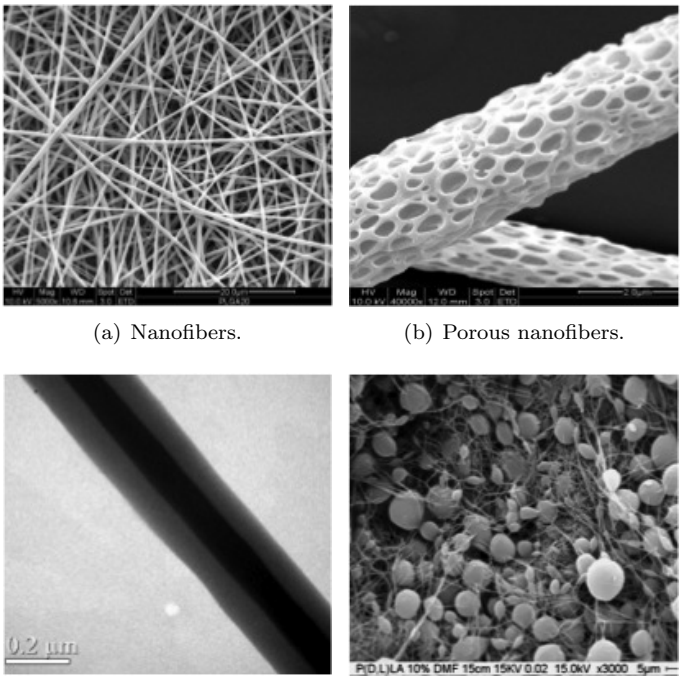

(a) Nanofibers. (b) Porous nanofibers.

(c) Core-shell nanofibers. (d) Pearly nanofibers.

Figure 2.2: Different kind of nanofibers.

- process conditions parameters: voltage, feedrate, temperature, motion/shape of the collector, needle diameter and needle tip - collector distance;
- ambient conditions: humidity, type of atmosphere and pressure.

Polymer solution parameters

The chemical characteristics of a polymer solution have the most significant influence on the final morphology of the fibers. High molecular weight leads the formation of the entaglements of the molecular chain which maintain a continuous solution jets and allow the formation of the nanofibers. If the solution is made with monomeric polymers, the electrospinning takes the name "electrospray" since the polymer is spread instead of spun. Molecular weight also affects the viscosity of the solution which is important to maintain the continuity of the process, as well as the polymer chains. Although a minimum amount of polymer chain entaglements, and thus viscosity, is needed, a too high viscous solution becomes very difficult to be processed and pumped to the needles. Moreover the solution may dry at the tip of the needle before the spinning process begins. It was found that at a low viscosity it is common to have deformations along the linear-shape of the fibers, called "beads", as shown in Figure 2.2(d).
The initiation of electrospinning requires that the charged solution overcome its surface tension. However, as the jet travels towards the collection plate, the surface tension may cause the formation of beads along the jet. Surface tension has the effect of decreasing the surface area per unit mass of a fluid. Solvents

such as ethanol have low surface tension and may be added to encourage the formation of smooth fibers.
Electrospinning involves stretching of the solution caused by repulsion of the charges at its surface. Thus the more the conductivity of the solution is increased, the more charges can be carried by the electrospinning jet. Beads formation will occur if the solution is not fully stretched. Therefore, sometimes a small amount of salt or polyelectrolyte is added to the solution with the purpose to increase the charges carried by the solution and the stretching of the jet. As a result, smoother fibers are formed which may otherwise yield to beaded fibers. The increasing in stretching the solution also will tend to yield fibers of smaller diameter.
The last important process condition is the effect of the solvents, which have a significant influence on the electrospinning. Generally, a solution with greater dielectric property reduces the beads formation and the diameter of the resultant electrospun fiber. Solvents such as N,N-Dimethylformamide (DMF) may be added to a solution in order to increase its dielectric property.

Process conditions parameters

A crucial element in electrospinning is the application of a high voltage between the needls (and thus the solution) and the collector. The high voltage induces the necessary charges on the solution and together with the external electric field will initiate the electrospinning process when the electrostatic force in the solution overcomes its surface tension. Generally, both high negative or positive voltage of more than $6kVs$ are able to cause the solution drop at the tip of the needle to distort into the shape of a Taylor cone during jet initiation. Depending on the feedrate of the solution, a higher voltage may be required so that the Taylor cone is more stable. The Columbic repulsive force in the jet will then stretch the viscoelastic solution. If the applied voltage is higher, the greater amount of charges will cause the jet to accelerate faster and more volume of solution will be drawn from the tip of the needle. This may result in a smaller and less stable Taylor cone. When the drawing of the solution to the collection plate is faster than the supply from the source, the Taylor cone may recede into the needle. As both the voltage supplied and the resultant electric field have an influence in the stretching and the acceleration of the jet, they will have an influence on the morphology of the fibers too. In most cases, a higher voltage will lead to greater stretching of the solution due to the greater Columbic forces in the jet as well as the stronger electric field. These have the effect of reducing the diameter of the fibers and also encourage faster solvent evaporation to yield drier fibers. When a solution of lower viscosity is used, a higher voltage may favour the formation of secondary jets during electrospinning. Another factor that may influence the diameter of the fiber is the flight time of the electrospinning jet. A longer flight time will allow more time for the fibers to stretch and elongates before it is deposited on the collection plate. Thus, at a lower voltage, the reduced acceleration of the jet and the weaker electric field may increase the flight time of the electrospinning jet which may favour the formation of finer fibers. In this case, a voltage close to the critical voltage for electrospinning may be favourable to obtain finer fibers. At higher voltages, it was found a greater tendency for beads formation and it is also reported that the shape of the beads changes from spindle- to spherical-like increasing the voltage.

It is observed that increasing voltage the beads density increases as well, and at an even higher voltage, the beads will join to form a thicker diameter fiber. Since the electrospinning is caused by charges on the jet, these charges can be influenced by the external electric field which will in turn affect the jet path. It is thus not surprising that there are several attempts to control the jet by changing the electric field profile between the source of the electrospinning jet and the collector. This can be achieved by using auxiliary electrodes or by changing the orientation or shape of the collector. Aligned and even patterned nanofibers can be obtained by clever manipulation of the electric field. In particular in Figure 2.3, some results are presented: random oriented fibers (Figure 2.3(a)), aligned fibers (Figure 2.3(b)), layered cross fibers (Figure 2.3(c)), star shaped fibers (Figure 2.3(d)) and radial fibers (Figure 2.3(e)) are shown.

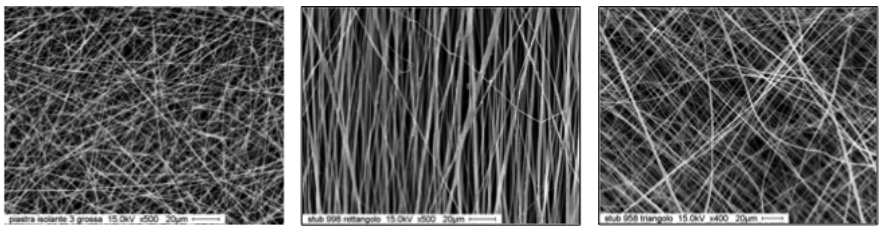

(a) Random fibers. (b) Aligned fibers. (c) Layered-cross fibers.

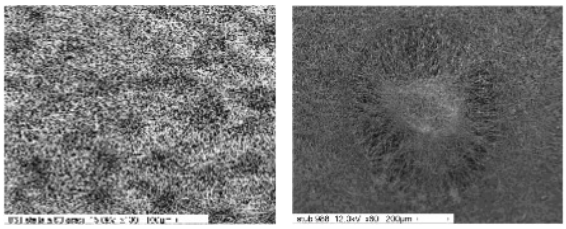

(d) Star shaped fibers. (e) Radial fibers.

Figure 2.3: Kind of nanofibers obtained changing the motion of the collector or manipulating the electric field.

The feedrate determines the amount of solution available for electrospinning in the unity of time. For a given voltage, there is a corresponding feedrate to maintain a stable Taylor cone. When the feedrate is increased, there is a corresponding increasing in fiber diameter or beads size, due to a greater volume of solution drawn away from the needle tip.
The temperature at which the electrospinning is processed has the double effect to increase the evaporation rate of the solvents and to reduce the viscosity of the solution. Increased molecules mobility due to increased temperature also allows the Columbic force to stretch the solution further. However, in cases where biological substances such as enzymes and proteins are added to the solution for medical purposes, the use of high temperature may cause the substance to lose its functionality.
The internal diameter of the needle or the pipette orifice has a certain effect on the electrospinning process. A smaller internal diameter was found to reduce the clogging as well as the amount of beads. Decreasing the internal diameter

of the orifice is also found to cause a reduction in the diameter of the fibers. When the size of the droplet at the tip of the orifice is decreased, such as in the case of a smaller internal diameter of the orifice, the surface tension of the droplet increases. For the same voltage supplied, a greater Columbic force is required to cause jet initiation. As a result, the acceleration of the jet decreases and this allows more time for the solution to be stretched and elongated before it is collected. However, if the diameter of the orifice is too small, it may not be possible to extrude a sufficient droplet of solution.
The last process important condition hereby introduced is the distance between the tip and the collector, which influences both the flight time and the electric field strength. When the distance between the tip and the collector is reduced, the jet may do not have sufficient distance to travel up to the collector plate. Moreover, the electric field strength increases at the same time pushing the acceleration of the jet to the collector. As a result, there may not have enough time for the solvents to evaporate before the jet hits the collector. When the distance is too short, excess solvent may cause the fibers to merge where they contact to form junctions resulting in inter- and intra-layer bonding. This interconnected fiber mesh may provide additional strength to the resultant scaffold. Depending on the solution property, the effect of varying the distance may or may not have a significant effect on the fiber morphology. Decreasing the distance has the same effect as increasing the voltage supplied and this will cause an increased in the field strength. As mentioned above, if the field strength is too high, the increased instability of the jet may encourage beads formation. However, if the distance is such that the field strength is at an optimal value, there is less beads formed as the electrostatic field provides sufficient stretching force to the jet.

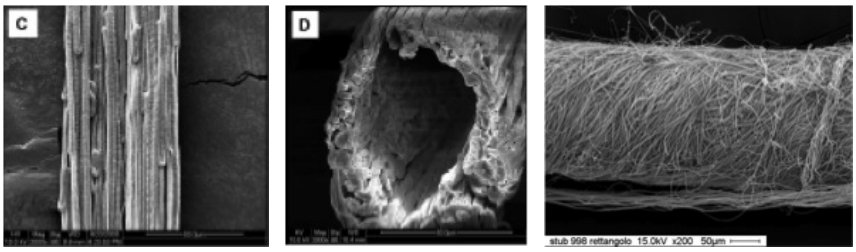

(a) Yarn. (b) Hollow yarn. (c) Bundle.

Figure 2.4: Various type of fiber morphology.

Ambient parameter

The humidity of the electrospinning environment may influence the polymeric solution during electrospinning. At high humidity, it is likely that water condenses on the surface of the fiber when electrospinning is carried out under normal atmosphere. As a result, this may have an influence on the fiber morphology especially for those polymers dissolved in volatile solvents. However, high humidity during electrospinning will cause circular pores to form on the fiber surfaces (Figure 2.2(b)). This may also happen during electrospinning as water vapour may condense on the surface of the jet due to cooling down as a

result of rapid evaporation of the volatile solvent. Pores are created when both water and solvents eventually evaporates. Although pores formed on thin film, due to breath figures are uniform, pores seen on electrospun fibers are not and this may be due to the dynamic condition of the electrospinning jet as compared to static condition where the effects of breath figures are seen on thin films. The humidity of the environment will also determine the rate of evaporation of the solvent in the solution. At a very low humidity, a volatile solvent may dry very rapidly. The evaporation of the solvent may be faster than the removal of the solvent from the tip of the needle. As a result, the electrospinning process may only be carried out for a few minutes before the needle tip is clogged.
The composition of the air in the electrospinning environment will have an effect on the electrospinning process. Different gases have different behavior under high electrostatic field. For example, helium breaks down under high electrostatic field and thus electrospinning is not possible. However, when a gas with higher breakdown voltage is used, such as Freon, the fibers obtained have twice the diameter of those electrospun in air given all other conditions equal.
Under enclosed condition, it is possible to investigate the effect of pressure on the electrospinning jet. Generally, reduction in the pressure surrounding the electrospinning jet does not improve the electrospinning process. When the pressure is below atmospheric pressure, the polymer solution in the syringe will have a greater tendency to flow out of the needle and there causes unstable jet initiation. As the pressure decreases, rapid bubbling of the solution will occur at the needle tip. At very low pressure, electrospinning is not possible due to direct discharge of the electrical charges.

2.2. Applications

Recently, researchers have begun to look into various applications of electrospun fibers and mats as these provide several advantages such as high surface to volume ratio, very high porosity and enhanced physics-mechanical properties. Manipulation of the solution and process parameters can be easily done to get the desired fiber morphology and mechanical strength to the nanoreinforce. In addition, electrospun fibers are required in small amount and the electrospinning process itself is very versatile as the fibers can be spun into any shape using a wide range of polymers. Electrospun nanofibers are broadly applied in biomedical applications, as tissue engineering scaffolds, wound healing, drug delivery, filtration, affinity membrane, immobilization of enzymes, small diameter vascular graft implants, healthcare, biotechnology, environmental engineering, defence and security, energy storage and generation and in various researches that are ongoing. In the paper published by Zucchelli at al. [42] a deep review of the application of nanofibers is presented.
Regarding the patents, approximately two-thirds of all electrospinning applications are in the medical field and of the remaining patents, one half deals with filtration applications.
Present work deals with integration of polymeric electrospun nanofibers into epoxy-based composite materials to improve delamination resistance and fracture toughness of interfaces and in the next section a review of the works already published on this topic is presented.

2.2.1. Nanofibers in composite material

This work deals with the introduction of nanofibers into epoxy-based composite laminate material following a patent owned by Dzenis and Reneker [44]. They proposed to use a nano-interlayer in the form of polymeric nanofibrous non-woven mat fabricated trough the electrospinning process into ply-to-ply interfaces of composite laminates. In their patent authors demonstrated that a fiber reinforced composite laminate with polymeric electrospun nanofibrous mats placed at one or more ply interfaces is characterized by an improved delamination resistance. Indeed, composite laminates incorporating nanofibrous reinforcements are expected to have an improved interlaminar fracture toughness, strength, and delamination resistance towards static, fatigue, and impact loadings. In particular, the nanofibrous reinforcement can be useful in suppressing and arresting delamination from any source, including matrix cracks, free edges, notches or holes, ply drops, bonded joints, bolted joints, out-of-plane loading, and so on.
It has been widely demonstrated that long fibers reinforced plastic materials are capable to carry out the reinforcing function, when they fulfil the following requirements: (a) suitable mechanical properties in terms of strength and stiffness with respect to the matrix; (b) large aspect ratio; (c) high surface area to volume ratio; (d) good fiber-matrix adhesion; (e) good dispersion and embedding in the polymer matrix; (f) proper orientation with respect to the applied external load. Since it is expected that nanofibers may have the potentiality to greatly satisfy all the above listed characteristics, it can be easily understood the engineering idea to use nanofibers to fabricate high-performance FRP composite structures, with further enhanced structural properties, is attracting growing interest nowadays. In terms of fiber mechanical properties, going from micro- down to nano-dimensions, fibers are expected to show an improved elastic modulus and strength at break, thanks to their internal structure consisting of highly aligned macromolecular chains, especially in the case of fibers fabricated through spinning technologies. In addition, the greater the fiber diameter, the greater the probability to find a high density of flaws along fiber section, which are responsible of reducing fiber strength.
The main function of nanofibers is to reduce the stress concentration due to mismatch of ply properties and to bond adjacent plies, without a reduction of in-plane properties and without increasing either the composite weight or the laminate thickness. Nanofibers can be small enough to reinforce regions of the matrix located in between adjacent plies of the laminate [45]. In addition, incorporating in laminated composites an entangled nanofiber layer, characterized by a combination of interlocked in-plane and out-of-plane nanofibers, might improve interlaminar fracture resistance, much like the "hooks and loops" in Velcro [5]. Following the pioneer idea of Dzenis and Reneker, other researchers have been investigated the use of electrospun polymeric nanofibers to enhance the mechanical performances of laminated composites. However, at present only few papers are available in the literature.
The term "electrospinning" was introduced in 1994 but only few years later researches started to focus their attention into this new technology [46]. The first interesting papers are dated 1999 [45] and 2001 [6]. For the first time a deep investigations on the electrospinning process and its potentiality were performed. Kim et al. [45] performed mechanical test under Mode I frac-

Figure 2.5: nanocomposites structure [5].

ture mechanics conditions incorporating Poly-Benzimidazole (PBI) electrospun nanofibers into brittle epoxy resin and Styrene-Butadiene Rubber (SBR) and attested significant improvement in the mechanical parameter they investigated (Young's module, K_{IC}, and G_{IC}) for nanomodified specimens, in particular concerning the rubber. Koombhongse [6] explored how many cross-sectional shape of nanofibers it is possible to manufacture by the electrospinning technique: branched fibers, flat ribbons, ribbons with other shapes, and fibers that were split longitudinally from larger fibers were produced (Figure 2.8). The work was interesting because it experimented the use of a large number of polymers, such as Poly(2-hydroxyethyl methacrylate) (HEMA), Polystirene (PS), Poly(vinylidene fluoride) (PVDF) and Poly(ether imide) (Ultem® 1000).

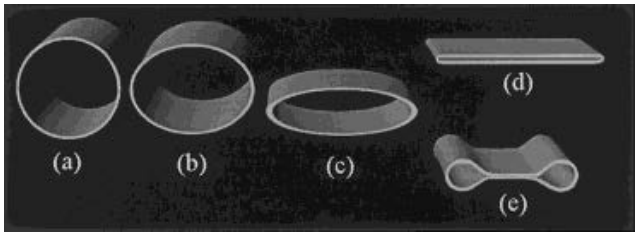

(a) Collapse of the skin on a jet.

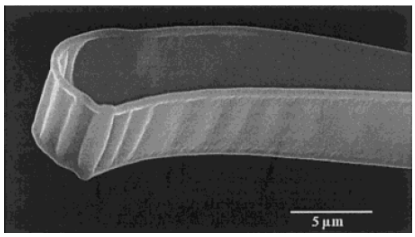

(b) Ribbons from 10% poly(ether imide) in hexafluoro-2-propano.

Figure 2.6: Nanofibers cross-section shapes[6].

In 2003 Finnegan et al. [47] and Wu [48] in his PhD thesis with professor Dzenis explored the use of two different material for manufacturing nanofibers through electrospinning: Carbon and PolyAcryloNitrile (PAN) respectively. Finnegan manufactured their carbon nanofibers through the vapour-grown technique and investigated the damping of carbon nanofiber/polypropylene composites. They

performed experiments by a Dynamic Mechanical Thermal Analysis (DMTA) and built an analytical model able to predict the damping of the structure. With their experiments they have found that composites having very low fiber aspect ratios (I/d) should have higher damping than those having high fiber aspect ratios, and that the carbon nanofiber aspect ratios of approximately 19 are in the range which yields the highest predicted damping. They also concluded that the storage and loss moduli and damping loss factor are proportional to the fiber aspect ratio. From this paper, many researchers started to deal with carbon nanofibers: some works performed mechanical tests on epoxy matrix enriched with random aligned carbon nanofibers [49–52], while others interleaved nanofibers among carbon- [53–55] or glass- [56] reinforced epoxy matrix.
Lee et al. [49] considered two sets of nanocomposites: an acrylic acid-coated carbon nanofiber-reinforced epoxy and polystyrene-coated carbon nanofiber-reinforced polystyrene composites. Carbon nanofibers were coated with polyacrylic acid or polystyrene using a plasma polymerization process. The aim was to investigate mechanical properties such elastic modulus via tensile and indentation tests. Both the techniques showed the similar trend with carbon nanofiber content: the elastic modulus increases until the carbon nanofiber content reaches the 3 wt%, and then a rapid decrement is registered further increasing the carbon content. Zhou et al. [50] confirmed the results and performed tensile, fatigue and fracture tests on unfilled, 1wt.%, 2wt.% and 3wt.% of Carbon Nano Fibers (CNF) filled SC-15 epoxy to identify the effect of adding CNF on the mechanical properties of epoxy. Their results were found to be similar to those obtained by Lee since they found an optimum value for the nanofiber content: the highest improvement in strength was obtained with 2wt.% loading of CNF. Moreover the tensile and flexural strengths improved by 11 and 22.3%, respectively, compared to the composite without CNF. The fatigue strength was also improved significantly.
Among the works that use carbon nanofiber to reinforce a glass- or carbon-fiber reinforced plastic, Bortz et al. [55] investigated fatigue performance and constant life diagrams of hierarchical carbon fiber/nanofiber epoxy composites. Authors reported the results of an extensive multi-stress ratio experimental study on the axial fatigue behavior of an all-carbon hierarchical composite laminate, in which carbon nanofibers (CNFs) are utilized along-side traditional micron-sized carbon fibers. Their results indicate that the CNF-reinforced composites collectively possess improved fatigue and static properties over their unmodified counterparts. Large mean lifetime improvements of 150-670% were observed in fully compressive, tensile and tensile dominated loadings. They attributed the enhancements to the high interface density and the damage shielding effect of the CNFs within the matrix. These results highlight the ability of a nanometer-sized reinforcing phase to actively participate and enhance matrix properties while moving toward a cost effective alternative to current material solutions.
Arai et al. [54] performed Mode I and Mode II fracture mechanics tests on carbon fiber/epoxy laminates toughened by a carbon nanofiber/epoxy interlayer by standard DCB and ENF tests. Experimental results of the DCB tests confirm that mode I interlaminar fracture toughness for hybrid laminates is about 50% greater than the base laminates. Furthermore, the results of the mode II fracture toughness tests confirm that the interlaminar fracture toughness for hybrid laminates is 2-3 times greater than base CFRP. An interesting result regards the fact that authors recommended a range of CNF interlayer thickness between 100

and 150 μm (approximately $20 g/m^2$ carbon nanofiber area density), confirming the fact that there exists an optimum value in adding nanofibers into interlayers of composite laminate. Sadeghian and their research group [56] interleaved carbon nanofibers into polyester/glass fiber composite to improve its interlaminar fracture properties. Surfactant-treated CNF were dispersed in polyester resin and then the CNF-resin suspension was infused to impregnate a glass fiber preform using Vacuum Assisted Resin Transfer Moulding (VARTM) process. The critical energy release rates of Mode I delamination (G_{IC}) were characterized for several composite specimens with 1 wt% CNF concentrations and for those with pure resin. Significant improvement in the G_{IC} was consistently observed as 1 wt.% CNF were added to toughen the polyester resin.
In 2007 two researchers, Jana [57] and Zhamu [58] investigated reactive graphitic nanofiber interleaved into epoxy matrix and performing flexural and DMTA tests. They tested composites with different amount of graphitic nanofibers and have found the best results with a content of 0.3wt.% of nanofiller, which is around 1/10 of what other researchers have found by using carbon nanofibers. Carbon and carbon-derived nanofibers and nanotube are proved to be probably the best nanofiber-reinforce for composite laminates but at the same time they present some risks for health if not managed with care [59, 60]. Then, because of this, the great part of the literature is focused of polymeric nanofibers, and most of them are manufactured by electrospinning. First works with electrospun nanofibers dealt with Policarbonate (PC). Moon [61] in his work presents a full investigation on the properties of PC nanofibers providing useful information about the process parameters (§2.1.1) and detected that the mechanical properties were dependent upon the fiber morphology. Sinh et al. [62] laid up laminates with and without the nano-interlayers in a proper stacking sequence and tested them under uniaxial tensile loading. They have found that first-ply-failure and delamination stresses, and ultimate strength increase 8.4%, 8.1% and 9.8% respectively with the addition of the nano-interlayers as compared with the pristine specimens. Furthermore the number of microcracks at the delamination stress decrease significantly by 21.6% with the addition of the nano-interlayers. In 2008 Li et al. [7, 63] investigated the properties of polysulfone (PSF) which is particularly interesting. In all the cases above it was important that during the curing process, the temperature remains lower respect to the T_G of the polymers, otherwise fibers could lost their morphology. By using polysulfone this idea is overcame. They toughened carbon fiber/epoxy composite by electrospun PSF nanofibers and compared the fracture toughness of the composite to those of composite toughened by PSF films prepared by solvent method and to those non-modified. During the laminate curing process PSF nanofibers lost their morphology and becomes spheres with uneven sizes uniformly dispersed through the interleaves of the composite. Researchers performed Mode I fracture mechanic tests and discovered a strong effect of the interleave: mode I fracture toughness of the nanofibers toughened composite was $0.869 kJ/m^2$ for 5.0 wt.% PSF nanofibers content, which was 140% and 280% higher than those of PSF films toughened and untoughened composite respectively due to the uniform distribution of PSF spheres (Figure 2.7). Such a behavior is a unique in the nanofibers-reinforced-laminate environment.
Zhang et al. [64] present an interesting discussion about the efforts to obtain optimal process parameter to electrospin Polycaprolactone (PCL), Polyvinylidene fluoride (PVDF) and Polyacrylonitrile (PAN) nanofibers. They performed Mode

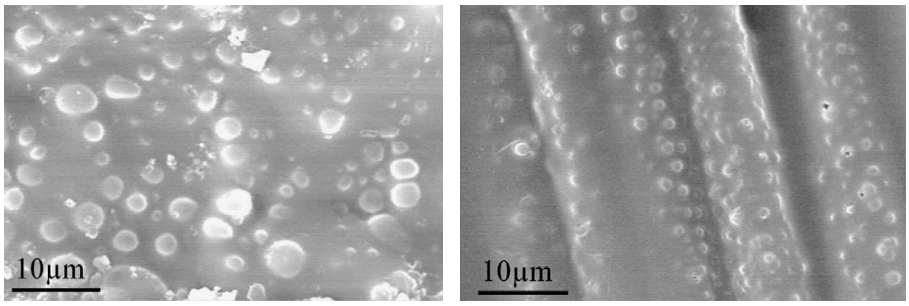

(a) Composites toughened by PSF nanofibers. (b) Composites toughened by PSF films.

Figure 2.7: SEM observations of PSF fracture surfaces [7].

I fracture mechanic and DMTA tests to determine the conditions which allow the best mechanical performances. Their findings show an optimal concentration of 15 wt.% of PCL solution for electrospinning to produce composites with enhanced mode I interlaminar fracture toughness (G_{IC}), stable crack growth and maintained flexural strength and modulus. Chen et al. [65] investigated the effect of the alignment of Polyimide (PI) nanofibers in Polyamide 6 (PA6) resin. They performed tensile tests on the PI/PA6 composite containing a 50 wt.% of aligned PI nanofibers and showed improved tensile strength and modulus around 700% and 500% respectively as compared to neat PA6. Kelkar et al. [66] electrospun tetra-ethyl-orthosilicate (TEOS) nanofibers and interleaved glass fiber/epoxy resin laminate. This paper presents two methods and material systems to process and integrate the nanomaterial constituents, namely: (a) dispersing alumina nanoparticles using high energy mixing (using ultrasonication, high shear mixing and pulverization) and (b) electrospinning technique to manufacture nanofiber. While the electrospun nanofibers provide bridging through-the-thickness reinforcement, the use of the nanoparticles influences the thermo-physical properties and provides an effective means from commercially available nanolevel material configurations to form reinforced polymer nanocomposites. Their paper discuss the experimental study of the processing and delamination (interlaminar failure) characteristics (via Mode I fracture toughness assessment) of reinforced composite systems. Another interesting polymer is the polyetherketone-cardo (PEK-C), used also to electrospun nanofibers directly deposited on carbon fabric. Zhanga [67] investigated the influences of nanofiber diameter and interlayer thickness on the Mode I delamination fracture toughness, flexure property and thermal mechanical properties of a CFRP interleaved with nanofibers. They have achieved considerably enhanced interlaminar fracture toughness with the wt. loading as low as 0.4%. Finer nanofibers result in more stable crack propagation and better mechanical performance under flexure loading. Composites modified by finer nanofibers maintained the glass transition temperature (T_G) of the cured resin and increasing nanofiber interlayer thickness improving the fracture toughness while compromising the flexure performance.
The last paper hereby presented is particularly interesting since it is the only one that deals with glass nanofibers: Chen et al. [68] have in fact electrospun glass nanofibers (EGNF) into glass microfiber/epoxy resin composite laminate.

The experimental results revealed that EGNFs substantially outperformed conventional glass fibers in both tension and impact tests, and led to the same trend of improvements in strength, stiffness, and toughness at small mass fractions of 0.5 and 1%. The tensile strength, Young's modulus, work of fracture, and impact strength of the nano-epoxy composite resins with EGNFs were improved by up to 40, 201, 67, and 363%, respectively. The study suggests that electrospun glass nanofibers can be used as reinforcement and/or toughening agent for making innovative nano-epoxy composite resins, which would be further used for the development of high-performance polymer composites
Among the researches it was also found some papers which attest that nanofibers decrease the mechanical properties of the laminate they are interleaved in [69–71].

2.2.2. Nylon 6,6

In previous paragraph a deep review of the progresses achieved with composites interleaved with nanofibers is presented. The author would focus its attention on nanofibers manufactured by electrospinning on Nylon 6,6. This polymer is particularly suitable for the purpose to reinforce epoxy interfaces, since:

- it exhibits high melting temperature, which allows the nanofibers to maintain their morphology during the curing process of the laminate (at around 130°C, Figure 3.2);
- it possesses very good mechanical characteristics (see Table 3.1), compared to other polymers;
- the cost of the raw polymer and its relative solvents (in this work Formic acid and Chloroform are used) is not so high;
- the viscosity of the solution is low enough to make the solution well processable;
- it shows good compatibility to be bonded with epoxies;
- many different molecular weights are available in the market.

Few works are published in literature concerning the use of Nylon 6,6 and the two most important ones are addressed to Shivakumar [72] and Akangah [73]. The first one performs a deep experimental campaign to prove that Nylon nanofibers interleaved into unidirectional CFRP are able to enhance dynamic properties, impact damage resistance, fracture toughness and resistance, and delamination onset life. In their work researchers performed DMA, impact and Mode I fracture mechanics tests. In DMA and Impact tests, 6 and 16 ply-laminates respectively were manufactured with nanofibers placed in all the interlayers. Mode I and fatigue tests were performed on a 20 layers specimen. By increasing the laminate thickness and weight by an order of 1%, the influence of Nylon nanofibers on the mechanical parameters investigated is substantial. Results of this study showed that nanomodified specimens exhibit an increased damping by 13%, a one-third reduced impact damage size, a 1.5 times increased fracture toughness and resistance, a significantly increase in delamination onset life, and also an increased fatigue threshold energy release rate by two-thirds.

Akangah et al. [73] investigated the same raw material of Shivakumar but they focused their attention on the impact behavior of nanofibrous-interleaved CFRP. They manufactured and impacted sixteen-ply quasi-isotropic composite laminates to assess the improvement in impact resistance by interleaving electrospun Nylon 6,6 nanofabric. The impact velocity, force, and energy ranged from 2.0 to 4.0 m/s, from 900 to 2100 N and from 0.46 to 1.80 J, respectively. Results showed that polymer nanofabric interleaving marginally increased the laminate thickness, by about 2.0%, while substantially increased the threshold impact force by about 60%, reduced the rate of impact damage growth rate to one-half with impact height and reduced impact damage growth rate from 0.115 to 0.105 mm^2/N with impact force.

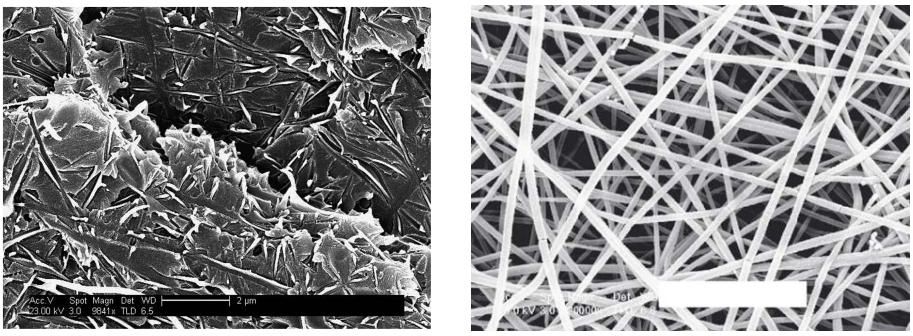

(a) SEM image of the fracture surface of the nanofabric interleaved specimen [72].

(b) SEM detail of Nylon 6,6 nanofibers [73].

Figure 2.8: SEM images of Nylon 6,6 nanofibers.

Present work attempts to make further steps from these presented papers on some aspects:

1. both Mode I and Mode II fracture mechanics tests are performed in order get a full comprehension of the delamination propagation into nanomodified interlayers;
2. acoustic emission analysis is also conducted in order to better understand the fracture propagation mechanism;
3. different configurations of nanofibers are tested in order to understand how some parameters (nanolayer thickness, nanofibers diameter and orientation) can affect the behavior of the whole laminate when loaded;
4. vibration analysis of both pre-impacted and impacted laminates (both nanomodified and non-nanomodified) are registered to verify the damage-arrest-capability of the nanointerlayers;
5. damping of the specimens are also measured before and after impacts;
6. impact experimental campaign on different configuration of laminates and with different energies is performed in order to understand how nanofibers can reduce the damaged area due to low velocity impacts.

In the next chapter the methods and procedures followed to reach the scope of the work are deeply illustrated.

3. Materials, techniques and experiments

Se c'è un modo di fare meglio,
trovalo!
T.A. Edison - inventore

In the following section a deep overview of the materials, techniques, and the experiments adopted in this work is presented.

3.1. Materials

3.1.1. Nylon 6,6 and nanofibers

Nanofibers were manufactured by means of electrospinning (§3.3.1) of Nylon 6,6 *Zytel*® E53 NC010 (Table 3.1) polymer, kindly provided by DuPont company.

Property	**Value**
Yield Stress (MPa	84
Nominal Strain at Break (%)	> 50
Yield Strain (%)	4.4
Tensile Modulus (MPa)	3000
Notched Charpy Impact Strength (kJ/m^2)	7

Table 3.1: Nylon 6,6 properties (Source: DuPont).

When electrospun and interleaved into the laminate, Nylon nanofibers exhibit a very good adhesion with both resin and matrix, as shown in Figure 3.1.
In Figure 3.1(a) a carbon microfiber surrounded by Nylon nanofiber is shown. In Figure 3.1(b), it is shown that Nylon and epoxy are very well compatible each other, since no voids between fibers and resin are shown. This is important to avoid stress concentration due to a non-complete fulfilling of the interface.

3.1.2. Prepreg

Specimens were manufactured with a 0/90 woven carbon fiber/epoxy resin prepreg (GG205PIMP503) (Table 3.2), kindly provided by Impregnatex Com-

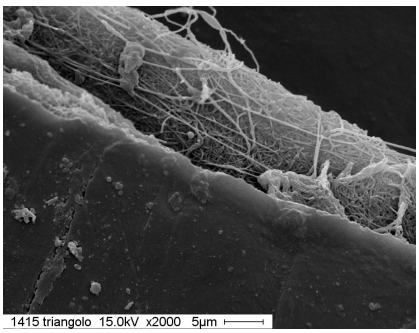

(a) Nanofibers and microfiber.

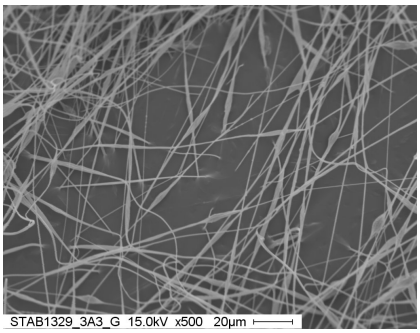

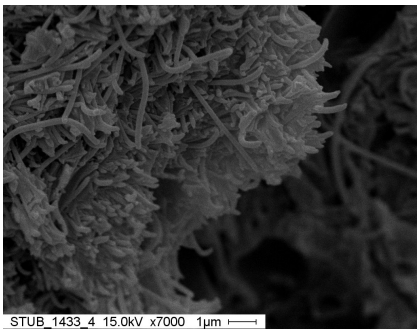

(b) Nanofibers and resin.

Figure 3.1: Nanofibers embedded into composites.

positi company (Milan, Italy). The epoxy resin was based on diglycidyl ether of bisphenol A prepolymer.

Property	**Value**	**Mech. properties**	**Value**
Density	1.5 g/cm^3	Bending resistance	850 MPa
Weight	353 g/m^2	Bending modulus	59 GPa
Resin Amount	42%	Tensile resistance	650 MPa
Post cured thickness	0.2 mm	Tensile modulus	59 GPa
T_G (DSC)	125°C	Short beam shear	65 MPa

Table 3.2: GG205IMP50 properties (Source: Impregnatex Compositi).

Panels were fabricated by hand lay-up process, stacking plies with fiber directed parallel to the laminate borders. From each lamina, many specimens were cut out, depending on the geometry requested by each test. Samples were cut from the panels using a high-speed rotating diamond disc. Nanofibers were placed into specific interfaces during the lay-up depending on the kind of test. After the lay-up, panels were cured by using a vacuum bag in autoclave according to process specifications provided by the supplier. Vacuum, pressure and temperature cycles are shown in Figure 3.2.

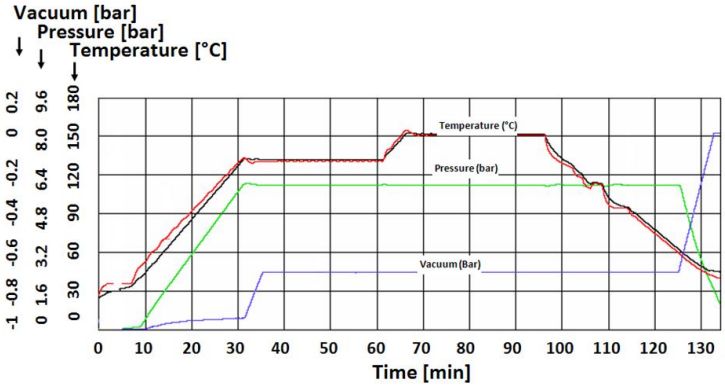

Figure 3.2: Cure-cycle in autoclave.

3.2. Specimen fabrication

3.2.1. DCB and ENF specimens

Samples for Mode I and Mode II tests were fabricated stacking twenty plies with fiber directions parallel to the laminate borders. An initial delamination is required, in the mid-thickness of the specimen, and the electrospun nanointerleave is placed in this interface. Initial delamination was provided by a $15\mu m$ thick nylon sheet placed during the lay-up process. Tests, carried out on virgin and nanomodified specimens will be detailed described on §3.4.
These experiments have the purpose to investigate two main aspects of the nanointerleaved interfaces:

1. fracture mechanics behavior. Both DCB and ENF tests mainly act on the nanomodified interfaces and researches can evaluate the effect of the nanointerleave by comparison of tests performed on virgin specimens to those performed with nanomodified ones. Delamination propagation, stiffness, energy release rate and energy absorption capability are some of the aspects that will be investigated;

2. the effect of the geometry and the morphology of the nanointerlayer. As previously introduced, the effect of three morphological parameters is investigated: nanolayer thickness, nanofibers orientation and fibers diameter:

   - nanoreinforce of 2 different thicknesses were electrospun: 25 and 50 μm. By increasing the electrospinning duration process of three times the nanolayer thickness was doubled;
   - nanoreinforce with 2 different nanofiber orientations were electrospun: random and aligned fibers. By the use of a rotating collector, and increasing its speed up to $6500rpm$ it was possible to obtain aligned nanofibers (Figures 3.3(a) and 3.3(b)). Then, oriented nanofibers will be placed in the direction of the length of the beams;
   - nanofibers with 2 different diameters were electrospun: 150 and 500 nm. Fiber diameter is mainly dependent on the concentration of the

polymer into the solution: Nylon concentrations of 14% and 25% have been used to obtain fibers with 150 and 500 nm diameter respectively (Figures 3.3(c) and 3.3(d)).

Fiber diameter distribution was determined by measuring 200 fibers per sample, with an image acquisition software (EDAX Genesis). Thus a full experimental campaign with 3 parameters and 2 factors were carried out: it leads to 8 different nanofibers configuration to manufacture and test as shown in Figure 3.3.

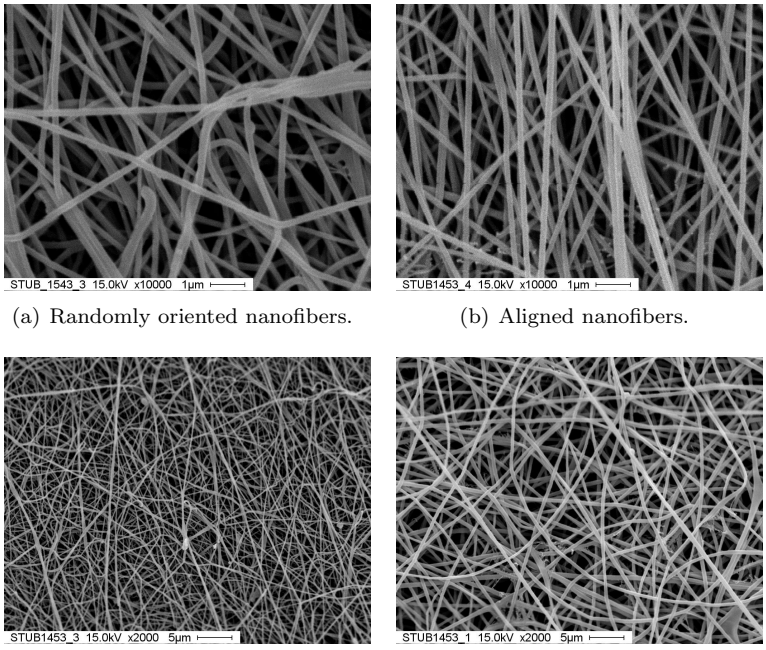

(a) Randomly oriented nanofibers.

(b) Aligned nanofibers.

(c) 150 nm diameter nanofibers.

(d) 500 nm diameter nanofibers.

Figure 3.3: Overview of the nanofiber morphologies use in this work.

Every configuration was then named, with a code formed by 4 character:

- the first two, numbers, indicate the concentration of the polymer into the solutions and they counts for the *nanofiber diameter*: if 14, the diameter is 150 nm, if 25, the diameter is 500 nm;
- the third character is a letter related with the *nanofiber orientation*: R indicates Random fibers, while O is related to oriented aligned nanofibers;
- the last one is a letter which indicates the *nanolayer thickness*: B indicates a thin film ($25\mu m$), C indicates the thicker one ($50\mu m$).

Configurations and codes are summarized in Table 3.3.
One of the most important consequence of the fiber morphology is the porosity of the nanoreinforce: the more nanoreinforce is porous, the better the resin can flow through it and the better adhesion is obtained between the layers. From the samples presented in Figure 3.3 it appears that oriented nanofibers exhibit a lower porosity with respect the random fibers; indeed, at the same

Thickness	Orientation	Diameter	Code
25 μm	Random	150 nm	14RB
		500 nm	25RB
	Aligned	150 nm	14OB
		500 nm	25OB
50 μm	Random	150 nm	14RC
		500 nm	25RC
	Aligned	150 nm	14OC
		500 nm	25OC

Table 3.3: Nanofibers configurations.

time their direction can be placed according to the expected loads and give a better contribution in the delamination assessment. In similar way, thicker nanolayers, have a larger amount of nanoreinforce, but at the same time they will make a bigger stand to the resin movement. Experiments have the purpose to find the optimum compromise between all these aspects in order to obtain the best performances from the laminate.
Moreover, an acoustic emission monitoring is performed (see §3.3.2) to better investigate the crack propagation.

3.2.2. Bump and LVI specimens

Panels were fabricated stacking ten plies with fibres parallel to laminate borders. Since this kind of test involves interlaminar properties of the whole laminates, many interfaces have been nano-addicted and two different nanomodified configurations were manufactured. The tested configurations are summarized in Figure 3.4.

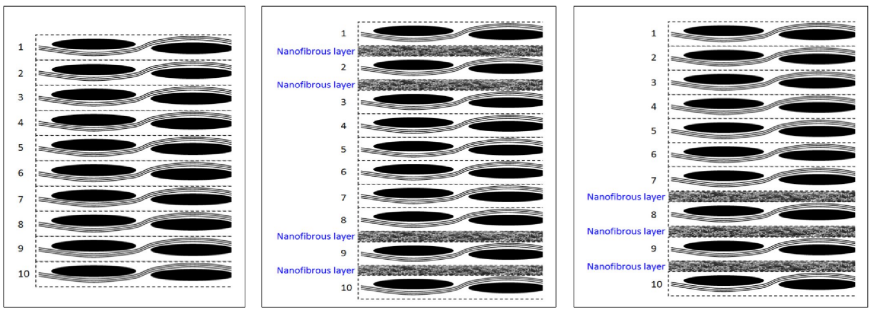

(a) Virgin configuration. (b) Nano1 configuration. (c) Nano2 configuration.

Figure 3.4: Virgin and nanomodified specimen configurations.

Configuration Nanomodified 1 (called "Nano1", Figure 3.4(b)), is symmetric while into Nanomodified 2 configuration (named "Nano2", Figure 3.4(c)), nanofibers are placed in the lower interfaces. This latter is manufactured since in low velocity impact in thin specimens, delamination cone starts from the impacted side and goes larger through the thickness down to the other [74]: in this configuration, nanofibers are placed where bigger delamination is expected,

with the purpose to better evaluate their reinforce effect. The nanolayer used in this specimens is the one that better improve the performances of the laminate, determined through the process illustrated is §4.1. After the lay-up, panels were cured in autoclave according to process specifications provided by the supplier. Final thickness was 2.27 ± 0.13 mm. All the specimens are manufactured at the same production batch. Presence of nanofibers did not cause significant increase in thickness.

3.3. Techniques

3.3.1. Electrospinning process

The polymer used for the experiments was the Nylon 6,6 Zytel®E53 NC010 kindly provided by DuPont company, dissolved in a solution made of Formic Acid and Chloroform (50:50 v/v) purchased by Sigma Aldrich, used without further purification. Polymer was dissolved at a concentration of 14% w/v. Electrospun non-woven mats were fabricated by using a SPINBOW S.r.l. electrospinning semi-automatic machine (Figures 3.5(a) and 3.5(b)), composed of a high voltage power supply, a double syringe pump, two chambers containing the polymeric solution (each one equipped with four stainless-steel blunt-ended needles and connected with the power supply electrode) and a grounded plane collector positioned 10cm away from the tip of the needles. The electrospinning process was carried out under the following conditions: applied voltage 22-26 kV, feed rate 0.3mL/h per nozzle, at room temperature and relative humidity RH = 40÷50%. Electrospun non woven mats (Figures 3.5(c) and 3.5(d)) were 25± 8 μm thick and kept under vacuum at room temperature overnight to remove residual solvents before the lay-up inside laminates. Thermal properties of Nylon 6,6 electrospun mat were investigated by means of differential scanning calorimetry (DSC) using a TA Instruments Q100 DSC equipped with the LNCS low-temperature accessory. Nanofibers show excellent impregnation to epoxy matrix and they are characterized by a high-melting crystal phase (Tm = 262°C, ΔH_m = 65J/g, by DSC). Therefore prepreg curing treatment (at temperature of 130°C) is below the Nylon 6,6 melting temperature: autoclave process does not cause any modification at mat shape or fiber morphology.

3.3.2. Acoustic Emission

Acoustic emission (AE) technique was used in order to monitor the material damage onset and progression during the quasi-static tests DCB and ENF. Acoustic emission data acquisition system (PAC) PCI-2 with a maximum sampling rate of 40MHz was used to record AE events. A broadband, resonant-type, single-crystal piezoelectric transducer from Physical Acoustics Corporation (PAC), called PAC R15, was used as the AE sensor. The surface of the sensor was covered with grease in order to provide good acoustic coupling between the specimen and the sensor. The signal was detected by the sensor and enhanced by a PAC pre-amplifier. The gain selector of the pre-amplifier was set to 40dB. The test sampling rate was 10MHz. Prior to the damage check, the data acquisition system was calibrated for each kind of specimen, according to a pencil lead break procedure. The pencil lead break procedure enables the generation of waves at the specimen surface that were used for device calibration.

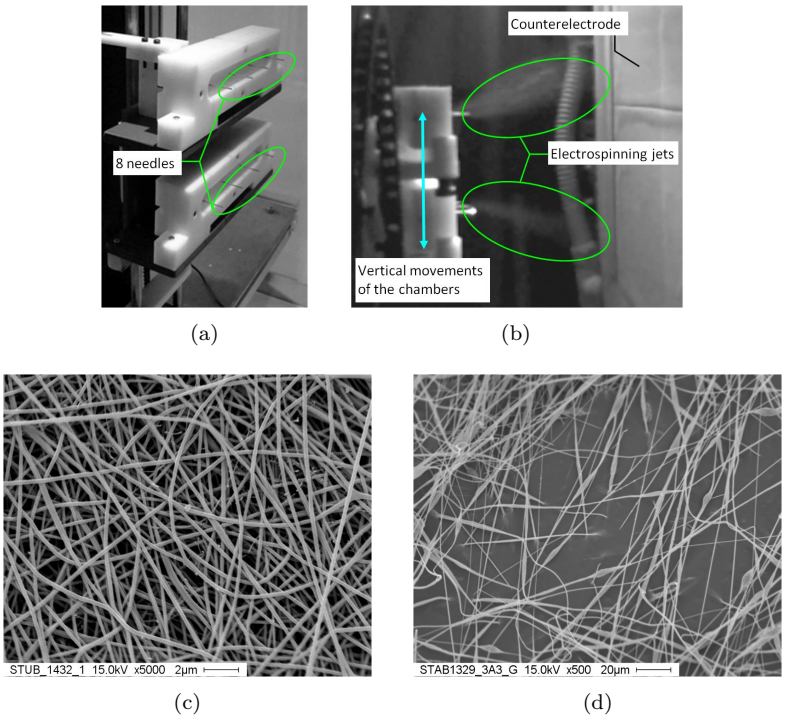

(a) (b)

(c) (d)

Figure 3.5: *a*): detail of the electrospinning machine; *b*) electrospining process; *c*) nanofibrous mat; *d*) nanofibers into the resin.

At the same time, the velocity and attenuation of the AE waves were measured. After the calibration step, AE signals were recorded during mechanical testing. The AE data analysis were performed by a parametric approach, considering the main AE events features (hits, counts, amplitude, frequency and energy) and in particular the AE events energy was used for a detailed discussion of test results. Moreover, an advanced and novel function, called sentry function, was used in order to have a deeper understanding of results. The sentry function is based on the idea that during the loading process a material is able to store strain energy and, at the same time, part of the stored energy is released due to internal failures. The AE events energy represents an important part of the released energy and can be used to weight the strain energy storing capability of the material. As greater is the damage due to internal failure as the cumulated AE increases and, at the same time, the strain energy storing attitude is reduced. The proposed function thus compares the mechanical energy stored in the material (E_s) to the released energy in the form of acoustic energy (E_a) by using their ratio (E_s/E_a). It was proved that the best way to represent such a ratio is to consider its natural logarithm ($Ln(E_s/E_a)$)) [75], that is referred as sentry function. It was also experimentally seen that the integral of the sentry function, over the AE domain, is directly related to the material damage, and to the delamination strength of composite materials. Because of its characteristics, the sentry function has been successfully applied to study the damage progression of some composite laminates [75], to estimate the static and the

fatigue residual strength of composite plates subjected to indentation processes [75–77], and to estimate the residual torsional strength of a composite laminate tubes subjected to a lateral impact [78]. Moreover the sentry function has been also used to detect the initiation of the delamination [79] and to estimate the G_{IC} [80] in composite laminate materials.

3.4. Experiments

Mechanical tests were performed to assess the effect of the nano-interleaves on the mechanical behaviour of CFRP laminates. Static DCB and ENF tests were performed on laminates interleaved with different configuration of nanofibers, in order to optimize the nanoreinforce. With the obtained configuration of nanofibrous mats, rectangular panels were then manufactured for dynamic tests. Prior the dynamic tests, flexural static tests were performed on cantilevered panels in order to collect direct information about their stiffness. Following, vibration experiments were performed on the same cantilevered panels and the first harmonic frequencies were extracted to measure the stiffness of the materials before and after the impact, for the virgin and the nano-modified configurations. For each tests many panels were manufactured and the results for each one are given in terms of the averages and standard deviations.

3.4.1. Double Cantilever Beam test

Mode I fracture test was performed according to ASTM D5528 [81]: 20 plies, 130mm x 20mm x 4mm laminate Double Cantilever Beam (DCB) specimens were manufactured as shown in Figure 3.6(a). Initial delamination was provided by Teflon sheet, 25 mm in length, that was placed in the mid-interface at one of the edges of the specimens.

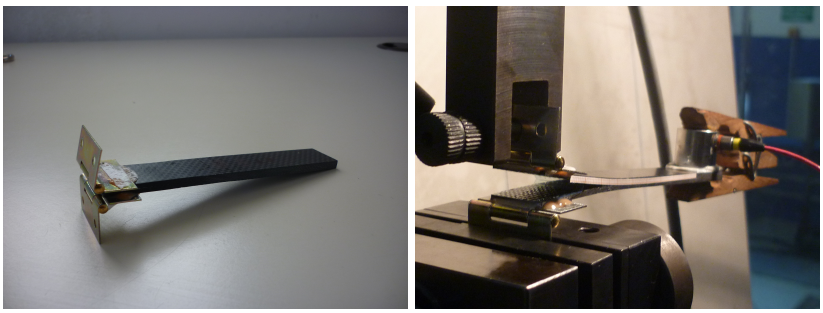

(a) DCB specimsn. (b) DCB test.

Figure 3.6: DCB.

Experimental tests were performed under displacement control condition at constant crosshead rate of 1.5mm/min in a servo-hydraulic universal testing machine Instron 8033 (Figure 3.6(b)) with a force capacity in the range 5-250 kN. Load and crosshead displacement were recorded 10 times per second during the test, while crack length was measured by visual inspection. Energy release rate for Mode I fracture testing is given by the Mixed Mode Theory presented in the

ASTM standard:

$$G_{IC} = \frac{3P\delta}{2b(a + |\Delta|)} \cdot \frac{F}{N} \tag{3.1}$$

where: P and δ are applied load and opening displacement respectively, b and a are the specimen width and crack length respectively, Δ is determined experimentally by generating a least squares plot of the cube root of compliance as a function of a; F and N are correction factors needed in order to account for the presence of the end hinges and large opening displacement.
According to the theory of linear fracture mechanics, fracture toughness G_{IC} for the crack extension can be obtained by substituting to P, in Equation 3.1, the critical load P_C which is the maximum load when the delamination extends from the initial point, and its relative a_C. Nanomodified specimens had a nanofibrous sheet placed in the opening inter-face. From the force history maximum load, absorbed energy and G_{IC} were determined for each specimen, for both the conditions, nanomodified ad non-nanomodified, and compared.
For each configuration, 5 specimens were tested, and the results are given by the average of all the tests.

3.4.2. End Notched Flexure test

The End Notched Flexure (ENF) test (Figure 3.7) is widely used for experimental evaluation of resistance to in-plane shear stress and it load the interested surface in Mode II fracture mechanism. This is a three point bending test where the specimens are characterized by an initial delamination. The latter is 25 mm long, provided by a 15μm thick Teflon sheet placed in between the 10^{th} and 11^{th} ply, i.e. the region where the shear stress reaches its maximum. Specimens were 20 plies, 160mm long, 20mm wide and 4mm thick and the support spam was 100mm. Tests were performed under controlled displacement condition with 1.5mm/min constant crosshead rate; acquisition frequency was 10Hz. Nanomodified specimens had a nanofibrous sheet placed in the mid-thickness, into the delaminated surface, like in the DCB case. Maximum tension, flexural modulus and absorbed energy were determined for each specimen, both nanomodified and non-nanomodified configurations and compared.

Figure 3.7: ENF Tests.

Stress (σ), Strain (ϵ) and Flexural Modulus (E^{flex}) were calculated for each

test using the international standard ASTM 7246 [82]:

$$\sigma = \frac{3}{2}\frac{PL}{bh^2} \qquad \epsilon = \frac{6\delta h}{L^2} \qquad E^{flex} = \frac{L^3 m}{4bh^3} \tag{3.2}$$

where P and δ are applied load and opening displacement respectively, L, b and h are the specimen length, width and thickness respectively, m is the slope of the secant of the force-deflection curve.
Energy absorption was also calculated for each tests. For each configuration, 5 specimens were tested, and the results are given by the average of all the tests.

3.4.3. Flexural test

For those panels subjected to impact and vibration tests, flexural stiffness was preliminary measured. Plate-shape laminates were cantilevered in one edge and subjected to a quasi-static load (Figure 3.8(b)), while two strain gauges (Vishay Micro-Measurement N2A-13-T004R-350) measured the longitudinal deformation of the external skin (Figure 3.8(a)). The flexural tests measured the deflection of the plates under a known load to evaluate the bending stiffness. It was performed before and after the impact. The experiment was performed 5 times per specimen and the results is given in terms of the average of all the tests for each configuration. Due to the fact that nanomodified 2 panels have a non-symmetric placement of nanoreinforce, two flexural tests were done: one by placing under tension the nanomodified side and the other by placing the same side under compression.

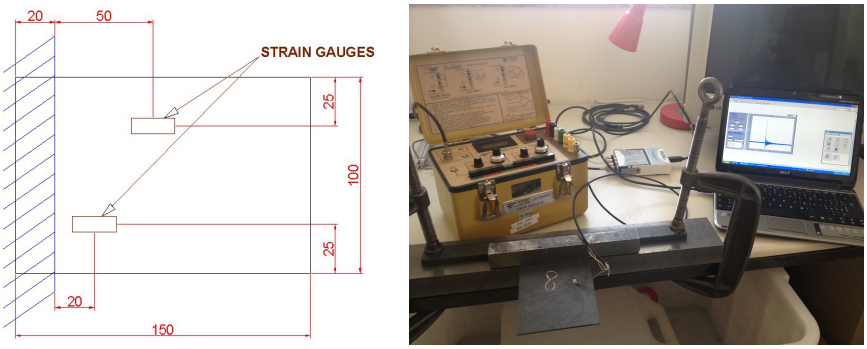

(a) Flexural test.

(b) Bump test equipment.

Figure 3.8: Flexural and bump tests configuration.

3.4.4. Dynamic/vibration testss

Free decay vibration tests were carried out under one edge cantilever condition as presented in §3.4.3. External excitation was provided by a steel hammer, after which the free vibration response of the plates was measured by the two strain gauges. The natural frequencies of the plate were determined using the Discrete Fourier Transform. The damping ratio ξ was calculated for the first mode by a logarithmic decrement method [83]. The test was repeated three

times each configuration. The measurement chain consisted of a strain gauge powered by a P-3550 Strain Indicator; the signal was then digitalized by an analogical-to-digital acquisition device (NI9215). The signal was acquired in a personal computer by a Labview executable program (Figure 3.9). A sampling frequency of 10 kHz and 6 seconds of acquisition time were chosen. Test was performed 5 times per specimen and the results are given in terms of the average of all the tests for each configuration.

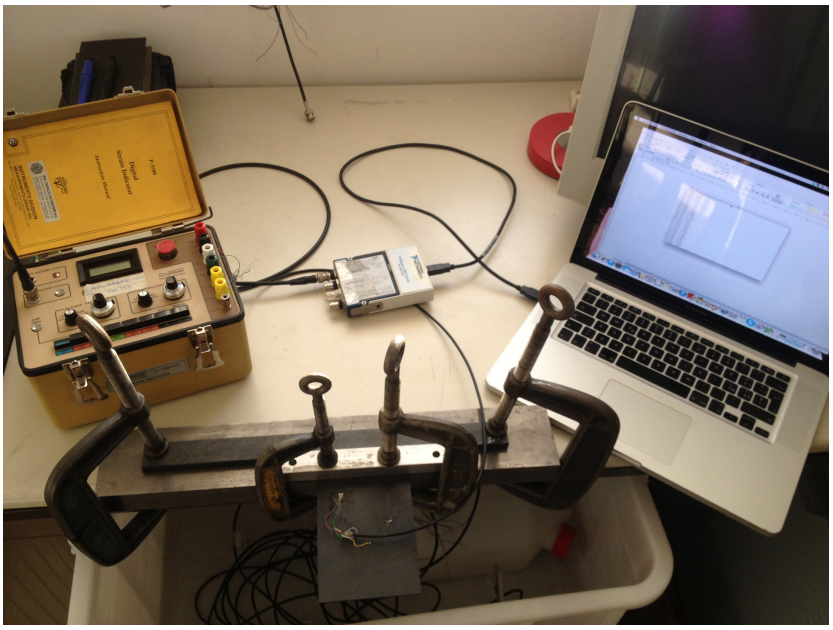

Figure 3.9: Measure chain for bump tests.

3.4.5. LVI TESTS

LVI tests were carried out in a drop-weight machine (Figure 3.10(a)) equipped with a laser device to determine the position of the impactor and with a piezoelectric load cell inside the tip of the impactor which measured contact force history. The load cell was equipped with a hemispherical 12.7mm diameter head, the impactor mass was 1.22 $\pm$ 0.01 kg. Multiple collisions were avoided by means of an electromagnetic braking system. The load cell was switched on 30 minutes before the tests to ensure the full charge of piezoelectric. A detailed description of the machine can be found in [84]. Three different drop heights of 0.25, 0.5 and 1 m were chosen, corresponding to a nominal potential energy of 3, 6, and 12 J respectively. Three specimens were tested for each energy level. The laminates were placed in a clamping fixture of four rubber pins as shown in Figure 3.10(b).
Data acquisition was made using the same NI9215 acquisition devices that were used for bump tests. Load cell and laser signals were acquired at the sampling frequency of 100kHz without any filtering except the intrinsic one due to the measurement chain. The maximum force during impact and absorbed energy were the two parameters chosen to measure in order to investigate the nano-

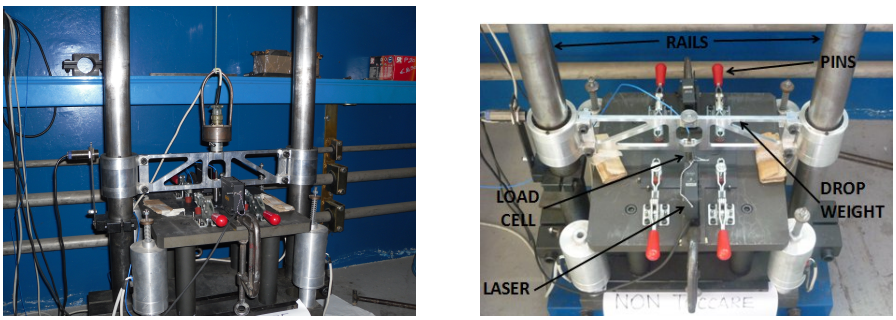

(a) Drop weight machine. (b) Specimen constrain.

Figure 3.10: Impact tests equipment.

layers effect. Peak forces were directly determined by the load cell, absorbed energies are calculated by the integration of the force-displacement curves and the rebound velocities were determined by the derivation of laser signals.

In the next chapter experimental results are presented and deeply discussed.

4. Results and discussion

One more thing...
S. Jobs - imprenditore

4.1. Effect of the nanolayer architecture

As introduced in §3.2.1, fracture mechanic tests have two main purposes:

1. evaluate the effect of the nanointerleaves by comparison of the tests performed on virgin and nanomodified specimens;
2. understand the effect of the architecture of the nanointerlayers on the mechanical behavior of the laminates.

In Figure 4.1 there are presented SEM images of fractured nanomodified surface.

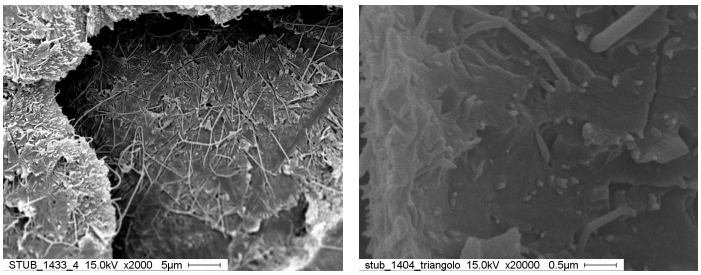

(a) Well-cured anomodified surface.

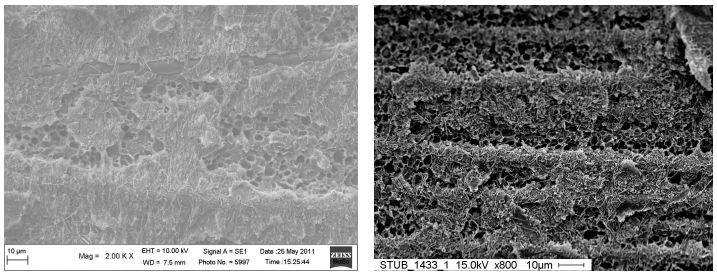

(b) Residual voids into nanomodified interface.

Figure 4.1: Fracture nanomodified surfaces.

In Figures 4.1(a) it is possible to observe how no voids or bubble are present in between the matrix or in the nanofiber-matrix interface. It means that during the curing process, the resin flowed correctly in the interface and was able to permeate the nanofibers fulfilling all the voids. In this way the interface is totally covered with resin, ensuring the best adhesion and mechanical properties. Figures 4.1(b) are related to an interface nanomodified with aligned nanofibers. It clearly appears how the amount of voids is significantly increased with respect those in Figures 4.1(a). As it is possible to observe also from Figures 3.3(a) and 3.3(b), aligned nanofibers present themselves more compact and with a lower grade of porosity. It leads to the risk that interface presents higher grade of voids respect to interface with random nanofibers and higher porosity.
In a similar manner, thickness of nanolayers influences the permeability of the interface. Increasing the thickness of nanoreinforce leads to two opposite effects:

1. decreasing of the permeability of the interface, since the resin finds more difficult flowing through the nanofibers;

2. increasing of the reinforce capability due to the greater amount of nanofibers.

Similar consideration can be also done for the diameter of the fibers.
From all these consideration the importance of a correct optimization of the architecture of the nanoreinforce is enhanced. Designers who want to introduce nanofibers into their composite must take care of these aspects, and this work intents to give a useful tool to choose the proper reinforce.
For this purpose, 8 configurations of nanomodified specimens were tested (Table 3.3) together with the virgin one under Mode I and Mode II fracture mechanic loading conditions. As described in §3.4 5 specimens were manufactured and tested for each configuration and the results are given by the average of the results of each experiment. To better understand the graphs, Figures below only show the most representative curve of each configuration.

4.1.1. DCB result overview

From DCB tests, force-displacement curves were recorded and are presented in Figure 4.2.

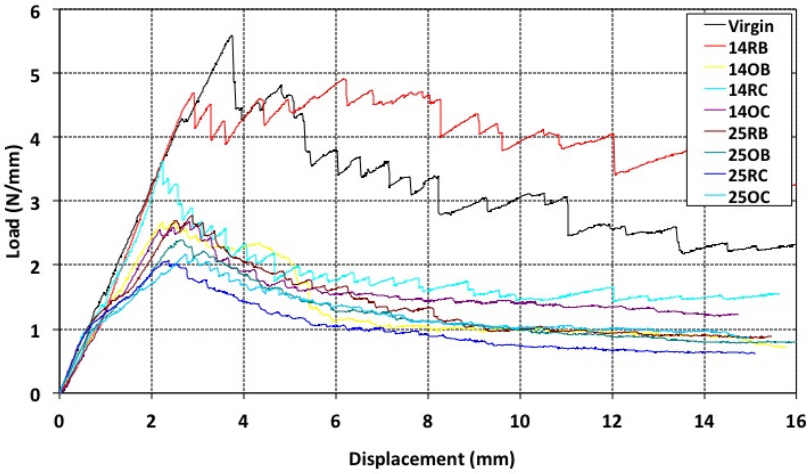

Figure 4.2: DCB tests. Black lines refer the virgin specimens.

Black line is related to the virgin interfaces and each colour represent a different configuration of nanomodified interfaces, as illustrate in the key. From a first view it clearly appears that nanofibers interleaved into delaminated interface strongly influence the mechanical behavior and the performances of the samples. In particular, it is enhanced the importance of an accurate optimization of the nanoreinforce architecture, since in many configurations it may weak the interface. For each tests mechanical parameters were used for the comparative analysis, and in particular, for DCB tests, maximum force and absorbed energy were calculated. Results are shown in Table 4.1 and Figure 4.3.

	F_{max} (N/mm)		E_{nergy} (J/m)	
	μ	$\sigma/\mu\%$	μ	$\sigma/\mu\%$
Virgin	5.61	1.72	45.55	2.54
14RB	4.92	3.34	55.29	8.39
25RB	2.79	7.38	25.20	5.91
14OB	2.68	7.90	19.60	2.85
25OB	2.41	1.44	17.33	4.57
14RC	3.63	0.59	26.05	1.63
25RC	2.08	12.90	14.97	8.78
14OC	2.70	15.26	22.50	17.86
25OC	2.18	7.23	18.26	7.52

Table 4.1: DCB mechanical results. Energy absorbed was calculated at 14 mm of displacement.

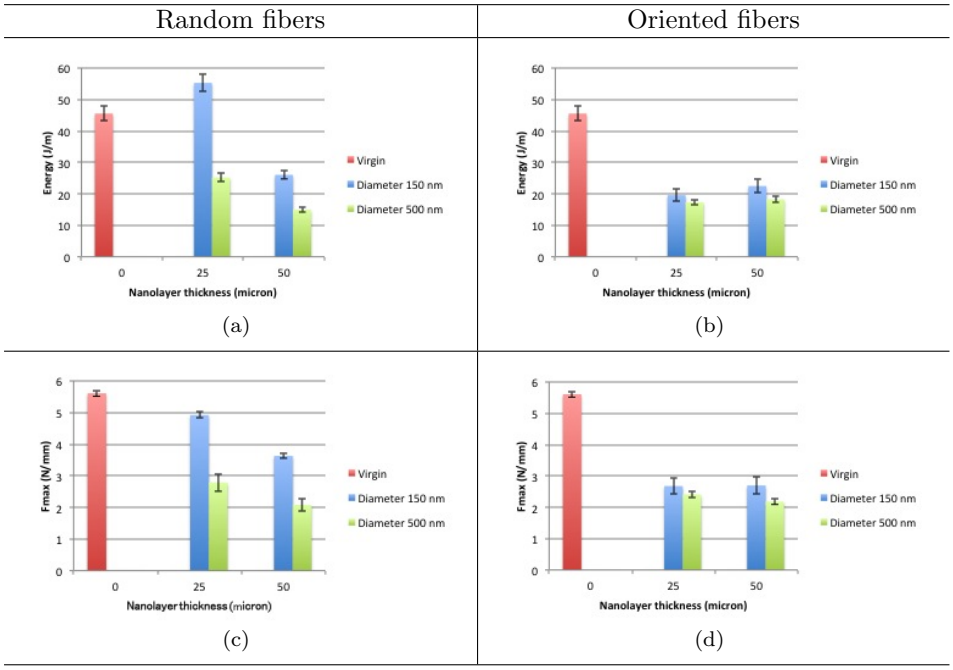

Figure 4.3: DCB mechanical result summary.

In contrast with literature results, Nylon nanofibers do not seem to able to mitigate delamination propagation in Mode I conditions, in the range of the nanolayer parameters here considered. Improvements are only registered with $150nm$ diameter nanofibers, thin layer, randomly oriented fibers (14RB configuration, Figure 4.2). In §4.2 this case will be deeper investigated. Figure 4.3 confirms that nanolayers lead to weaker interfaces for all the configurations but the 14RB. It is probably due to the low permeability of the resin through the thickness of the nanoreinforce which left voids into the cured laminates, weakening the interfaces.

4.1.2. ENF result overview

Black line is related to the virgin interfaces and each colour represent a diferent configuration of nanomodified interfaces, as illustrate in the key. From each ENF test force-displacement history was recorded, and by the formula introduced in Equations 3.4.2, stress and strain were calculated and plotted in Figure 4.4.

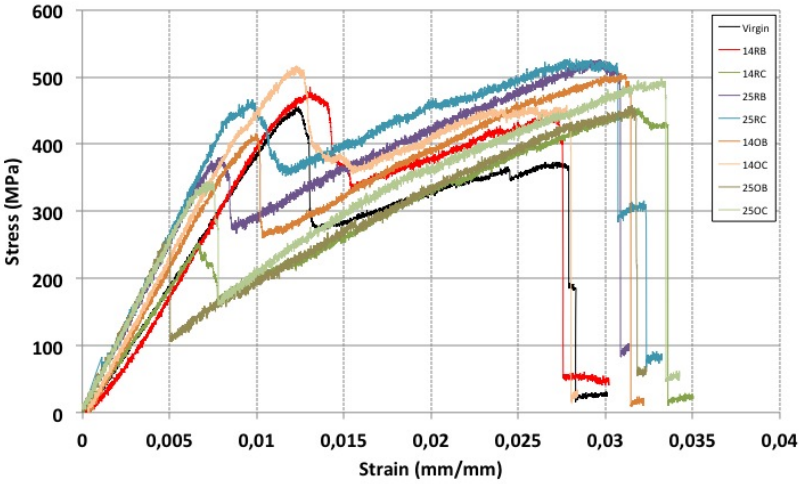

Figure 4.4: ENF tests. Black lines refer the virgin specimens.

Figure 4.4 present a different situation with respect those found with Mode I tests. Mode II experiments reveal the benefits of introducing nanofibers, for almost all the configurations. For all the test, an increasing strain-to-failure is registered, and in many configurations mechanical performances of the laminates are improved. From ENF tests, absorbed energy, stiffness and maximum tension (σ_{max}) were calculated and reported in Table 4.2 and Figure 4.5.

	E_{nergy} (J/cm^3)		$S_{tiffness}$ (GPa)		σ_{max} (MPa)	
	μ	$\sigma/\mu\%$	μ	$\sigma/\mu\%$	μ	$\sigma/\mu\%$
Virgin	7.30	9.76	42.34	3.56	459	6.55
14RB	7.87	4.06	45.05	2.30	504	2.00
25RB	6.42	3.92	51.36	0.70	347	0.17
14OB	6.28	7.14	46.56	1.79	333	21.75
25OB	5.21	4.53	52.20	0.41	256	5.77
14RC	5.87	1.79	38.82	3.44	287	10.63
25RC	6.64	11.00	52.21	1.85	424	8.84
14OC	7.60	4.29	48.19	1.52	507	3.08
25OC	5.67	1.23	50.54	0.57	323	8.44

Table 4.2: ENF mechanical results. Energy absorbed was calculated at 11.4 mm of displacement.

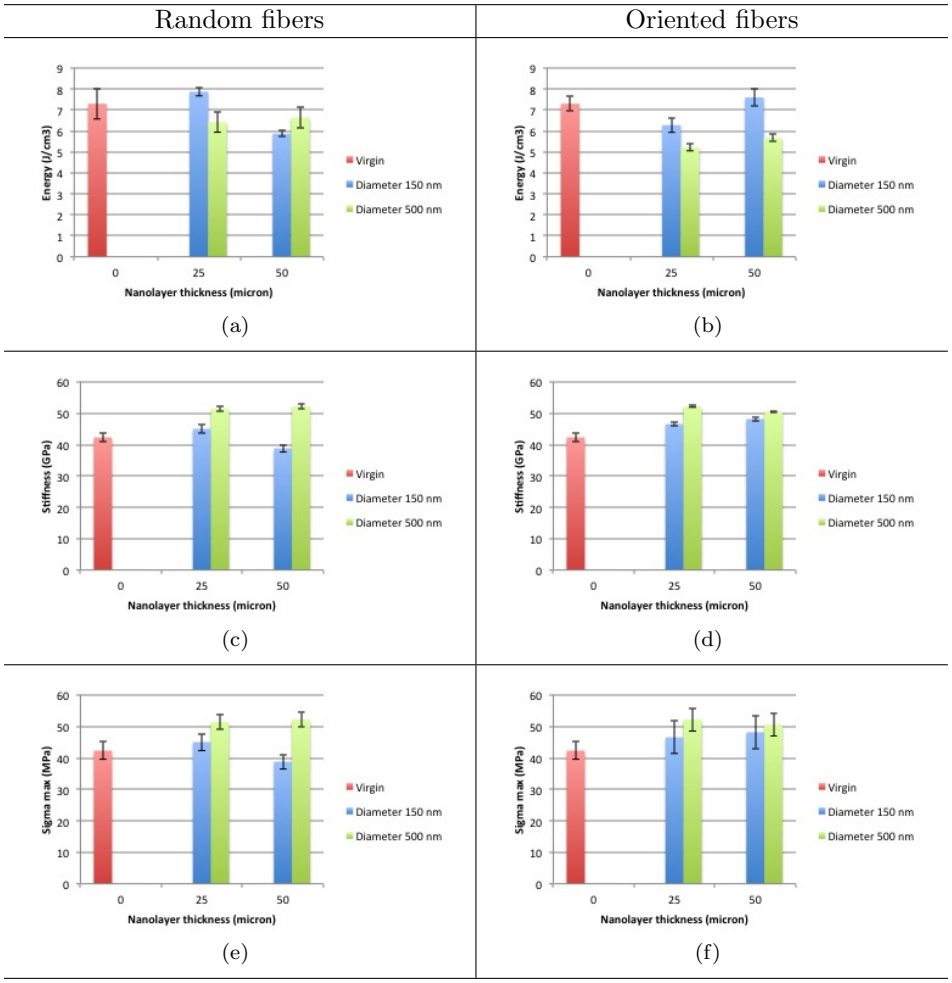

Figure 4.5: ENF mechanical result summary.

From an overview of the table and the graphs proposed, an increasing in the maximum tension after first fail is registered for all the configurations. The different behavior observed with respect the Mode I samples lies on the direction of the loads. In DCB tests load is perpendicular to the nanomodified interface plane and the weakening effect caused by the void left in the resin is prominent respect to the reinforce effect of the fibers. In Mode II, the solicitation induced in the nanomodified interface is in shear-mode and the nanoreinforce effect of the fibers overcome the lack in resin into the interface.
In the next paragraphs a detailed analysis of the results is presented. The effect of three morphology parameters will be separately discussed in order to give a full comprehension of all the aspects of the phenomena.

4.1.3. Influence of nanolayer thickness

In this section the effect of nanolayer thickness is considered: Figures 4.6 and 4.7, enhance the effect of nanolayer thickness in the tests. Figure 4.6 presents the load-displacement curves for DCB tests.

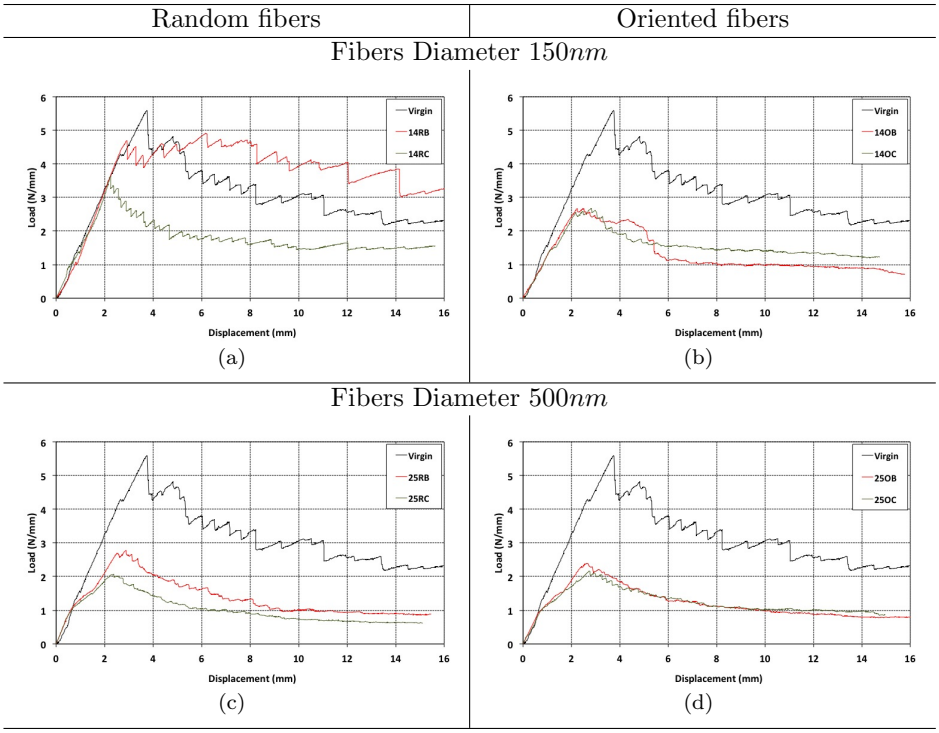

Figure 4.6: Thickness effect in DCB tests. Blue lines: virgin specimens - Red lines: 25μm layer - Green line: 50μm layer.

Experiments show that for non oriented fibers (graphs in Figures 4.3(a) and 4.3(c), and curves in 4.6(a) and 4.6(c)) it clearly appears that the thicker is the nanoreinforce, the lower are the energy absorbed and the peak force.
For the oriented fibers (Figures 4.3(b) and 4.3(d)) no particular effect can be recorded, since the two mechanical properties appear to be very similar for both the thicknesses.
Thus it is possible to state that, among the range of thickness hereby used, that thinner reinforce are more suitable to reinforce an interface subjected to a Mode I load.
Figure 4.7 collects the stress-strain curves from ENF tests.
Paying attention on the effect of the thickness of the nanoreinforce, Figure 4.5 gives some important informations. Absorbed energies diagrams (Figures 4.5(a) and 4.5(b)) show that using 500nm diameter fibers (green bars), thickness does not seem to influence the results. Different consideration can be done for 150nm fibers: for random nanolayers clearly the thicker is the reinforce, the lower is the energy absorbed, and vice versa for oriented fibers.
Stiffness of the specimens (Figures 4.5(c) and 4.5(d)) is not influenced by the thickness of the nanolayers. In almost all the configuration an increase of stiff-

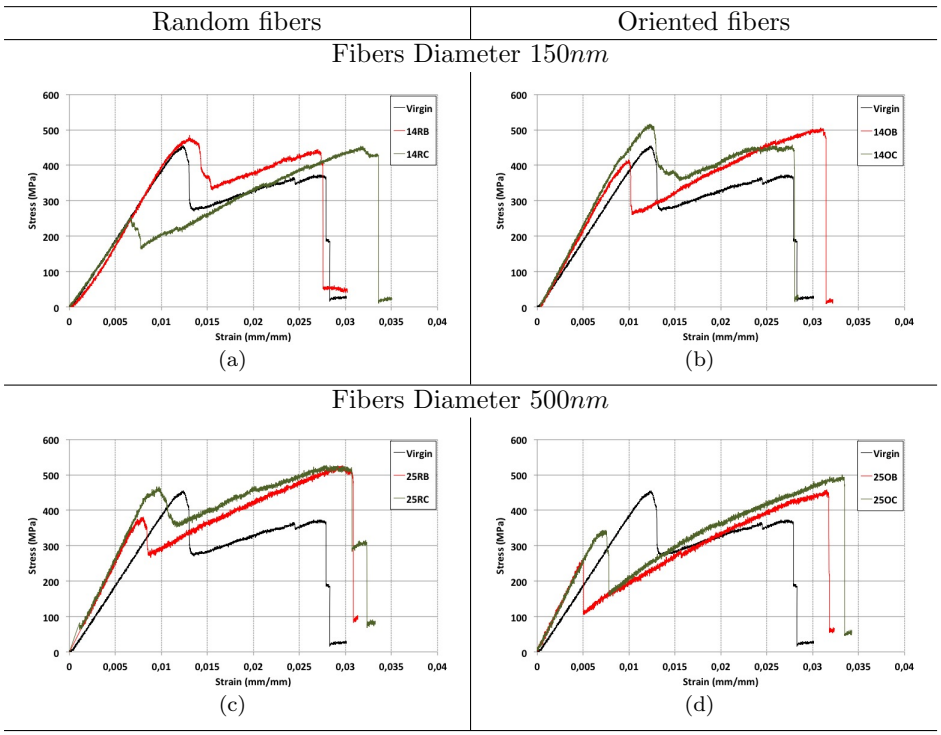

Figure 4.7: Thickness effect in ENF tests. Black lines: virgin specimens - Red lines: $25\mu m$ layer - Green line: $50\mu m$ layer.

ness is measured compare to the virgin configuration, but no appreciable differences can be registered among the two nanolayer thicknesses.
Maximum tension bars (Figures 4.5(e) and 4.5(f)) reveals the same results: a sensible increase is registered with respect the virgin specimens, but no appreciable difference in thickness can be recorded.
Concluding, it is possible to state that thickness of nanolayer, in the range of value hereby used, does not significantly affect the mechanical properties of interface it in interleaved in.

4.1.4. Influence of nanofibers orientation

In Figure 4.8 load-displacement curves of DCB test are presented in the way to enhance the nanofiber orientation effect.

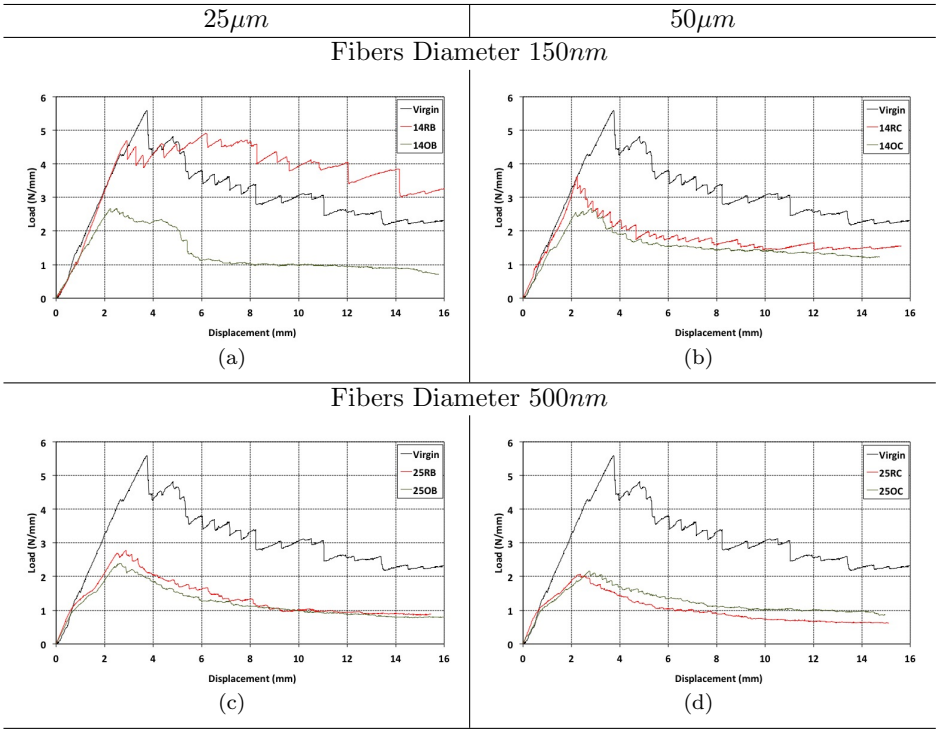

Figure 4.8: Orientation effect in DCB tests. Black lines: virgin specimens - Red lines: random fibers - Green lines: aligned fibers.

As described at the beginning of this chapter, the effect of nanofibers in a layer subjected to mode I fracture mechanics conditions, in the range of geometry and parameters considered in this work, is not able to reinforce the interface but in one case. In this part, the work is focused on the effect of the geometrical parameters of the fibers, and the effect of the orientation of fibers is here presented. Figures 4.8 and 4.3 state that the orientation of fibers is a very important parameter. Comparing Figure 4.3(a) with 4.3(b) and 4.3(c) with 4.3(d), it is clear that for $150nm$ diameter, orientation effect has a significant effect on the mechanical performance of the laminate: random interleaves lead to much better results with respect the oriented ones. For fiber of $500nm$ diameter, the same effect is not detected, and both the absorbed energy and peak force are very close for both the orientations. Concluding it is possible to state that in Mode I loading conditions, random fibers would be preferable respect the oriented ones.
Figure 4.9 presents the stress-strain curves for ENF tests and the effect of the orientation of the fibers is enhanced.
Figures 4.4 and 4.9 give contrasting results in terms of orientation effect for Mode II specimens. The energy absorption capability seems to slightly decrease when the nanofibers are oriented in the length direction of the specimens. Fur-

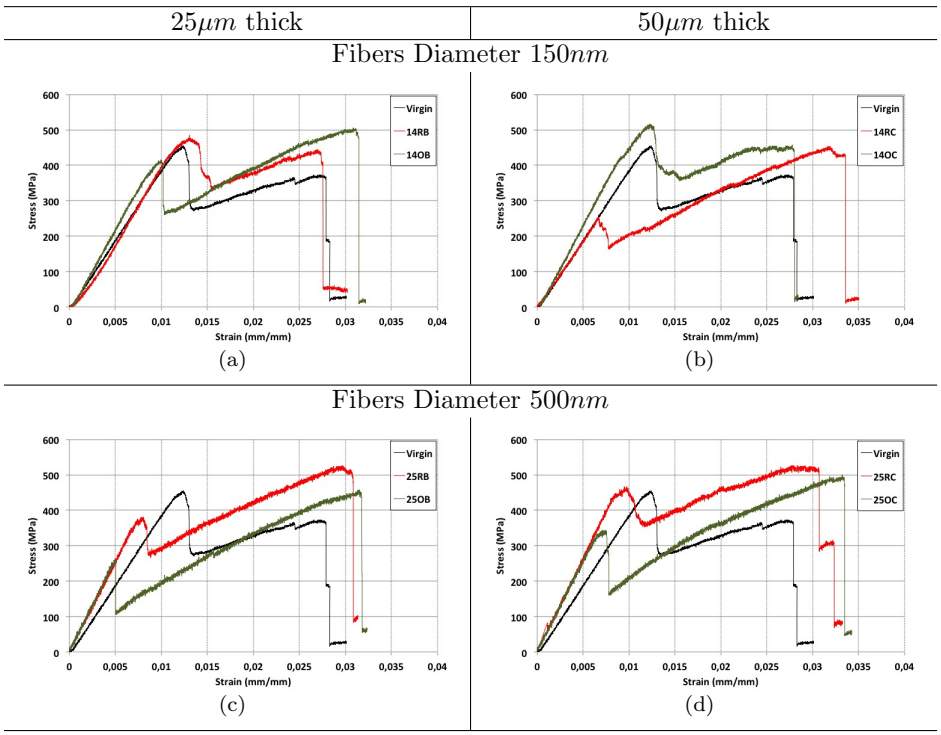

Figure 4.9: Orientation effect in ENF tests. Black lines: virgin specimens - Red lines: random fibers - Green lines: aligned fibers.

thermore, for $500nm$ fibers, no significant different are registered in terms of stiffness (Figures 4.5(c) and 4.5(d)) and maximum tensions (Figures 4.5(e) and 4.5(f)) among the two orientations of the fibers. For $150nm$ fibers, it seems that oriented fibers sensibly increase the stiffness and maximum tension with respect the random ones.
Concluding it is possible to say that form Mode II loading conditions, oriented fibers are slightly preferable with respect the random ones.

4.1.5. Influence of fibers diameter

The last parameter investigated is the fiber diameter. In Figure 4.10 its effect on DCB tests is enhanced.

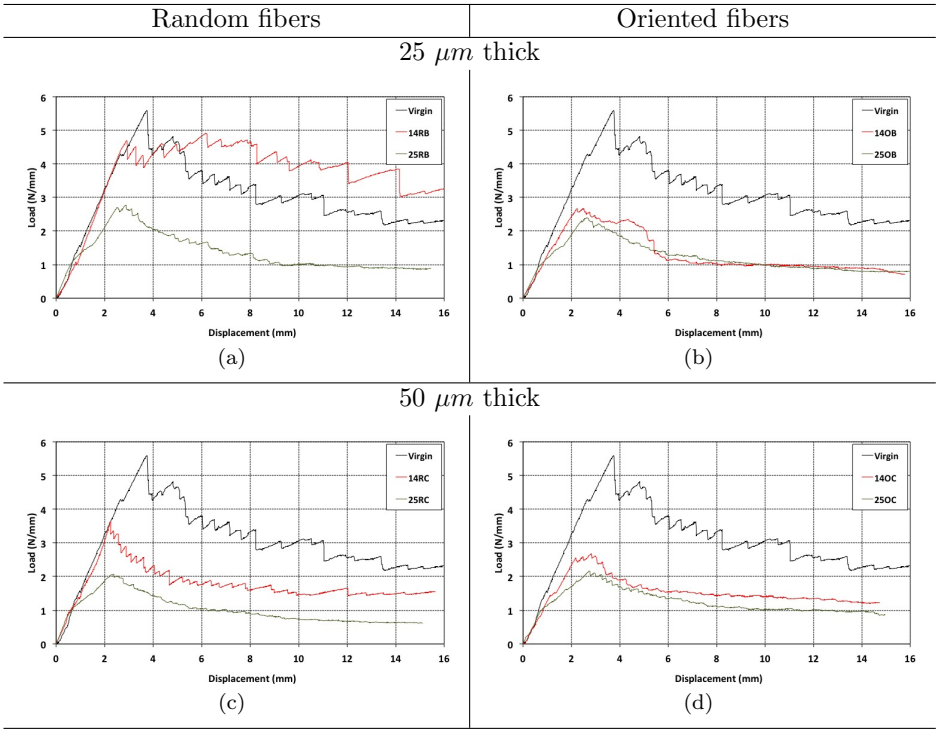

Figure 4.10: Fibers diameter effect in DCB tests. Black line: Virgin specimens - Red line: 150nm diameter - Green line: 500nm diameter.

The effect of fiber diameter in DCB experiments can be easily detected from Figure 4.10: the red curves, related to 150nm diameter, are greater than the green ones, related to 500nm diameter fibers, in all the diagrams. Results presented in table 4.1 and Figure 4.3 confirm that the smaller is the diameter, the better are the performances of the reinforce.
In Figure 4.11, nanofiber diameter effect in ENF tests is enhanced.
For Mode II tests, the effect of fiber diameter is not as clear as it appeared for the Mode I tests. In Figure 4.5, from the energy point of view (Figures 4.5(a) and 4.5(b)) specimens nanointerleaved with 150nm diameter fibers are capable to absorb a greater amount of energy with respect to those interleaved with 500nm fibers.
Regarding stiffness and maximum tension, it appears that for specimens interleaved with random nanofibers (Figures 4.5(c) and 4.5(e)), 500nm diameters lead to better results, compared to those obtained with 150nm interleave. At the same time, for specimens reinforced with nanolayers made by oriented fibers (Figures 4.5(d) and 4.5(f)), no significant differences can be appreciated between 150 and 500nm reinforce.
Concluding, it is possible to summarize that small nanofibers are preferable if the purpose of the nanoreinforce is to increase the energy absorbing capability of

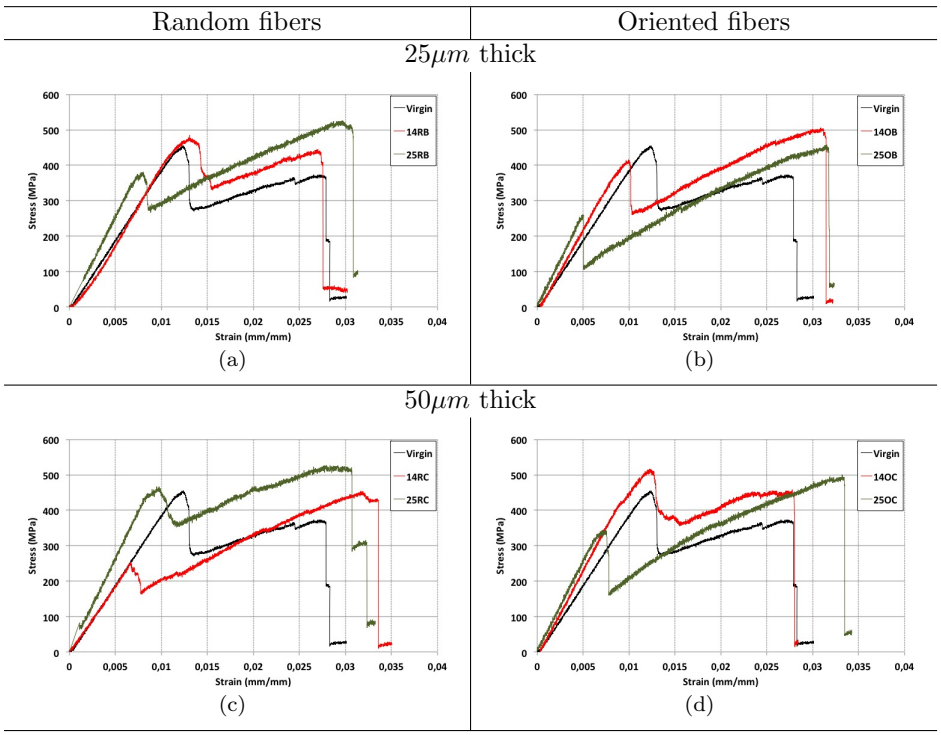

Figure 4.11: Fibers diameter effect in ENF tests. Black line: Virgin specimens - Red line: 150nm diameter - Green line: 500nm diameter.

the laminates; if the goal is to increase the maximum load, then big nanofibers are more suitable than smaller ones.

4.1.6. Summary

A full description of the mechanical tests performed on laminates subjected to Mode I and Mode II fracture mechanics has been reported. The effect of three morphological variables of the nanoreinforce on the mechanical performances of the composites is investigated. Fiber diameter, fiber orientation, and nanolayer thickness have been considered as parameters. Results can be summarised as follow:

- Mode I loading condition: for the considered range of variables, results presented a global decrease of the mechanical properties of the delaminated interface. Among the 8 different tested configurations only one has shown improvements form mechanical point of view. Regarding the effect of the parameters it is possible to say that:
  - in the considered range, the thinner is the reinforce, the better are the mechanical performances of the laminates;
  - random fibers leads to better results than oriented ones;
  - the smaller is the fiber diameter the higher are the performance of the nanoreinforce.
- Mode II loading conditions: a global improvement of the mechanical characteristic of the nano-modified specimens with respect the virgin configuration is enhanced. In particular, in the range of the parameters here considered, it has shown that:
  - the grater is the thickness on nanolayer, the better is the mechanical response, even if the difference between the two considered thicknesses is not particularly relevant;
  - oriented nanofibers are slightly preferable to random ones;
  - small diameters are more advisable than bigger with the purpose increasing the energy absorption capability of the specimens.

With the above considerations, it was decided to continue the experimental campaign with the nanofiber configuration that better increase properties of the laminates in both the loading modes and to use the 14RB configuration: nanofibers non-oriented, $150nm$ average diameter and low-thickness mats.

4.2. Mode I fracture mechanic tests

In this section a full dissertation of what happens into laminate interface when it is loaded in Mode I fracture mechanics condition is presented. As explained in the previous chapter, nanomodified specimens are interleaved with thin layer of nanofibers ($25\mu m$), characterized by $150nm$ diameter of non-oriented fibers.
Load-displacement and energy absorbed-displacement curves from DCB test are detailed presented in Figure 4.12. In Table 4.3 the mechanical parameters extracted from the curves are listed. Both the force and the mechanical energy values were normalized to specimen's width.

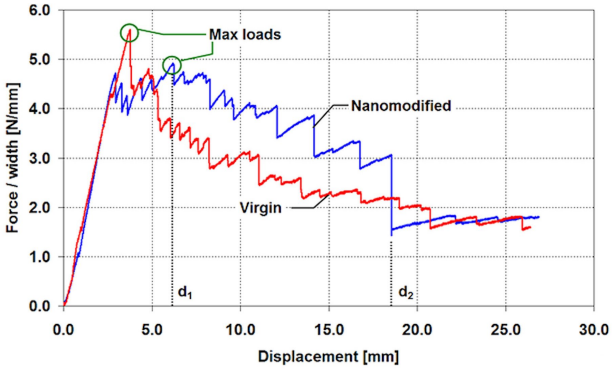

(a) Load-to-width vs. displacement.

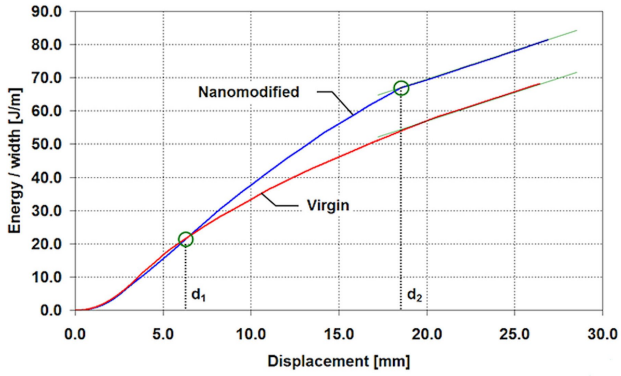

(b) Energy-to-width vs. displacement.

Figure 4.12: DCB mechanical test results.

In Figure 4.12(a) examples of force-displacement curves are reported for both the types of specimens, the virgin and the nanomodified one. From this diagram it is highlighted that the virgin laminate exhibits a higher maximum load with respect to the nanomodified one. Nevertheless, the load values of the nanomodified laminate for displacement higher than d_1, have a higher magnitude with

respect to the virgin laminate. Such a trend is confirmed by the mechanical energy calculated by means of the integration of the load-displacement diagram. In Figure 4.12(a) the diagrams of the mechanical energy plotted as a function of displacement are reported. In the mechanical energy diagrams it is interesting to note the presence of three test phases: (i) from the beginning of the test up to the displacement value d_1, the virgin and the nanomodified specimens have a similar energy trend, (ii) between the displacement d_1 and d_2 the nanomodified specimen supports a higher force value with respect to the virgin one and this causes the bifurcation of the energy trends, (iii) at the displacement d_2 the nanomodified specimen exhibits a force drop that causes a reduction in the slope of the energy trend, and after d_2 the energy slope of the nanomodified specimen is similar to the slope of the virgin one. From the force-displacement and energy-displacement diagrams the d_1 and d_2 displacement values discriminating the three phases of the test were identified. Such a behavior can be related to the presence of the nanofibrous layer that tends to obstacle the crack propagation in the opening Mode I.
The above reported comments are supported by the DCB results reported in Table 4.3 where the maximum load, the mechanical energy calculated at the $14mm$ of displacement, and the G_{IC} are summarized. As shown in Figure 4.12(a), the nanomodified specimens exhibit a maximum force value that is lower than the value of the virgin sample. In other words, it seems that when the nanofibrous mat is placed into the crack opening interface, the maximum sustainable force value is lower compared to the case of a virgin one: the maximum force value in the case of the nanomodified specimen is 12% lower than in the case of a virgin specimen. On the contrary, the presence of the nanofibrous mat at the crack opening interface enhances the mechanical energy that is absorbed during the crack propagation tests. It is estimated that the presence of the nanofibrous mat in the crack opening interface contributes to an increment in the absorbed energy of about 21% with respect to the virgin interface. Finally it is observed that the presence of the nanofibrous interlayer has a measurable influence also on the critical strain energy release rate: the G_{IC} in the case of nanomodified specimens is about 5% higher with respect to the virgin specimens.

	Virgin		Nanomodified		Δ
	μ	$\sigma/\mu\%$	μ	$\sigma/\mu\%$	
Max load (N/mm^2)	5.61	1.72	4.92	3.34	-12.3%
Mechanical energy* (J/m)	45.55	2.54	55.29	8.34	+21.4%
$\mathbf{G}_{IC}$ (J/m^2)	473	2,54	496	2.22	+4.9%

*mechanical energy has been calculated per width unit at 11 mm of displacement.

Table 4.3: DCB mechanical results. μ = mean value - σ = standard deviation.

The acoustic emission information were analysed considering the events trend and the distribution of the amplitude, of the duration and of the acoustic energy of each event.

By relating the amplitude and the duration in a double entry plot, Figure 4.13(a) and 4.13(b), it is possible to note that the distribution of the AE events released by the virgin interface have a different position with respect to the nanomodified one. In particular, in order to analyse the amplitude-duration scatter plot five regions were identified: (I) 55-65dB of amplitude and 0-2000sec of duration; (II) 65-85dB of amplitude and 0-2000 sec of duration; (III) 85-95dB of amplitude and 0-6000 sec of duration; (IV) 65-85dB of amplitude and 2000-4000sec of duration; (V) 85-95dB of amplitude and 6000-10000 sec of duration. The AE events from the virgin interface fit all the five regions (Figure 4.13(a)) while the AE from the nanomodified interface fill only the first three regions (Figure 4.13(b)). This means that the nanofibrous interlayer contributes to slow down and to homogenize the matrix breakage during the crack propagation. In other words, the nanofibrous interlayer sustains part of the applied force, thus reducing the overall matrix breakages. This finding is also confirmed by the cumulative event distributions reported in Figure 4.13(c) and the cumulative AE event energy diagram reported in Figure 4.13(d).

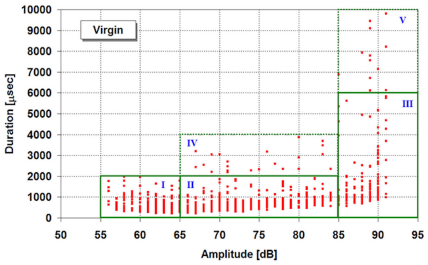

(a) AE events for virgin interface.

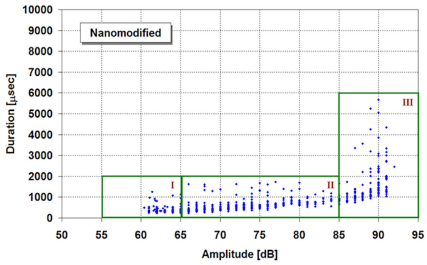

(b) AE events for nanomodified interface.

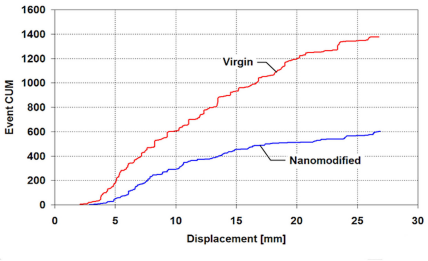

(c) Cumulative AE events vs. displacement.

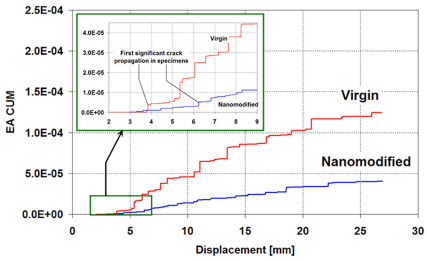

(d) Cumulative AE events energy (EA CUM).

Figure 4.13: DCB tests: plots of duration and amplitude of the AE events.

The total number of the AE events released by the nanomodified interface is lower than half of the total number of AE events released by the virgin interface. Likewise, the cumulative AE event energy related to virgin interface at the maximum value of the displacement (Figure 4.13(d)) is three times higher than the cumulative AE energy related to nanomodified one. Moreover, from the insert in the same Figure it is possible to note that the presence of the nanofibrous interlayer delays the first significant crack propagation with respect to what happens in case of the virgin interlayer. This fact is also related to the increment in the value of G_{IC} reported in Table 4.3.

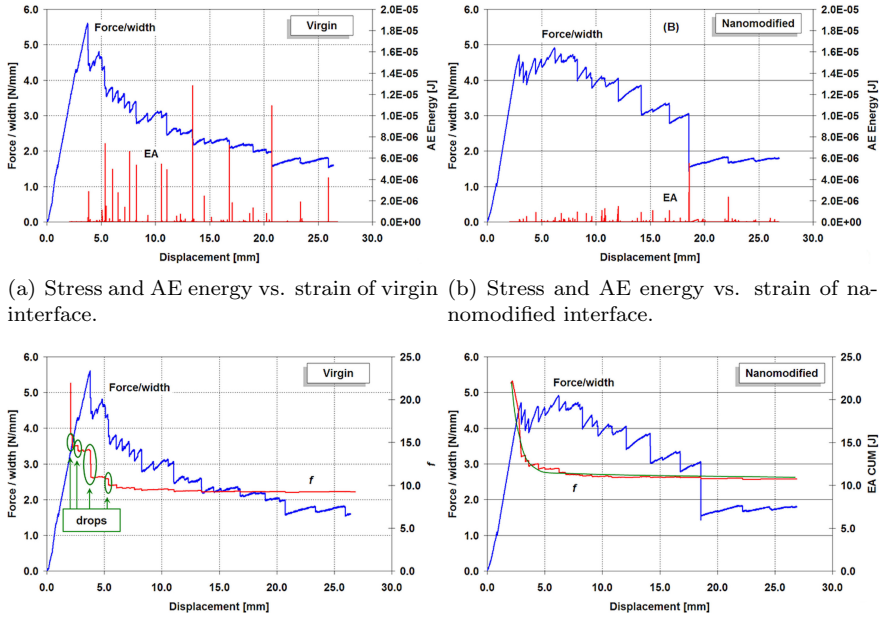

(a) Stress and AE energy vs. strain of virgin interface.

(b) Stress and AE energy vs. strain of nanomodified interface.

(c) Stress-strain and sentry function (f) of virgin interface.

(d) Stress-strain and sentry function (f) of nanomodified interface.

Figure 4.14: DCB tests: mechanical and AE results comparison.

In order to deeply understand the DCB results, mechanical and acoustic results are related and discussed together. In particular, two types of diagrams are considered in Figure 4.14 for each mechanical tests: a diagram that relates the force and the AE events energy to the displacement (Figures 4.14(a) and 4.14(b)) and a diagram where the force and the sentry function are referred to the displacement (Figure 4.14(c) and 4.14(d)). Figures 4.14(a) and 4.14(b) show that the AE events are very well related to the force drops. Moreover, considering the AE energy values it is possible to note that, in the case of the nanomodified interface, the energy of each single AE event is lower than that of the events released by the virgin interface. It is worth to note that the distribution of the AE events characterized by a high energy content from the virgin interface are more or less homogeneously distributed over all displacement domains. On the contrary, in the case of the nanomodified interface the most energetic AE events are released only near the end stages of the test, i.e. only when the interface is severely damaged. From diagrams 4.14(c) and 4.14(d) it is possible to note that the trend of f in the case of the nanomodified interface does not present important falls as, on the contrary, happens in the case of the virgin interface. This confirms that the nanofibrous interlayer reduces the number of catastrophic matrix failure events and it contributes to have a smooth stress redistribution meanwhile the crack propagates in the interface. A further information that can be extracted from the sentry function is the overall damage resistance capability. In fact, as previously reported, the integral of the sentry function can be used to estimate the materials attitude to resist against different types of damages. Indeed, if a material, let say material A, exhibits a higher

value of the integral of f with respect to another material, let say material B, this means that the material A mechanical energy storing capability is higher than that of the material B, or, in other words, the material A sensitivity to the damage progression is lower than that of the material B. In the present case the integral of the sentry function obtained by the virgin specimen is $95 \pm 5\ mm^{-1}$ while in the case of the nanomodified specimen the value is $281 \pm 9\ mm^{-1}$. The obtained values of the integral of the sentry function confirm the fact that the nanofibrous mat contributes to enhance the overall delamination resistance of the laminate under a fracture Mode I loading condition.

4.3. Mode II fracture mechanic tests

In this section a full dissertation of the results of Mode II fracture mechanics tests is presented.
Stress-strain and Energy absorbed-strain curves from ENF test are presented in Figures 4.15. In Table 4.4 the mechanical parameters extracted from the curves are listed. Mechanical energy values were normalized to specimen's width.

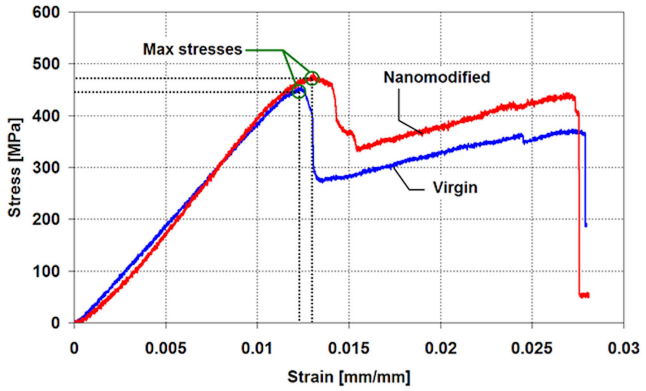

(a) Stress vs. strain.

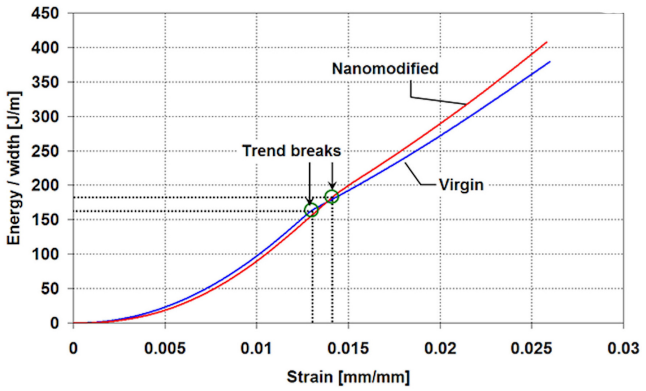

(b) Mechanical energy vs. strain.

Figure 4.15: ENF mechanical test results.

From Figure 4.15(a) and Table 4.4 it can be observed that the flexural modulus of the nanomodified and of the virgin laminate assume comparable values until the material exhibits a linear behavior. This experimental evidence is related to the fact that the nanofibrous mat is placed in the mid-plane of the laminate and to the fact that mat thickness does not significantly affect the total thickness of the laminate. Therefore, the linear elastic behavior of the two types of laminates can be considered the same. Nevertheless, differently to what observed for DCB tests, in the three point bending test the presence of the nanofibrous mat at the mid-interface contributes to increase the maximum value of the stress. In particular, considering the two curves in Figure 4.15(a) and the values in Table 4.4, it can be observed that the nanomodified specimen has a maximum

stress value that is about 10% higher than the maximum value of the virgin specimen. Likewise, it can be noted that in the case of the nanomodified laminate the strain value, when the maximum stress is reached, is higher than the strain value at the maximum stress of the virgin specimen. In summary, in the case of a end notched flexure laminate, the nanofibrous mat contributes to increase the maximum sustainable stress and, at the same time, it contributes to delay the first material crisis. Moreover, it can be observed that the general trend of the stress for the nanomodified specimen overcomes that of the virgin laminate. After the first stress drop it can be observed that the stress values of the nanomodified and of the virgin laminate increase following trends with a similar slope but different absolute values. In particular, the stress values of the nanomodified laminate always overcome the stress values of the virgin laminate. Such a behavior can be also evaluated by the mechanical energy diagram reported in Figure 4.15(b). From this diagram it can be noted that at strain values higher than those at which the laminate crisis takes place, after the two trend break points, the mechanical energy stored into the nanomodified laminate overcomes the energy stored into the virgin one. Mechanical energy data reported in Table 4.4 confirm these finding: the maximum mechanical energy that can be stored by a nanomodified laminate is about 8% higher than in the case of the virgin laminate.

	Virgin		Nanomodified		Δ
	μ	$\sigma/\mu\%$	μ	$\sigma/\mu\%$	
Flexural modulus (N/mm^2)	42.34	3.56	45.05	2.30	+9.6%
Maximum stress (MPa)	459	6.55	504	2.00	+6.4%
Mechanical energy* (J/cm^3)	7.30	9.76	7.87	4.06	+7.9%

*mechanical energy has been calculated per volume unit at 10 mm of displacement.

Table 4.4: ENF mechanical results. μ = mean value - σ = standard deviation.

The AE events distribution, amplitude, duration, and energy are considered to better interpret ENF results. In particular, the double entry plots relating the AE amplitude and the duration (Figures 4.16(a) and 4.16(b)) show that the virgin interface is characterized by points that have a different distribution with respect to the nanomodified one. In the case of ENF test, in the amplitude-duration space plot it is convenient to consider five regions organized as follows (Figure 4.16(a)): (I) 50-60dB of amplitude and 0-4000 sec of duration; (II) 60-85dB of amplitude and 0-4000 sec of duration; (III) 85-95dB of amplitude and 0-10000sec of duration; (IV) 60-85dB of amplitude and 4000-8000sec of duration; (V) 85-95dB of amplitude and 10000-16000 sec of duration. The AE events from the virgin interface fill all the five regions (Figure 4.16(a)) while the AE from the nanomodified interface fill only three regions (Figure 4.16(a)). As in the case of the DCB test, the nanofibrous interlayer sustains part of the applied force, thus reducing the overall matrix breakages. This fact is also confirmed by the cumulative event distributions reported in Figure 4.16(a) and by the cumulative AE event energy diagram reported in Figure 4.16(a).

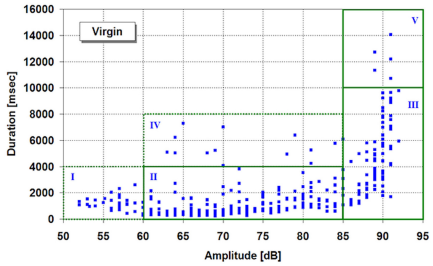

(a) AE events for virgin interface.

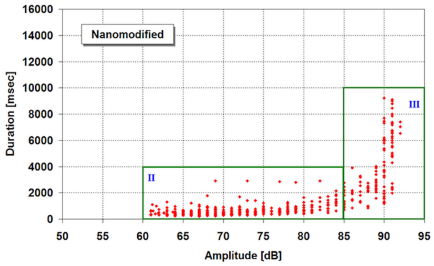

(b) AE events for nanomodified interface.

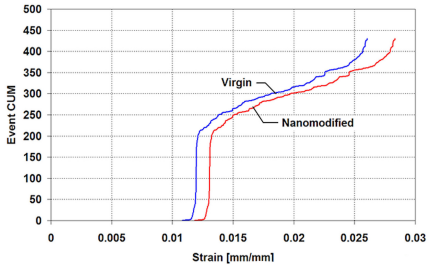

(c) Cumulative AE events vs. displacement.

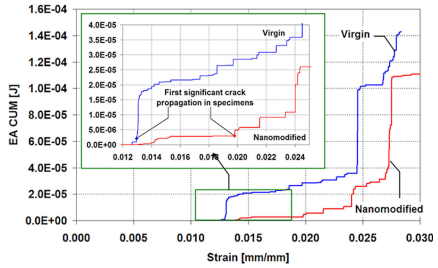

(d) Cumulative AE events energy (EA CUM).

Figure 4.16: ENF tests: plots of duration and amplitude of the AE events.

As it was observed in the case of the DCB test, the number of AE events released by the nanomodified interface is lower than the number of AE events released by the virgin interface as well as the cumulative AE energy of the events released by the virgin interface is higher than the cumulative energy of events coming from the nanomodified laminate. From Figures 4.16(c) and 4.16(c) it is possible to note that, as it was observed in the case of the DCB results, the presence of the nanofibrous interlayer delays the first significant crack propagation with respect to what happens in case of the virgin interlayer. In Figure 4.17 diagrams relating mechanical and acoustic informations to the strain are reported. In particular, in Figures 4.17(a) and 4.17(b), the force and the AE event energy are referred to the strain, while in Figures 4.17(c) and 4.17(d) the force and the sentry function are referred to the strain. Figures 4.17(a) and 4.17(b) show that the AE events are very well related to the force drops. Moreover, considering the AE energy values it is possible to note that, in the case of the nanomodified interface, the energy of each single AE events is lower than that of the events released by the virgin interface.

It is worth to note that, for both types of specimens, the distribution of the AE events characterized by a high energy content are released near the end stages of the test, i.e. only when the interface is severely damaged. Differently to what was observed in the case of DCB test, from Figures 4.17(c) and 4.17(d) it is possible to note that the trend of f presents important drops in the case of nanomodified laminates as well as in the case of virgin ones. Nevertheless, the drops that characterize the f function of a nanomodified laminate are smaller with respect to ones measured in the case of a virgin laminate. This fact confirms that the nanofibrous interlayer mitigates the catastrophic matrix failure events

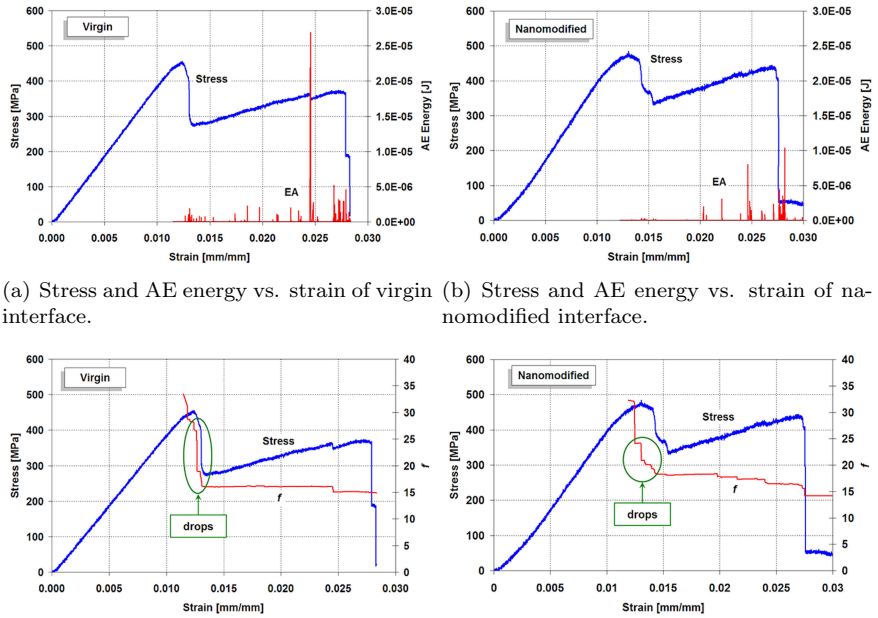

(a) Stress and AE energy vs. strain of virgin interface.

(b) Stress and AE energy vs. strain of nanomodified interface.

(c) Stress-strain and sentry function (f) of virgin interface.

(d) Stress-strain and sentry function (f) of nanomodified interface.

Figure 4.17: ENF tests: mechanical and AE results comparison.

and, at the same time, it contributes to have a smooth stress redistribution meanwhile the crack propagates in the interface. Considering also the integral of the sentry function it can be observed that in the case of virgin specimen its value is 100± 6 mm^{-1} while in the case of the nanomodified specimen its value is 130± 8 mm^{-1}. These values confirm the fact that the nanofibrous mat contributes to enhance the composite laminate damage resistance with respect to the Mode II of fracture.

4.4. Pre impact laminate micrography analysis

Micro-graphic analysis was performed for those specimens subjected to impact.
Figure 4.18 shows some micrograph images taken from the through-thickness section of virgin and nano-modified laminates.

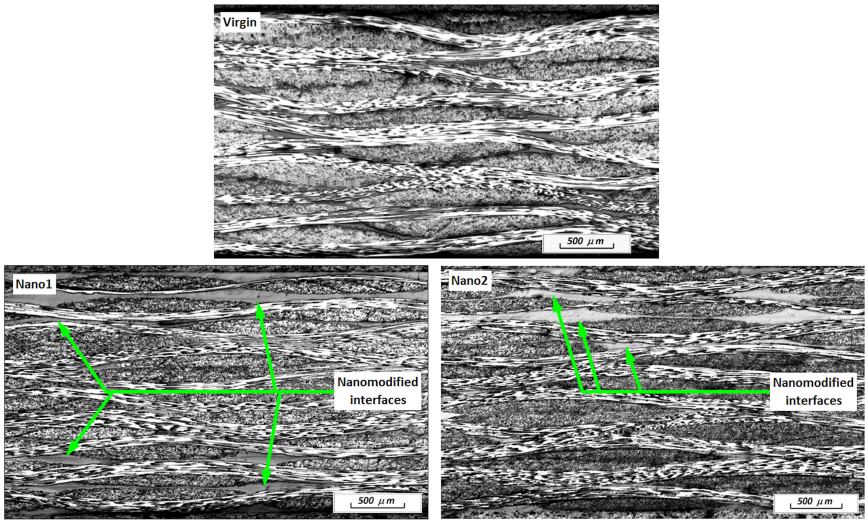

Figure 4.18: Through-thickness microscopy.

The horizontal lines are the fibers seen from aside, while the points are the sections of perpendicular fibers; the dark areas are the matrix. The upper picture shows the section of a virgin panel, while the lower two are related to nanomodified specimens: Nano1 configuration on the left and Nano2 on the right. In the nanomodified interfaces is it possible to observe the typical matrix enrichment due to the presence on the layer of nanofibers and the reinforce itself. They are the slightly darker lines particularly visible into the dark areas of the matrix. They are continuous from one side to the other of the pictures: 4 of them are detectable in Nano1 configuration, and 3 in the Nano2 one. It proves, before the Scanning Electron Microscope images presented later in this chapter, that the nanolayers are not melted after the cycle cure into the autoclave and also that, probably, the nanofibers maintained their original morphology.
Figure 4.19 shows a detailed comparison of the various types of nanomodified interfaces.
In this picture the presence of the nanoreinforce is highlighted, as well as the matrix enrichment into the nanomodified interfaces (pictures on the right).
Two types of interfaces were classified, according to the two orientations of the fibres: 0° (the horizontal direction of fibres in the plane of the photos) and the 90° (the perpendicular direction with respect to the plane of the photos). So the interface named type 1 is where the 0° fibres coupled with the 90° fibres of the adjacent ply; while the pair 0°/0° interface is classified as type 2.
For all the nanomodified interfaces it can be noted that the presence of the nano-fibrous mat induces the formation of an enriched interlayer matrix that is expected to influence the mechanical behaviour of the laminates as it will be

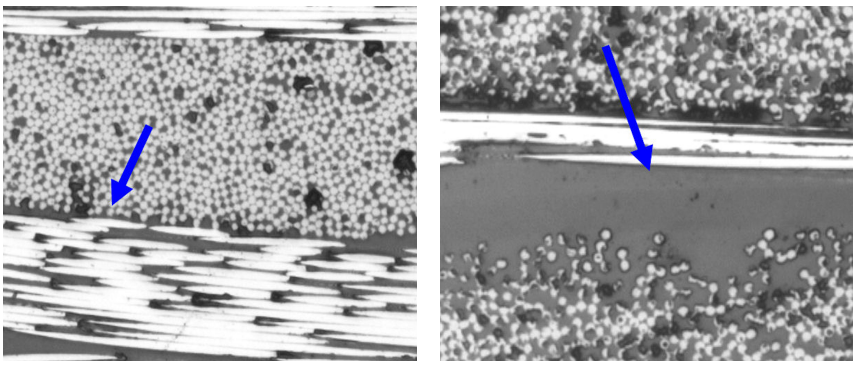

(a) Type 1 interface: fibres 90° vs fibres 0°.

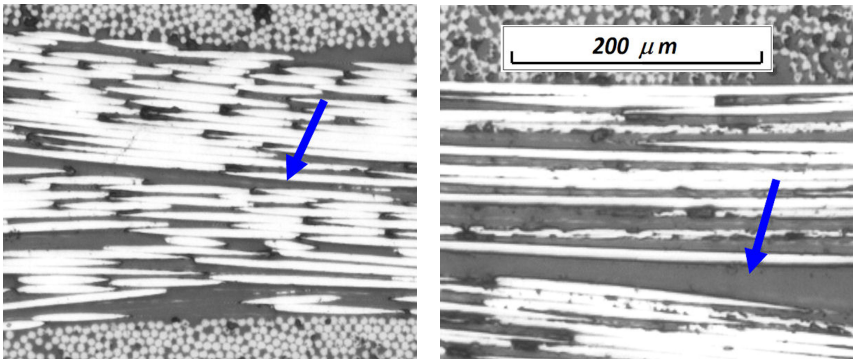

(b) Type 2 interface: fibres 0° vs fibres 0°.

Figure 4.19: Details of interfaces with (left) and without (right). *Length scale reported in the last picture is the same for the others.*

discussed later.

4.5. Pre impact flexural and free decay test

In this section the results of the tests performed before the impacts are presented and discussed. Table 4.5 shows the elastic moduli, the harmonic frequencies and the damping ratios determined by the flexural and the free decay tests before the impacts.

	Flexural stiffness (GPa)		**Free decay test** $\mathbf{f_1}$ (Hz)		**Damping ratio**	
	μ	$\sigma/\mu\%$	μ	$\sigma/\mu\%$	μ	$\sigma/\mu\%$
Virg	59.3	1.0	127.1	0.5	$4.0\ 10^{-3}$	6.3
Nano1	52.5	1.5	108.2	1.5	$9.9\ 10^{-3}$	7.4
Nano2	51.5	1.2	108.4	3.9	$6.5\ 10^{-3}$	14.9

Table 4.5: Pre impact results. μ = mean value - σ = standard deviation.

From the flexural test results it can be noted that the nano-modified panels

have a lower stiffness value with respect to virgin ones. This behaviour can be attributed to the fact that in the nano-modified laminates the the nano-fibrous mats keep part of the resin that would be squeezed out from the prepreg during the curing phase without the nanoreinforce. This causes the formation of the enriched matrix interfaces, (§4.4), which reduces the global stiffness of the laminate. By performing a percentage comparison of the flexural moduli of the tested panels it can be observed that the flexural moduli of Nano1 and Nano2 are 11% and 13% less than those of the virgin configuration respectively. Free decay test results on the pre-impacted specimens showed that virgin plates have a higher first natural frequency as compared to the nano-modified ones. This result agrees with the stiffness determined from the flexural tests: the presence of matrix enriched interfaces reduces the global stiffness and consequently the first natural frequency of the plate. No relevant differences can be found between the two nanomodified configurations. On the other hand, the analysis of vibrations revealed that the damping of the nano-modified laminates is higher than the one for virgin specimens. In particular, the first frequency of both nano-modified laminates is about 15% less than the one of the virgin specimens, whereas the damping of the Nano1 and the Nano2 plates is 149% and 62% higher than the damping of the virgin panels respectively.
Some previous studies performed mainly with carbon nanotubes revealed the same trend. Zhou et al [85] demonstrated that high damping can be achieved by taking advantage of the interfacial friction between the nano-reinforce and the polymer resin and introduced the concept of interfacial "stick-slip": a frictional motion between the nanoreinforce and the resin. Also Liang [86] addressed the greater energy dissipation to the fiction between fibers and resin. Gou [87] and Koratkar [88] in their works affirm that the energy dissipation is due to the cross-linkages within the nanofibers.

4.6. LVI RESULTS

The test is performed with three levels of impact energy: 3, 6 and 12J. In these tests force-versus-time and force-versus-displacement are recorded. Figure 4.20 presents examples of curves related to the impact process.

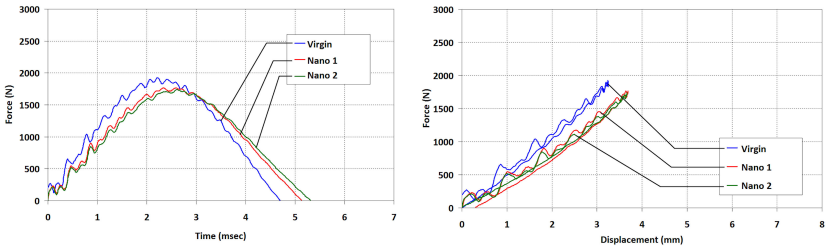

(a) 3J impact energy.

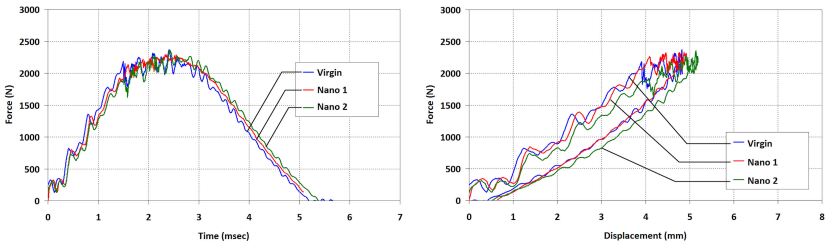

(b) 6J impact energy.

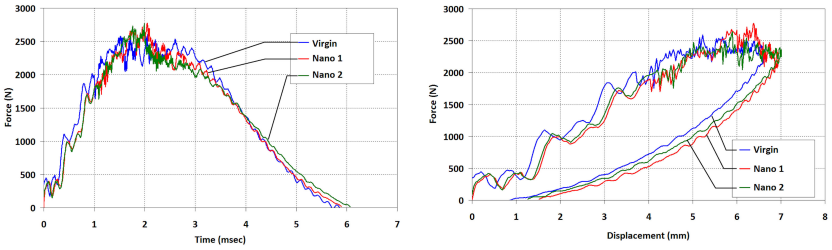

(c) 12J impact energy.

Figure 4.20: LVI curves.

The maximum impact forces and the absorbed energies are summarized in Table 4.6 and 4.7 respectively. From diagram shown in Figure 4.20(a) left, it can be noted that the 3J impacts in nanomodified specimens are longer in terms of time and lower in terms of force, compared to to the virgin ones. In particular, Table 4.6 shows that the maximum force of both the nanomodified specimens is about 8% less than the force measured for the virgin ones. Moreover, from Figure 4.20(a) right it can be seen that the loop area under the force-displacement curve is approximately zero for all specimens. Thus, no significant damage is induced to panels by the lowest impact energy. Such a conclusion is also supported by the results shown in Table 4.7: the energy absorbed for the lowest impact heights is related only to the elastic deformation.

Energy of	**Virgin**		**Nano 1**		**Nano 2**	
impact (J)	μ	$\sigma/\mu\%$	μ	$\sigma/\mu\%$	μ	$\sigma/\mu\%$
3	1905	1.15	1757	0.47	1762	6.25
6	2338	1.07	2288	1.48	2329	7.44
12	2703	1.59	2820	3.87	2730	14.86

Table 4.6: Impact results: maximum force (N). μ = mean value - σ = standard deviation.

Energy of	**Virgin**		**Nano 1**		**Nano 2**	
impact (J)	μ	$\sigma/\mu\%$	μ	$\sigma/\mu\%$	μ	$\sigma/\mu\%$
3	0.34	8.82	0.39	51.28	0.20	25.00
6	2.09	4.31	2.01	2.39	1.79	3.91
12	5.82	1.37	6.26	2.40	6.57	0.76

Table 4.7: Impact results: Absorbed energy (J). μ = mean value - σ = standard deviation.

Force-time curves corresponding to the $6J$ impacts are presented in Figure 4.20(b) left. The curves do not show any notable differences between virgin and nano-modified specimens; nevertheless for the $6J$ impact energy it can be noted that the absorbed energy by the nano-modified specimens is sensibly lower as compared to the energy absorbed by the virgin ones. In particular Nano1 and Nano2 configurations absorbed 3.8% and 14.3% less energy than virgin specimens, respectively. Such behaviour can be related to the fact that during the impact, nano-fibres play an important role in strengthening the interfaces and mitigating the damage propagation. Moreover the results confirm that since the delamination cone starts narrow in the impact zone and grows down through the thickness, nanofibers placed in the bottom layers allow a lower energy absorption from the specimen. The same behavior is also observed for the $3J$ impacted specimens, even if the specimens are not damaged. For $6J$ energy of impact, the only detectable damage is matrix breakage, as shown by Figures 4.22(a), 4.22(c) and 4.22(e). Figures present the bottom surface of the impacted specimens. Surface of virgin specimens appears clearly more damaged than those of nanomodified ones, in which only few sign of the impact can be observed.
Figure 4.21(a) shows pictures, produced by a Scanning Electron Microscope (SEM), of the nano-modified delaminated surfaces
From Figure 4.21(a) it can be observed that nanofibers stitch the two layers where they are put in between and many of the fibers still bridge with a net the two planes (this aspect will be further explained in §4.7). In Figure 4.22 the effect of the impact on the laminate surface is shown. Form the Figure 4.22(a) it is clear that the matrix of the bottom layer of the virgin laminates is damaged: fibers appear to be still unbroken, while the matrix exhibits some fails. After the same impact nanomodified specimen surfaces (Figures 4.22(c) and 4.22(e)) present a smoother and more intact surface compared to the virgin specimen one. It is due to the fact that delamination cone is much more smaller in the nanomodified specimens which significantly present themselves less undamaged.
From $12J$ energy force-time diagrams (Figure 4.20(c) left) no significant differences between virgin and nanomodified specimens can be observed. In fact

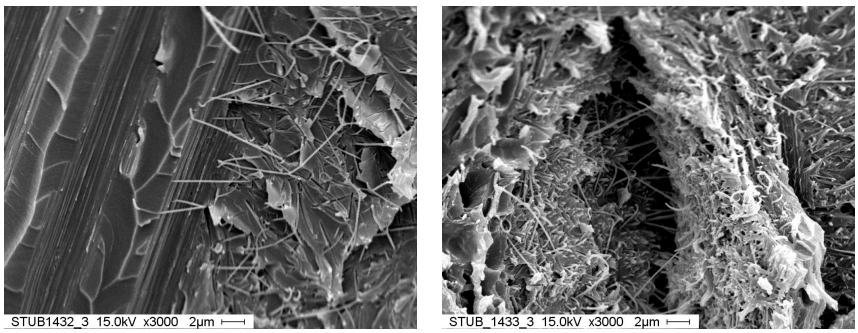

(a) $6J$ impact energy.

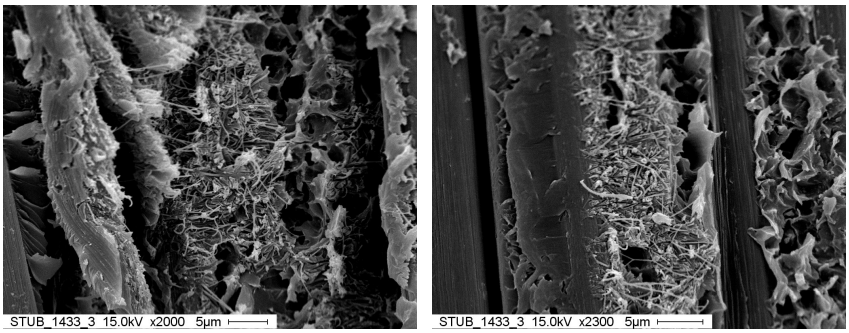

(b) $12J$ impact energy.

Figure 4.21: SEM investigation of nanomodified post impacted interface.

for virgin ad nanomodified laminate the maximum force values are similar as well as the impact duration. Nevertheless the analysis of the absorbed energy (Figure 4.20(c) right and Table 4.7) shows that nanomodified specimens have a higher absorption of energy than that of the virgin panels. In particular Nano1 and Nano2 configuration absorbed 7,5% and 12,9% higher amount of energy, compared to the virgin specimens, respectively. For this energy level, the trend for nanomodified specimens is inverted compared to what is found for 3 and $6J$ of impact: nanomodified specimens absorb more energy than virgin specimens, and Nano2 registers the highest value. Authors explain this behavior with the fact that at $12J$ of energy impact, the failure mode significantly changes and both matrix and fibers are cracked as presented in Figures 4.22(b), 4.22(e) and 4.22(f). From figures it is not appreciable a markable differences among the specimens: nanofibers are not able to resist to such a strong impact and few nanofibers are still linking the two adjacent layers (Figure 4.21(b)).

An interesting approach to evaluate the effect of an impact over a structure is the Ductility Index (DI), derived from load displacement diagram [89] and defined as the ratio of the post-peak-energy to the energy-to-peak:

$$DI = \frac{U_{post-peak}}{U_{pre-peak}} \tag{4.1}$$

This ratio should be equal to zero in the limit case of instant perforation of the

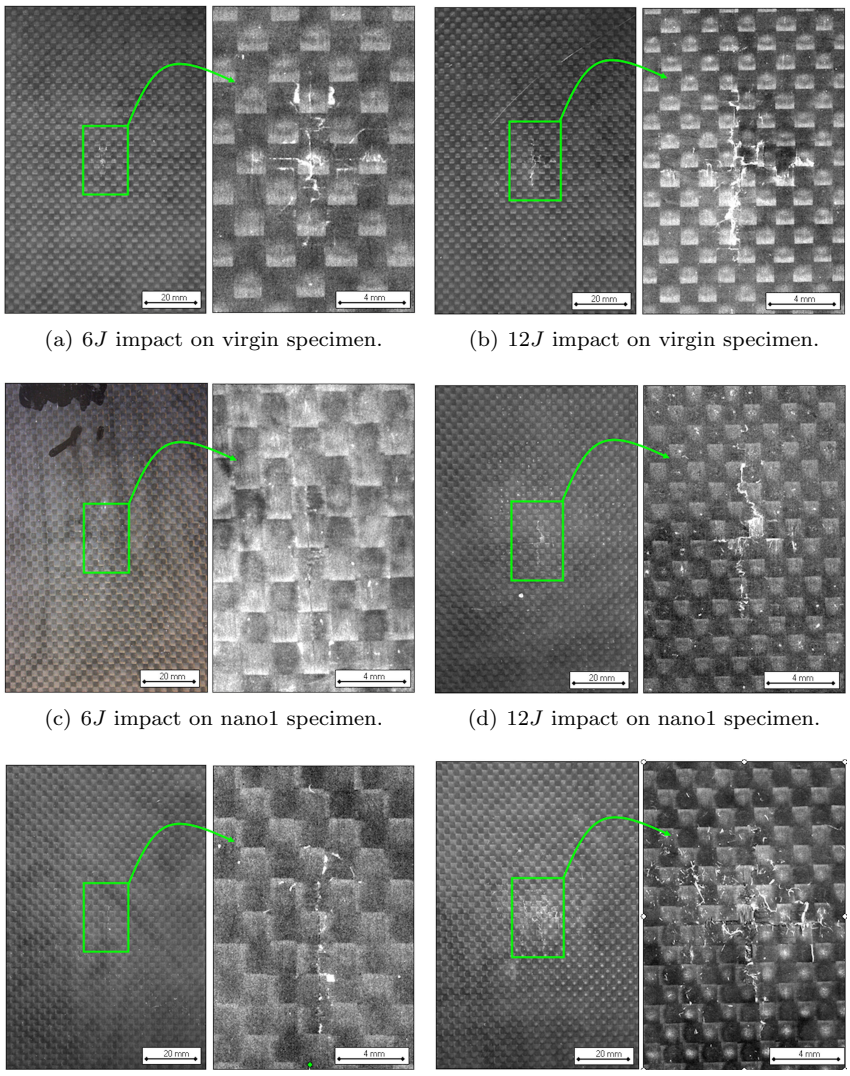

(a) 6J impact on virgin specimen.

(b) 12J impact on virgin specimen.

(c) 6J impact on nano1 specimen.

(d) 12J impact on nano1 specimen.

(e) 6J impact on nano2 specimen.

(f) 12J impact on nano2 specimen.

Figure 4.22: Post impact images of the lower surface.

structure, in which the peak of the force is immediately followed by a drop to zero. The opposite case-limit is the one in which DI is equal to 1 and the two amount of energy are equal: in this case all the energy provided by the impactor is totally released to it and the damage would be zero. Thus the DI is inversely proportional to the damage grade of the panel after impact: the closest to zero is the index, the more damaged is the panel
In Table 4.8 and Figure 4.23 the Ductility Index (DI) for all the configurations is presented.
In Figure 4.23 the blue line is related to the 3J impacts. DI is close to 0.9 for all the 3 configurations, and it confirms that that the panels are still undamaged or poorly damaged by the impactor. Even in this non-damaged condition it appears

Energy of	**Virgin**		**Nano 1**		**Nano 2**	
impact (J)	μ	$\sigma/\mu\%$	μ	$\sigma/\mu\%$	μ	$\sigma/\mu\%$
3	0.8916	1.68	0,9127	7.56	0.9421	0.53
6	0.6404	8.90	0.6573	1.22	0.6898	1.16
12	0.3247	2.16	0.3189	3.14	0.2635	0.38

Table 4.8: Ductility Index (DI). μ = mean value - σ = standard deviation.

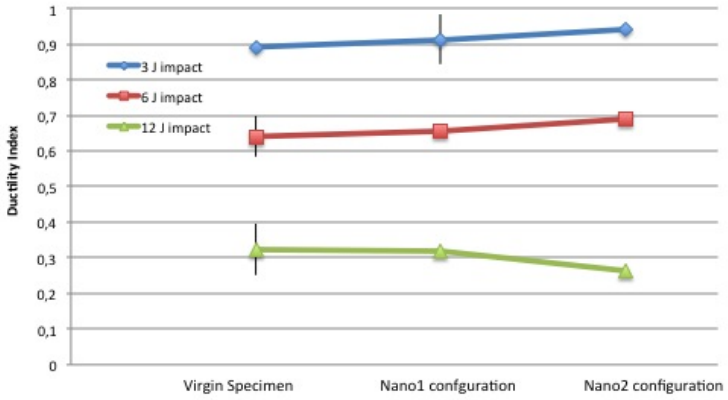

Figure 4.23: Damage calculated index for the 3 configurations at the 3 drop-levels.

that nanomodified specimens sensibly release a small greater amount of energy respect the virgin panels. The same behavior is highlighted for the $6J$ impact, in which, obviously, the DI is much lower: in this case the impact irreversibly and significantly damaged the specimens. Even for this case it is possible to see how nanomodified specimens, and in particular Nano2 configurations, release around a 8% more energy respect the virgin panels, confirming the results presented above. As it was see in Table 4.7, the $12J$ impacts appear to be slightly different, since the nanomodified specimens seems to behave sensibly worse than the virgin ones.

4.7. Post-impact mechanical tests and results

Flexural tests on impacted plates were preliminary performed to measure the variation of the laminate flexural stiffness modulus after the damage induced by impacts respect to the undamaged conditions. Table 4.9 summarizes the results.

Energy of	**Virign**		**Nano 1**		**Nano 2**	
impact (J)	μ	$\sigma/\mu\%$	μ	$\sigma/\mu\%$	μ	$\sigma/\mu\%$
0	59.3	1.0	52.5	1.5	51.5	1.2
3	57.9	0.4	54.2	3.7	52.8	5.5
6	56.0	0.3	60.1	5.9	56.4	2.2
12	54.4	0.9	56.8	5.4	53.5	2.8

Table 4.9: Flexural stiffness moduli after impact (GPa). μ = mean value - σ = standard deviation.

Comparing the results of the flexural tests obtained before and after impacts, it can be observed that the virgin and the nanomodified specimens exhibit two opposite behaviors. Virgin laminates presents, as expected, a stiffness reduction proportional to impact energy: in particular, in the case of $6J$ and $12J$ of impact energies the flexural stiffness of impacted panels is 6% and 8% less than the undamaged one respectively. On the contrary, the flexural modulus of the nano-modified specimens increases with the energies of the impacts: Nano1 panels impacted at $6J$ and $12J$ have a flexural stiffness 14% and 8% higher as compared to the undamaged ones respectively. In the case of Nano2 panels impacted at $6J$ and $12J$, the flexural modulus are respectively 9% and 3% higher than the undamaged ones. The modulus of Nano1 configuration appears to be higher, because the modulus on Nano2 is calculated by the average of two test, since the configuration is non-symmetric; nevertheless, the trend of both the configuration is very similar.
Similar results have been found with the dynamic tests. In virgin panels, increasing the energy of impact, the first harmonic frequency decreases as expected, in accordance with the flexural results. For nanomodified panels, again, increased harmonic frequencies have been found after impacts.
Table 4.10 presents the measured first harmonic frequencies for each configuration.

Energy of	**Virign**		**Nano 1**		**Nano 2**	
impact (J)	μ	$\sigma/\mu\%$	μ	$\sigma/\mu\%$	μ	$\sigma/\mu\%$
0	127.1	0.5	108.2	1.5	108.4	3.9
3	127.3	2.3	110.1	0.8	110.0	3.0
6	126.0	0.5	121.4	0.5	122.5	3.3
12	120.5	1.9	121.2	1.4	120.7	2.0

Table 4.10: First harmonic frequencies (Hz). μ = mean value - σ = standard deviation.

It can be observed that the results are in accordance with those presented in Table 4.9 for the stiffness. The first frequency of virgin laminates, by increasing the impact energy, decreases up to 5% for highest impact energy with respect

to the undamaged ones. In the case of impacted nano-modified panels, the first harmonic increases by 10% for Nano1 and up to 11% for Nano2 with respect to the undamaged ones.
In Figure 4.24 both trends of flexural stiffnesses and first harmonics versus impact energies are plotted.

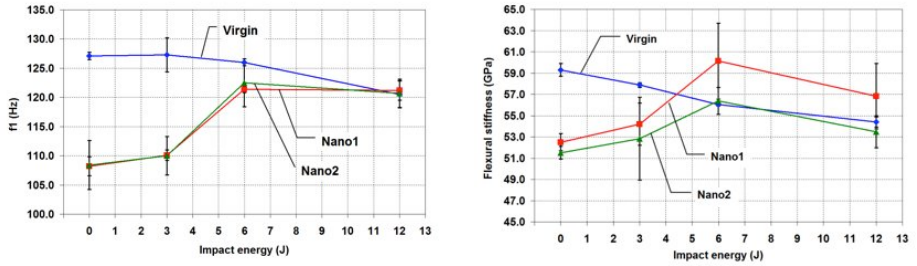

(a) First harmonic frequency.

(b) Flexural stiffness.

Figure 4.24: Post-impact harmonic frequencies and flexural stiffnesses.

Each diagrams plot the previously described trends for stiffness (Figure 4.24(a)) and first frequency (Figure 4.24(b)), and moreover, it is possible to appreciate the fact that by increasing the impact energy, the stiffnesses as well as first frequencies of both types of panels, virgin and nanomodified, tend towards the same values.
In the case of virgin panels, the reduction of both stiffness and first frequency observed by increasing the impact energy are due to the increment of the delaminated area. In the case of nanomodifed panels the increment of both stiffness and first frequency can be explained with the crack bridging effects acted by the presence of nanofibers between adjacent plies. Figure 4.25, which presents SEM micrography of nanomodified fractured surfaces after impact.
Figure shows that many nanofibers are still undamaged, particularly where the resin is broken. Pictures present the fact that despite the damage event (in this case the impact) and the consequent matrix rupture, nanofibers are still alive and able to link the layers. In particular Figure 4.25(b) clearly show that the nanofibers are in tension and still connecting the two plies where they are interleaved in between. Nylon is more ductile than the resin, and when this last brakes, nanofibers can slip over the matrix and become able to bridge the crack and reinforce the interface, even if the matrix is damaged. Once the impactor falls on the panel, the epoxy macrostructure is damaged, the matrix breaks and delamination propagates. After the impacts, nanofibers are free from the matrix and can play the role of a net-like reinforcing web, thus enabling a ply-to-ply bridging effect. Nevertheless when the energy of impact increases ($12J$) most of the nanofibers are broken as well, and the ply-to-ply bridging effect is reduced (Figure 4.21). In fact Figure 4.24 shows that both the first harmonic frequency and the stiffensses tent to the same value for all the configurations.
Damping ratios results are summarized in Table 4.11 and in Figure 4.26. The damping ratios are plotted with respect to the impact energy values. From the results presented in Table 4.11, it can be noted that by increasing the energy of impact, the damping ratio goes down for both virgin and nanomodified

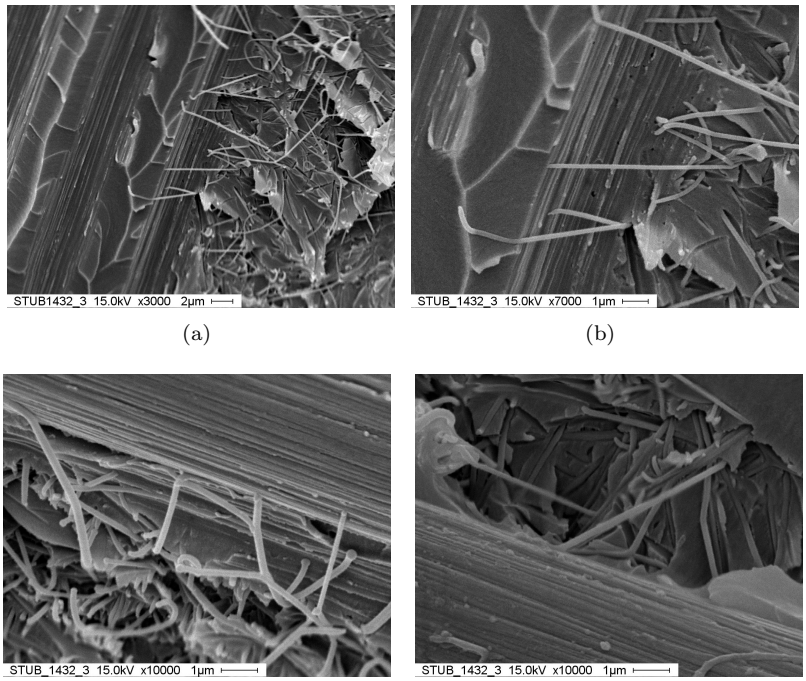

(a) (b)

(c) (d)

Figure 4.25: Naofibers still in tension after impact.

laminates and tends toward the same limit value ($2.9\ 10^{-3}$).

Energy of	**Virign**		**Nano 1**		**Nano 2**	
impact (J)	μ	$\sigma/\mu\%$	μ	$\sigma/\mu\%$	μ	$\sigma/\mu\%$
0	$4.0\ 10^{-3}$	6.3	$9.9\ 10^{-3}$	7.9	$6.5\ 10^{-3}$	14.9
3	$3.2\ 10^{-3}$	4.6	$4.3\ 10^{-3}$	4.0	$3.5\ 10^{-3}$	3.1
6	$3.0\ 10^{-3}$	7.9	$2.9\ 10^{-3}$	8.2	$3.2\ 10^{-3}$	4.4
12	$2.9\ 10^{-3}$	12.3	$2.6\ 10^{-3}$	4.2	$3.0\ 10^{-3}$	6.3

Table 4.11: Post-impact damping. μ = mean value - σ = standard deviation.

From a physical point of view it is interesting to compare the damping ratio of damaged and undamaged panels. As shown in Figure 4.26, when panels are undamaged the damping ratio of the nanomodified laminates is higher than the virgin ones. This can be explained by the fact that when nanofibers are embedded into the matrix, they are able to dissipate energy, giving to the nanomodified laminates a higher damping ratio value with respect to the virgin ones. So, in the case of undamaged laminates, nanofibers play the role of interlayer dampers. When panels are damaged some of the nanofibers are free from the matrix, (Figure 4.21), and they can contribute to increase the flexural stiffness and the first harmonic frequency by working as ropes in a Tibetan bridge. At the same time they are not able to dissipate energy as it was when they were embedded into the matrix.

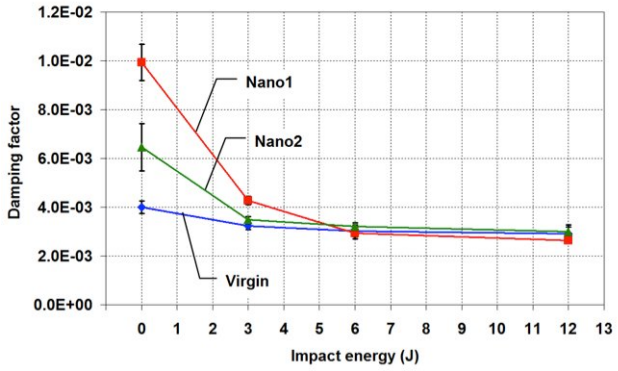

Figure 4.26: Diagrams of damping ratio; experimental points refers to the damping ratio of undamaged ($0J$) and impact-damaged panels ($3J$, $6J$, $12J$).

The pre-impact and post-impact results of both virgin and nano-modifed laminates can be summarized in the two diagrams presented in Figure 4.27. The diagrams show the damping ratio versus the flexural stiffness (Figure 4.27(b)) and versus the first harmonic frequency (Figure 4.27(a)). From the diagrams it can be observed that before the impact, in an undamaged status, nanomodified laminates have lower flexural stiffness modulus and first harmonic frequency than virgin panels; at the same time nanomodified panels present a higher damping ratio with respect to the virgin ones.

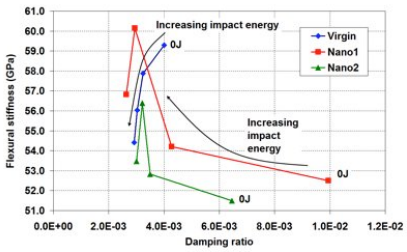

(a) Damping ratio vs flexural stiffness.

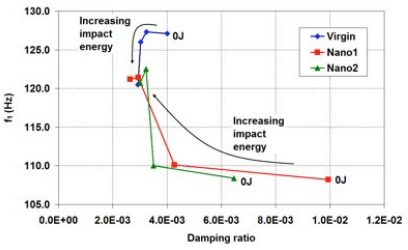

(b) Damping ratio vs first harmonic.

Figure 4.27: Summary results.

From the nano-modified panels that are subjected to impact it can be observed that the flexural stiffness and the first harmonic frequency increase with respect to the undamaged panels whereas the damping ratio decreases. So in the case of undamaged laminates, the nanofibers, that are embedded into the matrix play the role of dampers. When the nano-modified panels are damaged some of the nano-fibers are free from the matrix and they can work as internal links that contribute to increase the flexural stiffness and the first harmonic frequency, whereas their contribution as internal dampers is reduced with respect to the condition when they are embedded into the matrix.

5. Conclusion

Non giudicare sbagliato ciò che non conosci,
prendi l'occasione per comprendere
P. Picasso - pittore, scultore, artista

The aim of this dissertation is to understand the reinforce mechanism of polymeric nanofibrous interleave into CFRP laminates. The importance of carbon/glass fiber composite materials is increasing day by day even in everyday life and many efforts have been made to improve their performances. In the last decades, laminate composite materials have assumed a great importance since their high strength- and stiffness-to-weight ratios, their capabilities to be modelled under many shapes, and so on. In spite all their good characteristic, these new materials still present some weak aspects which must be improved: one of the most important is the delamination resistance. Many researches were carried out to face the problem and one the most promising technique is the one that involve the use of nanofibers. This work involves the use of Nylon 6,6 electrospun nanofibers as interleave reinforce material for carbon fiber/epoxy resin composite material. Electrospinning is probably the most versatile technique to obtain nanofibers and Nylon 6,6 is a polymer with high mechanical properties and that shows a good affinities with the epoxy resin that impregnates the fibers.
The purpose of the work was achieved through 4 steps:

1. definition of the architecture of the nanoreinforce. Three main features characterize a layer of nanoreinforce: its thickness, fibers diameter and orientation of them. When a nanofibrous sheet is placed into a laminate interface, each feature plays its own role in the reinforcement process. Preliminary activities presented in the work had the purpose to determine how these features change the mechanical behavior of the laminate in which they are interleaved in and to obtain the configuration that can ensure the best reinforcement for the laminate;

2. investigation of the reinforce mechanism in specimens subjected to quasi-static DCB and ENF tests. Fracture mechanics principles have been used to characterize delamination failures in composite laminates, and Mode I and Mode II tests have been performed on beam-like shape specimens. Maximum loads, absorbed energies, stiffness and G_{IC} were measured and used to determine the effect of the interleave. Acoustic emission technique was also used to understand the mechanism by which the nanofibers reinforce the interface meanwhile the crack propagates;

3. investigation of the reinforce mechanism in specimens subjected to dynamic LVI and bump tests. From the tests, harmonic frequencies, dumping, absorbed energy and stiffness were measured and used to determine the reinforce effect;

4. micrograph analysis of the fractured surface.

Each steps lead to important considerations, summarized in the following.

5.1. Architecture of nanoreinforce

Optimization process revealed the importance of an accurate selection of the nanoreinforce. DCB test results showed that under Mode I loads interleave can seriously weak the interface if not properly designed. Under Mode II quasi-static tests, the benefits of the nanoreinforce were more evident and many configurations led to improved mechanical performances. The wide experimental campaign revealed that the best reinforce was achieved with a thin layer of nanofiber ($25\mu m$ thick), with small diameter ($150nm$) randomly oriented. This configuration was then used to perform the experimental campaign core of the work, in which the nanoreinforce mechanism is investigated.

5.2. Quasi static tests

Twenty plies, woven carbon fibers/epoxy resin prepreg beam-shaped specimens were manufactured with a nanofibrous mat placed in the mid-plane and tested under Mode I and Mode II of fracture. The results can be summarized as follows:

- from the DCB tests the following conclusion notes can be reported:
  - nanofibrous mat reduces the maximum opening load that can be supported by stressed interfaces by about 12% compared to virgin ones;
  - presence of nanofibrous mat significantly increases the absorbed mechanical energy during all the test (about 21%);
  - G_{IC} of nanomodified specimens is 5% higher with respect to virgin ones;
- from the ENF tests the following concluding remarks can be listed:
  - flexural modulus is not significantly influenced by the presence of the nanofibers. It is due to the fact that the modified interface were in the middle of the specimens, thus in the neutral axe for bending;
  - nanofibrous mat enhances of about 10% the maximum value of the force that has to be applied to initiate the longitudinal crack propagation;
  - consistently to DCB results, nanomodified composite laminates subjected to the interlaminar crack propagation, can absorb a 8% higher amount of mechanical energy with respect to the virgin ones.

The AE analysis confirmed that the nanomodified laminates have a finer attitude to mitigate the crack onset and propagation. The released AE energy and the total number of events in the case of a nanomodified laminate are lower with respect to the virgin laminates.
Overall, DCB and ENF results demonstrate that the interleaved nanofibrous mat can enhance composite delamination strength and damage tolerance.

5.3. Dynamic tests

Ten plies, woven carbon fibers/epoxy resin prepreg plate-shaped specimens were manufactured and tested by LVI and free decay tests. Symmetric and non-symmetric lay-up configurations of nanomodified laminates were manufactured together with virgin one. On the first stage static and dynamic tests were done to measure the stiffness and the damping of the virgin composite panels. After that the specimens were subjected to LVI in order to induce damage in them. Then, the same static and dynamic tests were done on the damaged specimens. From the analysis of the test results it is possible to derive some important conclusions. First of all the damping of nanomodified laminates is higher than those virgins, thus the nano Nylon 6,6 inter-layers act as dampers before any damage is induced. At the same time nanointerleaves induce an expected reduction of the stiffness of the specimens. This is actually the expected behaviour after the introduction of new layers- they would decrease the stiffness making the material less tough and they may have a damping effect. When subjected to impact the nano-modified specimens reveal different behaviour as compared to the non-modified ones.
Regarding the LVI tests, an 8% lower peak force was measured during impact for the lowest energy level in nanomodified configurations and up to 14.3% less energy is absorbed by non-symmetric configuration with respect to the virgin one, with a clear reduction of the post-impact damage. Those results are enhanced for those specimens that present nanofibers concentrated on the lower layers, in which the expected delamination is bigger.
Post impact analysis revealed an unexpected behavior for nanomodified laminates, while virgin panels showed the expected decrease in stiffness and harmonic frequencies, proportional to the impact energy. Nanomodified panels showed an extraordinary reinforcement effect due to the presence of nanofibers: they display an increase of both the first harmonic frequency (up to 12%) and the stiffness (up to 14%), when impacted with 6 J of energy, compared to the non damaged condition. So in this case the nano Nylon 6,6 patches act as stiffeners and their stiffening effect increase up to a certain energy of the impact and up to a certain level of the damage introduced in the material. Thus there is a certain critical point in the damage state of the Nylon 6,6 modified CFRP up to which they get tougher and consequently are able to sustain the damage and prevent its increase. The further increase of the impact energy, after this critical point, brings the stiffness down, closely to the one measured for virgin panels. The same behavior is registered for the stiffnesses and it means that after a certain level the damage induced by the impact overcome the benefits of the interleave, and the presence of nanofibers become negligible. It is proven by the fact that, after $12J$ of impact, frequencies and stiffnesses of all the configurations tent to the same value.

5.4. Micrograph

Scanning Electron Microscope (SEM) was used to capture pictures of fractured surfaces to see the final state of the fibers into the interleave. Considerations have been done to give a physical explanation to the results previously found. SEM pictures showed that even when the matrix is broken nanofibers still link the layers they are inserted in between. Pictures show that they are able to continue to keep the layers together, even after that the macrostructure is irreversibly damaged. This mechanism is a self-stiffening effect that nanofibrous interlayers are capable to give to the whole panel once delaminated. The microscopic tests confirmed that after the impact the interleaves improve the quality of the specimens (up to a certain point of the energy increase) because they hold the fibers together once the matrix is damaged. After a certain level of energy, nanointerleaves cannot any longer sustain the impact since they are damaged and their stiffening effect is diminished.
On the other hand after the impact the nano-interleaves do not any longer have an increasing damping effect. They act as stiffeners but they do not contribute to the damping of the nano-modified specimens. After the impact and with the increase of the energy of the impact, which obviously increases the amount of damage in the material, the damping goes down. So the Nylon 6,6 indentations do not any longer act as dampers once a certain (even small) amount of damage is introduced in the material.

5.5. Concluding remark

At the end of this work, personal opinion of the author is that nanofibers really have the capabilities to solve some of the problems afflicting composite laminates due to the mismatch between two consecutive plies. Nylon is the most suitable material to produce nanofibers, and electrospinnig is proven to be a very good and versatile technique to manufacture them. The results show that nanofibers can play an important role into laminates, for whatever kind and direction of load. Specimens were subjected to static and dynamic tests, to in- and out-of plane loads and nanofibers always give their contribution. Interleaving composite laminate with polymeric nanofibers can be easily applied in a wide number of important practical applications and structures to mitigate the damage that these structures are subjected to, for the purposes of noise/vibration reduction, and many more.
At the state of the art, electrospinning technology needs to be improved, since it is still quite slow. Nanofibers can really become a worldwide useful toll to reinforce laminate if researchers will be able to develop a system capable to electrospin enough fibers per unit time. The machine used in this work is a laboratory prototype, and some research still has to be done in order to fix those problems related with the production rate.
In this work, together with the good results presented above, some limitation should be highlighted as well. Nanolayers were manufactured with the cited electrospinning machine in an aluminium plate, and then placed over the prepreg layer which is then cured. Results would be more reliable if nanofibers could be directly electrospun over the prepreg, in order to avoid steps that could introduce noise factors. Another limitation of this work is enhanced by the DCB

tests, for which, almost all the nanomodified configurations led to worse performances compared to virgin one. Results would suggest that a different range parameter would have been chosen, and that further investigation is required. An experimental campaign with a different parameter range for nanofibers is encouraged.
A next step could regard the modelling of nanointerleave. Present work lays down an accurate foundation for a numerical modelling process. Data collected by the experimental campaign, and the obtained results, can be used with numerical simulator to predict the characteristic of an interface nanofiber-addicted. This study is supposed to put the foundations in the research of the effect of Nylon 6,6 reinforcement on the mechanical properties of CFRP laminates. Further research is needed to e.g find the critical level up to which the indentations have a stiffening effect and/or regarding the optimal number and position of the interleaves and/or the best characteristics of a nanolayers, especially when interleaved in a laminated subjected to Mode I loads. More research in the area of the dynamic/vibratory behaviour is needed having in mind the fact that in most applications composite materials experience and are subjected to vibrations: the allowable and the optimal ranges of the amplitudes and the frequencies of these vibrations still need to be established.
In the very end, this work successfully attended to its purposes and some interesting steps on the understating of these new and fascinating materials have been done.

References

[1] British Petroil. Statistical Review of World Energy June 2008. Technical Report June, 2008.

[2] S.K. Mazumdar. *Composite manufactoring. Materials, Product and Process Engineering*. CRC Press, 2002.

[3] D. Gay, S.V. Hoa, and S.W. Tsai. *Composite material*. CRC Press, 2003.

[4] S. Sridharan. *Delamination behaviour of composites*. CRC Press.

[5] Y.A. Dzenis. Structural Nanocomposites. *Material Science*, 319(January):419–420, 2008.

[6] S. Koombhongse, W. Liu, and D.H. Reneker. Flat polymer ribbons and other shapes by electrospinning. *Journal of Polymer Science. Part B*, 39:2598–2606, 2001.

[7] G. Li, P. Li, Y. Yu, X. Jia, S. Zhang, X. Yang, and S. Ryu. Novel carbon fiber/epoxy composite toughened by electrospun polysulfone nanofibers. *Materials Letters*, 62(3):511–514, February 2008.

[8] A.P. Mouritz, E. Gellert, P. Burchill, and K. Challis. Review of advanced composite structures for naval ships and submarines. *Composite Structures*, 53(1):21–42, July 2001.

[9] L.C. Hollaway. A review of the present and future utilisation of FRP composites in the civil infrastructure with reference to their important in-service properties. *Construction and Building Materials*, 24(12):2419–2445, December 2010.

[10] S. Ramakrishna, J. Mayer, E. Wintermantel, and K.W. Leong. Biomedical applications of polymer-composite materials: a review. *Composites Science and Technology*, 61(9):1189–1224, July 2001.

[11] C. Soutis. Fibre reinforced composites in aircraft construction. *Progress in Aerospace Sciences*, 41(2):143–151, February 2005.

[12] R.M. Jones. *Mechanics of Composite Material*. Taylor & Francis, second edition, 1999.

[13] P. Davies, B.R.K. Blackman, and A.J. Brunner. Standard Test Methods for Delamination Resistance of Composite Materials : Current Status. *Applied Composite Materials*, 5:345–364, 1998.

[14] A.J. Brunner, B.R.K. Blackman, and P. Davies. A status report on delamination resistance testing of polymer/matrix composites. *Engineering Fracture Mechanics*, 75(9):2779–2794, June 2008.

[15] ASTM D5528. Standard Test Method for Mode I Interlaminar Fracture Toughness of Unidirectional Fiber-Reinforced Polymer Matrix Composites. *Annual Book of ASTM Standards*, 2007.

[16] ASTM D6671. Standard Test Method for Mixed Mode I-Mode II Interlaminar Fracture Toughness of Unidirextional Fiber Reinforced Polymer Matrix Composites. *Annual Book of ASTM Standards*, 2006.

[17] C. Marieta, E. Schulz, L. Irusta, N. Gabilondo, a. Tercjak, and I. Mondragon. Evaluation of fiber surface treatment and toughening of thermoset matrix on the interfacial behaviour of carbon fiber-reinforced cyanate matrix composites. *Composites Science and Technology*, 65(14):2189–2197, November 2005.

[18] M. Hojo, S. Matsuda, M. Tanaka, S. Ochiai, and A. Murakami. Mode I delamination fatigue properties of interlayer-toughened CF/epoxy laminates. *Composites Science and Technology*, 66(5):665–675, May 2006.

[19] T. Yang, C.H. Wang, J. Zhang, S. He, and A.P. Mouritz. Toughening and self-healing of epoxy matrix laminates using mendable polymer stitching. *Composites Science and Technology*, 72(12):1396–1401, July 2012.

[20] S.W. Tsai. *Theory of composite design.*

[21] E. Fuoss, P.V. Straznicky, and C. Poon. Effects of stacking sequence on the impact resistance in composite laminates - Part 1 : parametric study. *Composite Structures*, 41:67–77, 1998.

[22] E. Fuoss, P.V. Straznicky, and C. Poon. Effect of stacking sequence on the impact resistance in composite laminates. part 2: prediction method. *Composite Structures*, 41:177–186, 1998.

[23] P. Kere and J. Koski. Multicriterion stacking sequence optimization scheme for composite laminates subjected to multiple loading conditions. *Composite Structures*, 54(2-3):225–229, November 2001.

[24] H. Ghiasi, D. Pasini, and L. Lessard. Optimum stacking sequence design of composite materials Part I: Constant stiffness design. *Composite Structures*, 90(1):1–11, September 2009.

[25] H. Ghiasi, K. Fayazbakhsh, D. Pasini, and L. Lessard. Optimum stacking sequence design of composite materials Part II: Variable stiffness design. *Composite Structures*, 93(1):1–13, December 2010.

[26] A.B. Pereira, A.B. de Morais, A.T. Marques, and P.M.S.T. de Castro. Mode II interlaminar fracture of carbon/epoxy multidirectional laminates. *Composite Science and Technology*, 64(10-11):1653–1659, August 2004.

[27] N.J. Pagano. Influence of Stacking sequence on laminate strength. *Journal of Composite Materials*, 5:50–57, 1971.

[28] W.E. Howard, T. Gossard, R.M. Jones, and M.J. Robert. Reinforcement of composite laminate free edges with U-shaped caps. *AIAA Paper*, 1(86-09722), 1986.

[29] I.K. Partridge and D.D.R. Cartié. Delamination resistant laminates by Z-FibeR pinning: Part I manufacture and fracture performance. *Composites Part A: Applied Science and Manufacturing*, 36(1):55–64, January 2005.

[30] G. Tang, Y. Yan, X. Chen, J. Zhang, B. Xu, and Z. Feng. Dynamic damage and fracture mechanism of three-dimensional braided carbon fiberrepoxy resin composites. *Materials & Design*, pages 21–25, 2001.

[31] L. Chen. Analysis of Mode I and Mode II Tests for Composites with Translaminar Reinforcements. *Journal of Composite Materials*, 39(15):1311–1333, August 2005.

[32] A.P. Mouritz, C. Baini, and I. Herszberg. Mode I interlaminar fracture toughness properties of advanced textile fibreglass composites. *Composites Part A: Applied Science and Manufacturing*, 30(7):859–870, July 1999.

[33] J.F. Cooley. Apparatus for electrically dispersing fluids, 1902.

[34] W.J. Morton. Method of dispersing fluids, 1902.

[35] J. Zeleny. The electrical discharge form liquid points, and a hydrostatic method of measuring the electric intensity at their surfaces. *The Physical review*, 3(2), 1914.

[36] A. Formhals. Process and apparatus for preparing artificial threads, 1934.

[37] G. Taylor. Electrically driven jets. *Royal Society of London. Series A*, 313(1515):453–475, 1969.

[38] R. Gopal, S. Kaur, Z. Ma, C. Chan, S. Ramakrishna, and T. Matsuura. Electrospun nanofibrous filtration membrane. *Journal of Membrane Science*, 281(1-2):581–586, September 2006.

[39] T. Subbiah, G.S. Bhat, R.W. Tock, S. Parameswaran, and S.S. Ramkumar. Electrospinning of nanofibers. *Journal of Applied Polymer Science*, 96(2):557–569, April 2005.

[40] Y.K. Luu, K. Kim, B.S. Hsiao, B. Chu, and M. Hadjiargyrou. Development of a nanostructured DNA delivery scaffold via electrospinning of PLGA and PLA-PEG block copolymers. *Journal of Controlled Release*, 89:341–353, 2003.

[41] D. Liang, B.S. Hsiao, and B. Chu. Functional electrospun nanofibrous scaffolds for biomedical applications. *Advanced drug delivery reviews*, 59(14):1392–412, December 2007.

[42] A. Zucchelli, M.L. Focarete, C. Gualandi, and S. Ramakrishna. Electrospun nanofibers for enhancing structural performance of composite materials. *Polymers Advanced Technologies*, 22(3):339–349, 2011.

[43] S. Ramakrishna. *An introduction to electrospinning And nanofibers*. World Scientific, 2005.

[44] Y.A. Dzenis and D.H. Reneker. Delamination resistant composites prepared by small fiber reinforcement at ply interfaces, 1999.

[45] J.S. Kim and D.H. Reneker. Mechanical properties of composites using ultrafine electrospun fibers. *Polymer Composites*, 20(1):124–131, February 1999.

[46] Z.M. Huang. A review on polymer nanofibers by electrospinning and their applications in nanocomposites. *Composite Science and Technology*, 63(15):2223–2253, November 2003.

[47] I. Finegan. Modeling and characterization of damping in carbon nanofiber/polypropylene composites. *Composites Science and Technology*, 63(11):1629–1635, August 2003.

[48] X.F. Wu and Y.A. Dzenis. *Fracture of advanced polymer composites with nanofiber reinforced interfaces*. PhD thesis, University of Nebraska, 2003.

[49] H. Lee, S. Mall, P. He, D. Shi, S. Narasimhadevara, Y. Yun, V. Shanov, and M. Schulz. Characterization of carbon nanotube/nanofiber-reinforced polymer composites using an instrumented indentation technique. *Composites Part B: Engineering*, 38:58–65, January 2007.

[50] Y. Zhou, F. Pervin, S. Jeelani, and P. Mallick. Improvement in mechanical properties of carbon fabric/epoxy composite using carbon nanofibers. *Journal of Materials Processing Technology*, 198(1-3):445–453, March 2008.

[51] S. Bal. Experimental study of mechanical and electrical properties of carbon nanofiber/epoxy composites. *Materials and Design*, 31(5):2406–2413, May 2010.

[52] R. Chaos-Moràin, A. Salazar, and A. Urena. Mechanical analysis of carbon nanofiber/epoxy resin composites. *Polymer Composites*, 32(10):21–25, 2011.

[53] S. Sihn, J.W. Park, R.Y. Kim, and A.K. Roy. Improvement of delamination resistnce in composite laminates with nano interlayers. Technical report, 2006.

[54] M. Arai, Y. Noro, K. Sugimoto, and M. Endo. Mode I and mode II interlaminar fracture toughness of CFRP laminates toughened by carbon nanofiber interlayer. *Composite Science and Technology*, 68(2):516–525, February 2008.

[55] D.R. Bortz, C. Merino, and I. Martin-Gullon. Augmented fatigue performance and constant life diagrams of hierarchical carbon fiber/nanofiber

epoxy composites. *Composites Science and Technology*, December 2011.

[56] R. Sadeghian, S. Gangireddy, B. Minaie, and K.T. Hsiao. Manufacturing carbon nanofibers toughened polyester/glass fiber composites using vacuum assisted resin transfer molding for enhancing the mode-I delamination resistance. *Composites Part A: Applied Science and Manufacturing*, 37(10):1787–1795, October 2006.

[57] S. Jana, W. Zhong, and Y. Gan. Characterization of the flexural behavior of a reactive graphitic nanofibers reinforced epoxy using a non-linear damage model. *Materials Science and Engineering: A*, 445-446:106–112, February 2007.

[58] A. Zhamu, Y. Hou, W.H. Zhong, J.J. Stone, J. Li, and C.M. Lukehart. Properties of a Reactive-Graphitic-Carbon-Nanofibers-Reinforced Epoxy. *Polymer Composites*, 28(5):605–611, 2007.

[59] A. Genaidy, R. Sequeira, M. Rinder, and A. A-Rehim. Risk analysis and protection measures in a carbon nanofiber manufacturing enterprise: an exploratory investigation. *The Science of the total environment*, 407(22):5825–38, November 2009.

[60] P.A. Schulte, E.D. Kuempel, R.D. Zumwalde, C.L. Geraci, M.K. Schubauer-Berigan, V. Castranova, L. Hodson, V. Murashov, M.M. Dahm, and M. Ellenbecker. Focused actions to protect carbon nanotube workers. *Americal journal of industrial medicine*, 55:395–411, 2012.

[61] S.C. Moon and R.J. Farris. The morphology , mechanical properties , and flammability of aligned electrospun polycarbonate (PC) nanofibers preparation of polymer solution. *Polymer Engineering and Science*, pages 1848–1854, 2008.

[62] S. Sihn, J.W. Park, R.Y. Kim, W. Huh, and A.K. Roy. Prediction of delamination resistance in laminated composites with electrospun nanointerlayers using a cohesive zone modeling. In *47th AIAA*, number May, 2006.

[63] G. Li, P. Li, C. Zhang, Y. Yu, H. Liu, S. Zhang, X. Jia, X. Yang, Z. Xue, and S. Ryu. Inhomogeneous toughening of carbon fiber/epoxy composite using electrospun polysulfone nanofibrous membranes by in situ phase separation. *Composites Science and Technology*, 68(3-4):987–994, March 2008.

[64] J. Zhang, T. Yang, T. Lin, and C.H. Wang. Phase morphology of nanofibre interlayers: critical factor for toughening carbon/epoxy composites. *Composite Science and Technology*, 2011.

[65] Y. Chen, D. Han, W. Ouyang, S. Chen, H. Hou, Y. Zhao, and H. Fong. Fabrication and evaluation of polyamide 6 composites with electrospun polyimide nanofibers as skeletal framework. *Composites Part B: Engineering*, December 2011.

[66] A.D. Kelkar, R. Mohan, R. Bolick, and S. Shendokar. Effect of nanoparticles and nanofibers on Mode I fracture toughness of fiber glass reinforced polymeric matrix composites. *Materials Science and Engineering: B*, 168(1-3):85–89, April 2010.

[67] J. Zhang, T. Lin, and X. Wang. Electrospun nanofibre toughened carbon/epoxy composites- Effects of polyetherketone cardo (PEK-C) nanofibre diameter and interlayer thickness. *Composite Science and Technology*, 70:1660–1666, 2010.

[68] Q. Chen, L. Zhang, M.K. Yoon, X.F. Wu, R.H. Arefin, and H. Fong. Preparation and Evaluation of Nano-Epoxy Composite Resins Containing Elec-

trospun Glass Nanofibers. *Journal of Applied Polymer Science*, pages 21–25, 2011.

[69] L. Liu, M.Z. Huang, C. He, and X. Han. Mechanical performance of laminated composites incorporated with nanofibrous membranes. *Materials Science and Engineering: A*, 435-436:309–317, November 2006.

[70] L. Liu, Y.M. Liang, G.Y. Xu, H.S. Zhang, and Z.M. Huang. Mode I Interlaminar Fracture of Composite Laminates Incorporating with Ultrathin Fibrous Sheets. *Journal of Reinforced Plastics and Composites*, 27(11):1147–1162, April 2008.

[71] L. Liu, Z.M. Huang, G.Y. Xu, Y.M. Liang, and G.H. Dong. Mode II Interlaminar Delamination of Composite Laminates Incorporating With Polymer Ultrathin Fibers. *Polymer Composites*, pages 285–292, 2008.

[72] K. Shivakumar, S. Lingaiah, H. Chen, P. Akangah, G. Swaminathan, and L. Russell. Polymer nanofabric interleaved composite laminates. *AIAA Journal*, 47(7):1723–1729, July 2009.

[73] P. Akangah, S. Lingaiah, and K. Shivakumar. Effect of Nylon-66 nano-fiber interleaving on impact damage resistance of epoxy/carbon fiber composite laminates. *Composite Structures*, 92(6):1432–1439, May 2010.

[74] S. Abrate. *Impact on Composite Structures*. Cambridge University Press, 2005.

[75] G. Minak and A. Zucchelli. Damage evaluation and residual strength prediction of CFRP laminates by means of Acoustic Emission techniques. *Composites Part A: Applied Science and Manufacturing*, pages 165–207, 2008.

[76] G. Minak, F. Cesari, V. Dal Re, and A. Zucchelli. Damage and residual strength of laminated carbon-epoxy composite circular plates loaded at the centre. *Composites Part A: Applied Science and Manufacturing*, 38(4):1163–1173, 2007.

[77] G. Minak, P. Morelli, and A. Zucchelli. Fatigue residual strength of circular laminate graphite-epoxy composite plates damaged by transverse load. *Composite Science and Technology*, 69(9):1358–1363, 2009.

[78] G. Minak, S. Abrate, D. Ghelli, R. Panciroli, and a. Zucchelli. Residual torsional strength after impact of CFRP tubes. *Composites Part B: Engineering*, 41(8):637–645, December 2010.

[79] A.A. Bakhtiary Davijani, M. Hajikhani, and M. Hamadi. Acoustic Emission based on sentry function to monitor the initiation of delamination in composite materials. *Materials and Design*, 32(5):3059–3065, May 2011.

[80] A.R. Oskouei, A. Zucchelli, M. Ahmadi, and G. Minak. An integrated approach based on acoustic emission and mechanical information to evaluate the delamination fracture toughness at mode I in composite laminate. *Materials and Design*, 32(3):1444–1455, March 2011.

[81] ASTM D5528. Standard Test Method for Mode I Interlaminar Fracture Toughness of Unidirectional Fiber-Reinforced Polymer Matrix Composites. *Annual Book of ASTM Standards*, 2007.

[82] ASTM D7246/D. Standard Test Method for Flexural Properties of Polymer Matrix Composite Materials. *Annual Book of ASTM Standards*, 2010.

[83] E. Barkanov, W. Hufenbach, and L. Kroll. Transient response analysis of systems with different damping models. *Computer Methods in Applied Mechanics and Engineering*, 192(1-2):33–46, January 2003.

[84] G. Minak and D. Ghelli. Design of a drop-weight machine for composite

materials impact testing. In *5th International Congress of Croatian Society of Mechanics*, Trogir/Split, 2006.

[85] X. Zhou, Eungsoo Shin, K.W. Wang, and C.E. Bakis. Interfacial damping characteristics of carbon nanotube-based composites. *Composites Science and Technology*, 64(15):2425–2437, November 2004.

[86] F. Liang, Y. Tang, J. Gou, H. C. Gu, and G. Song. Vibration damping enhancement of polymer composites via carbon nanopaper sheets with different fiber reinforcements. In *Earth and Space 2010*, pages 3709–3720, Reston, VA, March 2010. American Society of Civil Engineers.

[87] J. Gou, S. O'Braint, H. Gu, and G. Song. Damping Augmentation of Nanocomposites Using Carbon Nanofiber Paper. *Journal of Nanomaterials*, 2006:1–7, 2006.

[88] N. Koratkar. Multifunctional structural reinforcement featuring carbon nanotube films. *Composites Science and Technology*, 63(11):1525–1531, August 2003.

[89] H.I. Wu and G. Springer. Measurement of matrix cracking and delamination caused by impact on composite plates. *Journal Of Composite Materials*, 22:518–532, 1998.

Acknowledgment

Author would like to acknowledge:

- professor *Andrea Zucchelli*[1], wise mentor and honest friend, for his very precious teaching and support all along my path;
- professor *Giangiacomo Minak*[2] for his always sharp and smart help, support during conferences and constant stimuli to work better and better;
- professor *Maria Letizia Focarete*[3] and doctor *Chiara Gualandi*[4] for the calm and patience demonstrated with a muddler engineer into a chemistry laboratory;
- *Riccardo*[5], *Daniele*[6] and *Ezequiel*[7], for their important help and support with daily problems and for all the funny time spent together;
- *Metal T.I.G company*[8] for its important help and support during lamination process;
- *Impregnatex Compositi s.r.l.*[9] for the prepreg used for all the experiments;
- *doctor Paolo Proli*[10] for his help and during lamination processes.

Bologna, March 26, 2013 R. P.

[1] Assistant professor, Engineering Faculty, University of Bologna.
[2] Associate professor, Engineering Faculty, University of Bologna.
[3] Assistant professor, Chemistry Faculty, University of Bologna.
[4] Ph.D., Chemistry Faculty, University of Bologna.
[5] Ph.D., Engineering Faculty, University of Bologna.
[6] Ph.D., Engineering Faculty, University of Bologna.
[7] Ph.D. student, Engineering Faculty, University of Bologna.
[8] via Flavio Gioia 11, 40024 Castel San Pietro Terme (BO) ✉info@metaltig@it
[9] via Tiepoli 19, 20022 Castano Primo (MI) ✉info@impregnatex.it
[10] II Engineering Faculty, University of Bologna, Forlì laboratories.